

AN ABSTRACT OF THE THESIS OF

JOHN NEIL GALLAGHER for the PH. D.
(Name) (Degree)

in GEOPHYSICS presented on January 28, 1968
(Major) (Date)

Title: A METHOD FOR DETERMINING THE SOURCE MECHANISM
IN SMALL EARTHQUAKES WITH APPLICATION TO THE
PACIFIC NORTHWEST REGION

Abstract approved: Redacted for privacy
Peter Dehlinger

A technique was developed in the present study to determine fault-plane solutions for small earthquakes. The method uses the direction and amplitude of initial P-wave motions recorded at a small number of seismic stations for epicentral distances less than 2000 km.

Seismic arrivals recorded on short-period seismograms were identified as p, P or Pn waves for crustal shocks and P waves for subcrustal shocks. Source amplitudes were converted from station amplitudes using known theoretical methods, based on determining angles of incidence at the surface of the earth and straight ray paths in experimental crustal models.

Source amplitudes were calculated for three stations and were then projected back to the earthquake source. The source amplitudes

were compared to amplitudes that correspond to more than 6000 theoretical amplitude patterns. The pattern which most nearly fitted the first motions was taken as the fault-plane solution. P-wave amplitudes, velocity structures, focal depth and wave attenuation were varied to show the relative deviations of the dip and strike in a fault-plane solution.

When the S-wave was identified, it was found that polarization could be determined for epicentral distances less than 20° .

Thirty-three earthquakes in the Pacific Northwest region were analyzed, and twenty-two fault-plane solutions were determined by the method described in this paper. Seven additional fault-plane solutions were determined using the well-known Byerly method.

The fault-plane solutions generally showed large dip-slip components. This was particularly evident in fault-plane solutions for earthquakes occurring off the coast of Oregon and northern California, and west of the Cascade Mountains. The solutions for earthquakes east of the Cascade Range and off the coast of British Columbia have either dip-slip or strike-slip components.

The solutions obtained by the present technique were compared with solutions for generally larger earthquakes in western North America as previously determined by other investigators, using the Byerly method. Satisfactory agreement was found between the two methods.

Two general tectonic hypotheses are proposed from the study of earthquake stresses in the Pacific Northwest region.

A Method for Determining the Source
Mechanism in Small Earthquakes With
Application to the Pacific Northwest Region

by

John Neil Gallagher

A THESIS

submitted to

Oregon State University

in partial fulfillment of
the requirements for the
degree of

Doctor of Philosophy

June 1969

APPROVED:

Redacted for privacy

Professor of Geophysics
in charge of major

Redacted for privacy

Chairman of Department of Oceanography

Redacted for privacy

Dean of Graduate School

Date thesis is presented January 28, 1969

Typed by Donna L. Olson for John Neil Gallagher

ACKNOWLEDGMENTS

This research was performed under the direction of Dr. Peter Dehlinger, Professor of Geophysics, Department of Oceanography, Oregon State University.

I am grateful to the Messrs. Richard W. Couch and William S. French for their helpful suggestions and discussions about the research.

I wish to thank Miss Ellen Gallagher for editing the manuscript, and my wife, Teresa, for typing the preliminary copies.

I am grateful to Dr. Gunnar Bodvarsson for his review of the mathematical aspects of the thesis and Dr. Donald Heinrichs for his review of the manuscript.

Seismograms were obtained through the courtesy of the Dominion Observatory, Ottawa, Canada; U. S. Coast and Geodetic Survey, Washington, D. C.; University of California, Berkeley, California; University of Washington, Seattle, Washington; and University of Utah, Salt Lake City, Utah.

This research was partially funded by the National Science Foundation Grant GP-5769, Expansion of the Computer Center and Office of Naval Research Nonr Contract No. 1286(10).

TABLE OF CONTENTS

	<u>Page</u>
INTRODUCTION	1
PREVIOUS WORK	4
THEORY	16
Classification of the P Waves	17
Determination of Incident Amplitude	19
Amplitude Conversion Factors for the Effect of the Crust and Upper Mantle	26
Correcting for Effects of Wave Attenuation	33
Method for Determining Fault-Plane Solutions	34
MATERIALS USED	39
Earthquakes and Stations	39
Assumed Crustal Sections	43
Calculation of Ground Velocities	49
PROCEDURE FOR DETERMINING FAULT-PLANE SOLUTIONS	52
Removing Surface Effects from Ground Motions	52
Removing Crust and Upper Mantle Effects	55
Calculation of the Fault-Plane Solution	68
DISCUSSION OF RESULTS	71
Comparison of Byerly Method and Present Method	71
Present Method Applied in Northwestern North America	84
Off the Coast of British Columbia	84
Off the Coast of Oregon and Northern California	87
West of the Cascade Mountains	87
East of the Cascade Mountains	90
Reliability of the Fault-Plane Solutions	94
Accuracy of First Motion Directions	94
Possible Measurement Errors	94
Variations of the Angles i_h and Amplitude Conversion Factors	95

	<u>Page</u>
Accuracy of Orientations for Obtaining Fault-Plane Solutions	97
Effect of Amplitude Deviations on Orientations	97
Effect of Wave Attenuation on Orientations	98
General Tectonic Forces in Western America	104
CONCLUSIONS	109
BIBLIOGRAPHY	113
APPENDIX I. THEORETICAL DEVELOPMENT OF THE HEAD WAVE EQUATION	121
APPENDIX II. DEPTH OF FOCUS DETERMINATION	130
APPENDIX III. COMPUTER PROGRAMS	132
APPENDIX IV. PRELIMINARY STUDY OF TRAVEL TIMES IN BRITISH COLUMBIA	142
APPENDIX V. THE TACOMA AND OTHER EARTHQUAKE FAULT-PLANE SOLUTIONS OBTAINED WITH THE BYERLY METHOD	149
APPENDIX VI. EXPERIMENTAL EARTHQUAKE DATA	156

LIST OF TABLES

<u>Table</u>	<u>Page</u>
I. Data for Thirty-Three Earthquakes in the Pacific Northwest.	41
II. Seismic Stations Used in Present Study.	44
III. Tabulation for Amplitude Conversion Factors.	65
IV. Summary of Fault-Plane Solutions Obtained in Present Study.	72
V. Summary of Fault-Plane Solutions Found by Other Investigators Using Byerly Method.	81
VI. Effect of Q Values on Source Amplitudes.	102
VII. Travel Times of Seismic Waves from British Columbia Earthquakes.	143

LIST OF FIGURES

<u>Figure</u>		<u>Page</u>
1.	Type I and II source mechanisms for P and S waves (after Byerly and Stauder, 1957).	5
2.	A spherical earth section showing seismic waves originating from crustal and subcrustal earthquakes.	18
3.	Apparent and true angles of incidence for a P wave at the surface of the earth.	20
4.	Horizontal (U) and vertical (W) ground displacement and incident amplitude (A) of a P wave at the surface of the earth. (determined from Bullen equations, 1963).	22
5.	Ratios of the transverse, radial and vertical displacements of the S wave at the surface of the earth. Inset shows phase relationship between vertical and radial components (after Nuttli, 1961).	25
6.	Geometrical spreading of the wave from focus to surface of the earth (after DeBremaecker, 1955).	30
7.	Angular rotations. (a), (b), (c) illustrate the three rotations due to Euler Angles between fixed and rotating co-ordinate systems (after Goldstein, 1959); (d) illustrates the nodes of a P wave fixed in the rotating system.	36
8.	Locations of thirty-three earthquakes in the Pacific Northwest used in this investigation.	40
9.	Ten crustal sections in the Pacific Northwest area based on analyses of gravity and seismic data.	47
10.	Calculated true angles of incidence at various seismic stations based on amplitudes of P waves.	53

11. Amplitude conversion factor of the Pn wave as a function of epicentral distance for different crustal sections and focal depths (use of ratio gives resultant displacement). 57
12. Amplitude conversion factor of the SVn wave as a function of epicentral distance for different crustal sections and focal depths (use of ratio gives resultant displacement). 58
13. Amplitude conversion factor of the SHn wave as a function of epicentral distance for different crustal sections and focal depths (use of ratio gives resultant displacement). 59
14. Variation of the angle of incidence i_h with epicentral distance for different focal depths and selected crustal sections. 60
15. Variation of the incidence angle (a) beneath the Moho, i_m , at the surface of the earth i_o and (b) at the source i_h with epicentral distance for different focal depths and selected crustal sections. 61
16. Amplitude conversion factors of P and p waves as a function of epicentral distance for different crustal sections and focal depths. 62
17. Amplitude conversion factors of P and p waves as a function of epicentral distance for different crustal sections and focal depths. 63
18. Amplitude conversion factors of the P wave as a function of epicentral distance for different crustal sections and focal depths above the Moho. 64
19. Partitioning of energy curves: 1 and 4 after Gutenberg (1944); 2 and 3 computed in present study. 67

<u>Figure</u>		<u>Page</u>
20.	Fault-plane solutions for earthquake of April 29, 1965 projected on top and bottom half of focal sphere.	75
21.	Fault-plane solution for earthquake of August 22, 1963 projected on top and bottom half of focal sphere.	75
22.	Fault-plane solution for earthquake of May 8, 1968 projected on bottom half of focal sphere.	76
23.	Reliability of fault-plane solution based on 5° and 10° increments of Euler Angles.	78
24.	Fault-plane solutions for earthquake of October 14, 1962 projected on top and bottom half of focal sphere.	79
25.	Fault-plane solutions for earthquake of March 7, 1963 projected on top and bottom half of focal sphere.	80
26.	Fault-plane solutions for earthquake of April 19, 1967 projected on top and bottom half of focal sphere.	86
27.	Fault-plane solution for earthquake of April 29, 1967 projected on bottom half of focal sphere.	86
28.	Fault-plane solution for earthquake of March 30, 1966 projected on bottom half of focal sphere.	86
29.	Fault-plane solution for earthquake of May 20, 1966 projected on bottom half of focal sphere.	88
30.	Fault-plane solution for earthquake of November 4, 1966 projected on bottom half of focal sphere.	88
31.	Fault-plane solution for earthquake of June 25, 1963 (08: 26: 21. 7) projected on bottom half of focal sphere.	88

FigurePage

32. Fault-plane solution for earthquake of June 25, 1968 (09:39:27.7) projected on bottom half of focal sphere. 88
33. Fault-plane solution for earthquake of July 4, 1963 projected on top and bottom half of focal sphere. 89
34. Fault-plane solution for earthquake of February 21, 1963 projected on top and bottom half of focal sphere. 89
35. Fault-plane solution for earthquake of November 6, 1962 projected on top and bottom half of focal sphere. 91
36. Fault-plane solution for earthquake of January 24, 1963 projected on top and bottom half of focal sphere. 91
37. Fault-plane solution for earthquake of September 26, 1962 projected on bottom half of focal sphere. 92
38. Fault-plane solution for earthquake of February 16, 1963 projected on bottom half of focal sphere. 92
39. Fault-plane solution for earthquake of October 18, 1962 (20:31:02.6) projected on top and bottom half of focal sphere. 92
40. Fault-plane solution for earthquake of October 18, 1962 (18:03:14.0) projected on top and bottom half of focal sphere. 93
41. Fault-plane solution for earthquake of January 6, 1963 projected on bottom half of focal sphere. 93
42. Fault-plane solution for earthquake of February 24, 1963 projected on bottom half of focal sphere. 93
43. Comparison of the effects of straight and curved ray paths on calculated source incidence angles. 96

FigurePage

44. Attenuation for $Q = 200$ and $Q = 400$ in relation to travel time for waves of one cps. 100
45. Fault-plane solutions for earthquake of February 16, 1963 using $Q = \infty$, $Q = 200$, and $Q = 400$. 101
46. Fault-plane solutions for earthquake of June 25, 1963 (09:39: 27. 7) using $Q = \infty$, $Q = 200$, and $Q = 400$. 101
47. Fault-plane solutions for earthquake of August 22, 1963 using $Q = \infty$ and $Q = 400$. 101
48. Location of earthquakes used in the present investigation. 105
49. Direction of maximum, intermediate, and minimum principal stresses found from fault-plane solutions determined by the Byerly method. Numbered earthquakes listed in Table V. 106
50. Direction of maximum, intermediate, and minimum principal stresses found from fault-plane solutions determined by the present method. Numbered earthquakes listed in Table IV. 107

A METHOD FOR DETERMINING THE SOURCE MECHANISM IN SMALL EARTHQUAKES WITH APPLICATION TO THE PACIFIC NORTHWEST REGION

INTRODUCTION

The objective of the present study was to develop a new technique for obtaining fault-plane solutions for local earthquakes. The method is based primarily on determining P-wave radiation patterns from seismic recordings at three stations near the epicenter. Thirty-three earthquakes were investigated by this method. These earthquakes occurred in the Pacific Northwest region (parts of the United States, Canada and coastal waters). Results of the technique described in this paper are presented as a contribution to the understanding of earthquake sources and tectonic processes in the area. The method developed is based on modifications of existing techniques for determining fault-plane solutions.

P-wave techniques developed by Byerly (1955) and subsequent investigators are well known. A world-wide distribution of seismic stations used in the Byerly technique has been employed successfully in determining fault-plane solutions for large earthquakes. However, small earthquakes, recorded only locally, are difficult to analyze by the Byerly method unless many seismic stations are located near the epicenter.

Other investigators using one or more stations have determined

fault-plane solutions by mathematical equations expressed in terms of P and S-wave amplitudes. The difficulty with this technique arises from the uncertainty in identifying S waves at epicentral distances between 5° and 12° .

The original objective of this research was to make separate investigations for using P waves to determine fault planes and S waves to determine source mechanisms. Attempts were made to identify S waves, calculate S polarization and evolve procedures for determining source mechanisms from the S wave. From these original investigations it was determined that the techniques of this study should be based entirely on P-wave radiation patterns determined from short-period seismograms. The study does not require the use of the S wave to obtain fault-plane solutions.

The following factors had to be evaluated in the development of the technique:

- (1) Effects of seismograph response characteristics on the incident wave.
- (2) Amplitude of the incident seismic wave at the surface of the earth.
- (3) Geometrical spreading of the waves; refraction and partitioning of energy at major interfaces; and wave attenuation.

A mathematical method utilizing a theoretically derived function for P-wave radiation was used to calculate P-wave amplitudes

for over 6000 possible radiation patterns. These calculated P-wave amplitudes were compared with experimentally determined P-wave amplitudes at three seismic stations to select a fault-plane solution.

PREVIOUS WORK

An earthquake mechanism may be described by the geometrical pattern of forces causing the source motion. Two earthquake mechanisms, known as Types I and II, were considered in determining the fault-plane solutions in this study (Figure 1). The forces of a Type I mechanism are consistent with elastic rebound, while those of the Type II mechanism correspond to orthogonal axes of compressive and tensile stress. These mechanisms, which were developed mathematically by Nakano (1923), frequently are used to characterize source motions. Radiation patterns of P waves in both Type I and II sources are identical, but for S waves they are different. S-wave radiation patterns must be known to distinguish between the two types.

The P-wave patterns can be delineated geometrically by two perpendicular planes. The two planes of zero P radiation separate four lunes. Each lune has a symmetrical P-wave radiation pattern, but the direction of P-wave motion changes alternately by lune. The planes represent a fault plane and an auxiliary plane in a Type I mechanism and nodes in a Type II mechanism. The line of intersection of the two planes is the null vector or null line.

In the Type I mechanism a single couple of vector forces, with moment, acts along one of the planes (the fault plane) and perpendicular to the other (auxiliary) plane. S-wave data are required to

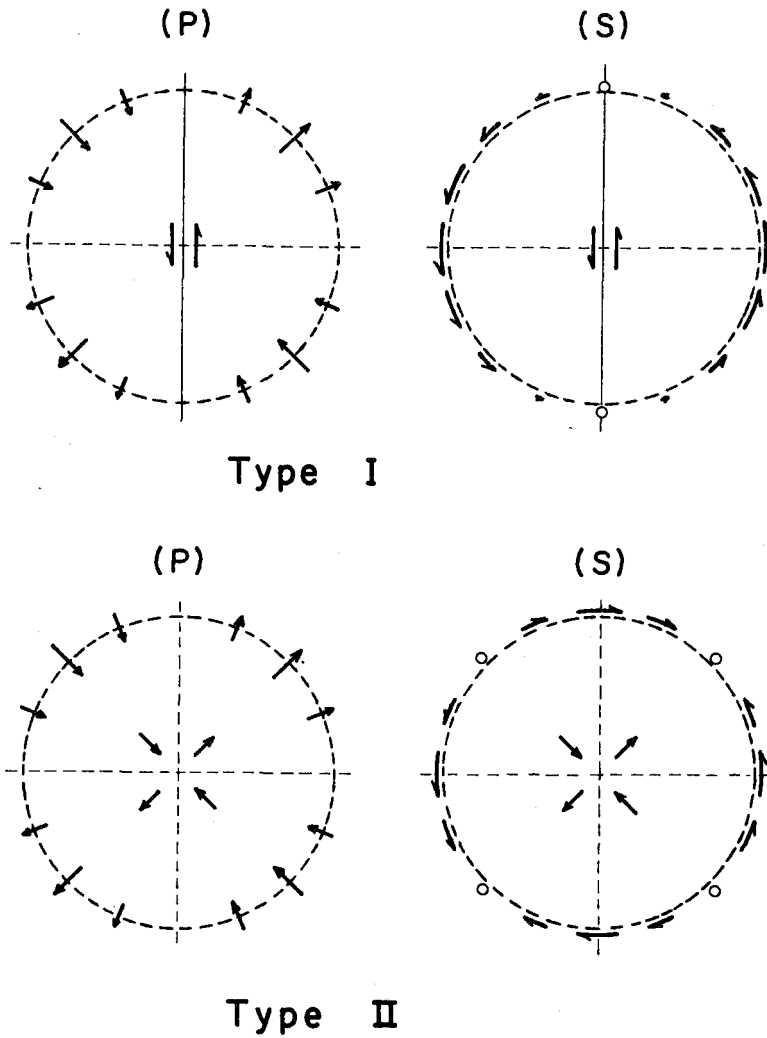


Figure 1. Type I and II source mechanisms for P and S waves (after Byerly and Stauder, 1957).

differentiate the two planes. The P-radiation pattern alone can provide the orientations of the two planes. In a Type II mechanism a double couple of vector forces, with moment, acts along both planes. Neither plane is a fault plane, but both are nodal planes separating zones of compression and dilatation.

The Type I mechanism can be visualized as a small sphere with the vector forces acting along a line through its center. The intersection of the line of vector forces with the surface of the sphere is the pole of the forces. The radiation of the S-wave, as produced by the vector forces, forms lines of polarization on the spherical surface.

Source mechanisms of earthquakes have been determined from directions of initial P and S-wave motions using various methods based upon geographical distribution of stations and focal depths.

Investigators in many countries have developed different approaches in determining the fault-plane solution of an earthquake. The Byerly (1955) method, which uses P-wave arrivals, is described in the following paragraphs. As many other methods involve similar concepts, only the essential variations of these methods from the Byerly technique will be given.

In various investigations, the initial motions of P waves have been plotted for determining the orientation of the fault or nodal planes at the earthquake source; in these methods, it is considered

essential to use large numbers of stations.

Byerly (1926) perceived the P-wave first motions of the 1925 Montana earthquake formed patterns, but he did not arrive at any conclusions on the force mechanism at the source. Two years later, Byerly (1928) showed that a P wave, traveling from the earthquake focus along a curved path, may arrive at a seismic station with a first motion that is inconsistent with first motions recorded at other stations. This phenomenon may be caused by the recorded seismic wave having originated on a side of the fault plane opposite to that of the station. Byerly (1928) removed the effects of curved rays by assuming a homogenous earth, permitting the wave of the earthquake to travel along straight paths. The station recording the wave for the curved ray path was projected to a new position on the earth, where the straight ray path would arrive. The relation between the actual and the projected positions of the seismic station was called the extended position. The extended position was determined from travel-time curves (for different focal depths).

Byerly (1938) projected the extended positions on an equatorial plane (extended distances) for a homogenous earth. In this projection the anticerter of the earthquake was used for the pole of the projection. The projection provides a simple device for plotting first motions of P waves at each seismic station and for drafting circles that represent fault planes and auxiliary planes, or the nodal planes

of a source mechanism.

In a study of the July 6, 1934 earthquake off the coast of northern California, Byerly (1938) unsuccessfully compared experimental amplitudes of the P wave in the vicinity of the fault plane with theoretical radiation patterns derived by Nakano (1923).

Soviet investigators (Byerly and Stauder, 1957) have reduced the seismic radiation on a heterogenous earth to that on a focal sphere (a unit sphere with the focus at its center) instead of using Byerly's concept of a homogenous earth. In the Soviet method, the angle of incidence must be determined for rays leaving the source.

American, Russian, Japanese and other investigators (Scheidegger, 1957) have used a variety of stereographic projections to determine fault-plane solutions. Scheidegger (1957) showed that many of these stereographic projections are geometrically equivalent.

Hodgson and Storey (1953) developed extended distance tables, as used in the Byerly method, for P waves at epicentral distances from 0° to 105° . They constructed these tables for different focal depths, using the Jeffreys-Bullen travel-time tables and regarding the earth as stripped to the focus (i. e., an earth in which all earth layers above the source have been removed). These tables convert epicentral distances to extended distances for a given station.

Hodgson and Storey observed that velocities from the tables were

low at short epicentral distances. They stated that extended distances may be of questionable accuracy due to this inconsistency in velocities.

To correct for the low seismic velocities which had been encountered in crustal earthquake shocks, Sutton and Berg (1958) revised the Hodgson-Storey (1953) tables. They observed that P waves travel from source to receiver in a curved path. P-wave incidence angles at the source decrease with increasing epicentral distance. However, the Pn wave (head wave) leaves the source within the crust at the same incidence angle for epicentral distances of about 1° to 10° . The extended distances are also the same in the 1° to 10° range. The loci of extended distances on the homogenous earth form a circle whose center is on the line passing from the epicenter to the antipode. This circle on the earth forms a circle on the projection, known as the critical circle.

As compensation for limited geographical station distribution on the Byerly type of projection plane, the Dominion Observatory, Ottawa, Canada (Hodgson and Adams, 1958) used several phases of P waves--PcP, PKP, PP and pP. These P-wave motions are designated as follows. PcP is a wave that is reflected from the outer surface of the core, PKP is a wave that has traveled through the core of the earth. PP is a wave that is reflected once at the surface of the earth but remains within the mantle and crust. pP is a

wave from a deep focus that is reflected at the surface of the earth near the epicenter. When the first motion and distribution of each of these phases was used, the distribution of P-wave first motions was enhanced, as these phases exhibit varied extended distances. However, Hodgson and Adams (1958) have investigated the inconsistencies of first motions in fault-plane solutions and found that the reflected phases (PP, PcP, pP) provided questionable data for these solutions.

Douglas (1967) investigated the complexities of P-wave amplitudes arriving at a seismic station in the first 30 to 40 seconds from the first arriving P wave. The complexities involved relative wave amplitudes of first and later arrivals. When the first arrivals were large and gradually diminished, the undulations were called simple. When the recorded amplitudes were irregular, they were termed complex. Douglas (1967) compared these simple and complex amplitudes near the nodes of experimental radiation patterns.

Polarization of the S wave from an earthquake has been used to determine the force pattern in Type I and II mechanisms. Neumann (1930), Gutenberg (1952), Nuttli (1961), and others have discussed the partitioning of S waves at the surface of the earth. SV waves (polarized vertically) arrive at incidence angles greater than the critical angle for P waves at epicentral distances between 0° and 30° (Gutenberg, 1952); therefore, S waves should be used to

determine the polarization of the S wave at epicentral distances between 30° and 80° . Gutenberg (1952) suggested the 80° upper limit because of the interference of other S phases at the greater epicentral distances. Stauder (1960c) and Monachov (1950) concluded that S polarization is unaffected by inhomogeneities of the earth, although Galitzin (1914) found that polarization is affected by earth boundaries.

Dehlinger (1952) determined S polarization directions for local earthquakes in southern California (epicentral distances less than 130 km) and showed that direct S waves are polarized in a direction related to the faulting at the earthquake source. The faults he used generated predominantly SH waves (polarized horizontally).

Based on recordings at one seismic station, Ritsema (1962) investigated S-wave polarization at epicentral distances of less than 20° . He concluded that polarization of the S wave can be determined for earthquakes under favorable conditions (low noise and elliptical polarization). Adams (1958) used polarization of S waves to determine a Type I mechanism. His technique employed two seismic stations located along different lines of polarization. The intersection of these lines determined the orientation of the pole of forces.

Stauder (1960b) distinguished between Type I and II focal mechanisms using hodographs (particle vector diagrams) to

determine the polarization of the S wave. He found that lines of polarization can be plotted on a central projection, which is the projection of the seismic stations on a tangent plane at the antipode of the earthquake. Other investigators have successfully used the amplitude ratios of SH/SV from the train of the S wave to determine the polarization of the S wave at a seismic station.

In many investigations both P and S waves have been used to determine fault-plane solutions. Nakano (1923) developed theoretical equations for particle accelerations of P and S waves for the various mechanisms of earthquakes. Honda (1956) derived similar equations for amplitudes of particle motions.

Honda (1957) stated that Japanese investigators have compared effectively P and S wave amplitudes recorded at seismic stations with theoretically determined amplitudes that are based on equations derived by Nakano (1923), Honda (1957), and others.

Seismic studies in Japan have utilized P, S and surface waves recorded at seismic stations that are restricted in azimuth to one quadrant to determine fault-plane solutions. According to Keylis-Borok (1957), in the Soviet Union, where there are few seismic stations, amplitudes and directions of first motions from SV, SH and P waves were utilized to give constraint in development of techniques. Investigators in the U.S.S.R. (Stauder, 1960b) also developed the mathematically constraining techniques that use amplitude ratios of

P/S_H, P/S_V and S_V/S_H for determining fault-plane solutions.

Ritsema (1967) suggested that, when an investigation is limited to a small closely grouped distribution of seismic stations, the amplitudes of the P wave sometimes can be used to determine P-wave gradients; i. e., the rate of change of P amplitude with epicentral distance. Then the ratio of P amplitude to P gradient at a seismic station could be used in determining nodal planes.

The ratio of P and S-wave amplitudes were studied by Ritsema (1962) from determined fault-plane solutions based on P and PKP first motions. Values were obtained (called C_i in the present paper) that are associated with the geometrical relationship between nodal planes and ratio of the P and S-wave amplitudes. The C_i values were found to vary at stations which could indicate possible errors in the P and/or S amplitudes and/or fault-plane solutions. As the fault-plane solutions were constrained by the first motions of P and PKP waves, errors evidently exist in determining the P and/or S-wave amplitudes.

Mikumo (1962) used P and S data from three local stations at epicentral distances of less than a degree to study small earthquakes ($1 < M < 3$). Using mathematically constrained techniques (Byerly and Stauder, 1957) and experimental crustal sections, Mikumo determined fault-plane solutions. Mikumo was able to determine the pole of force using one station, and fault-plane solutions using two

stations, assuming a Type I mechanism. Using more than two stations, he determined fault-plane solutions for Type II mechanisms.

Ben-Menahem (1967) determined that long-period P and S waves, as well as surface waves, can be used to determine fault-plane solutions by comparing experimental amplitude radiation patterns with theoretical radiation patterns. This technique, using P and S waves, has been applied to deep and intermediate shocks.

Recent investigators have developed computer programs to determine fault-plane solutions analytically by using least-square techniques with first motions of P waves or with S-wave polarizations.

Knopoff (1960) developed such a computer program, using a probability procedure which was based on initial motions of P waves, theoretical amplitude (a) and assumed constant noise (n). This procedure obtained the preferred fault-plane solution by maximizing the probability of selecting the correct direction of motions in relation to ratio of a/n . Kasahara (1963) extended Knopoff's approach by analyzing the directions of first motions of an earthquake as recorded at several seismic stations. A statistical reliability factor for the a/n relationship was also determined from a number of earthquakes.

Stevens (1967) successfully developed generalized equations that described all fault mechanisms (including Types I and II) found in earthquake studies. S-wave polarizations at seismic stations

were applied to the generalized equations, using least squares and other statistical techniques, to determine force mechanisms. Each force mechanism, determined by the S wave, then was compared with the fault plane determined by the P wave. When this technique was applied to previously determined fault-plane solutions, Stevens concluded that most of the solutions satisfied a Type II mechanism.

THEORY

The theory developed in this study was directed toward identifying the first motion of P and S waves and of source amplitudes so as to determine focal mechanisms. The source amplitudes were sought from the recorded amplitudes by correcting for the effects of the response of the recording instruments, the amplitude of the incident wave at the surface of the earth, partitioning of energy at major boundaries, geometrical spreading and wave attenuation.

In a homogenous, isotropic medium, two body waves are propagated with velocities

$$\alpha = \sqrt{\frac{\lambda + 2\mu}{\rho}} \quad \beta = \sqrt{\frac{\mu}{\rho}} \quad (1)$$

where: α is the P wave velocity, β is the velocity of the S wave, λ and μ are Lamé constants and ρ is the density of the medium.

The particle motion of the S wave is polarized elliptically in a direction normal to that of propagation. The S wave consists of two normal components; the SH wave characterized by particle motions in a horizontal plane, and the SV wave characterized by particle motions in a vertical plane.

The particle motion of the P wave at the surface of the earth in the direction of propagation is designated as a compression and the

motion in the opposite direction a dilatation.

The particle motion of the SV wave in the direction of propagation is designated as negative. The particle motion of the SH wave to the right, as observed at a seismic station looking toward the epicenter, is termed positive.

Classification of the P Waves

Classification of the first arrival of the P wave recorded at a seismic station is dependent on the focal depth of the earthquake. In the present study, three types of P waves, characterized by their ray path, will be used for foci above the Mohorovičić Discontinuity (Moho). These waves, shown in Figure 2, are:

- (1) the head wave (P_n) reaches the Moho at a critical angle, travels beneath the Moho and to the surface of the earth for epicentral distances from 0° to 15° .
- (2) the P wave travels from focus to the Moho, beneath the Moho and to the surface of the earth, and is refracted both above and beneath the Moho at less than the critical angle.
- (3) the p wave travels from the focus to the surface of the earth; it is the first arrival at epicentral distances 0° to 1° .

For foci beneath the Moho, only the P wave will be considered. This wave travels from focus to the station as a first arrival for

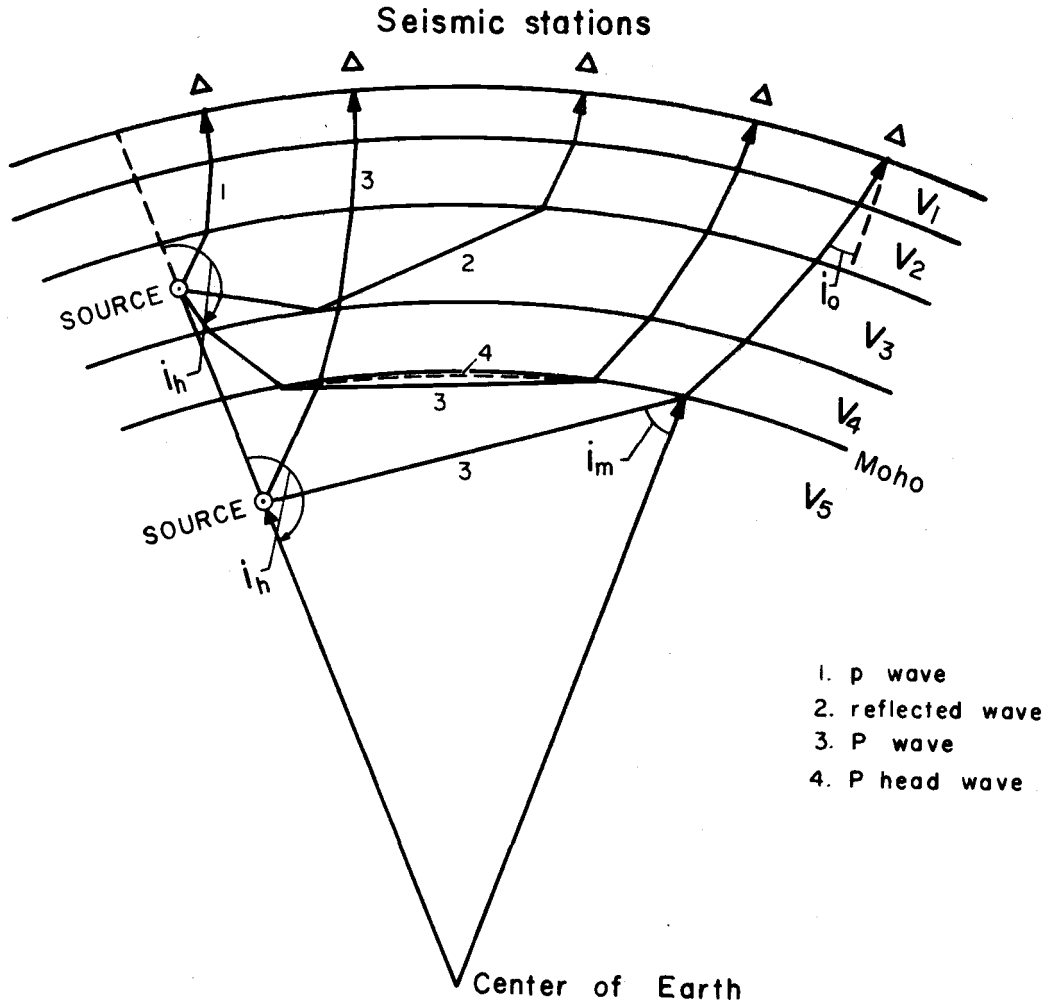


Figure 2. A spherical earth section showing seismic waves originating from crustal and subcrustal earthquakes.

epicentral distances of 20° or less. It travels mostly beneath the Moho for epicentral distances greater than 2° .

Determination of Incident Amplitude

The recorded P wave at the surface of the earth is a composite of the incident and reflected P waves and the reflected S-wave motions. Effects of the reflected wave motions must be removed to obtain the amplitude of the incident P wave. To determine the incident amplitude of the P wave from the recorded amplitude, the P wave angle of incidence must be obtained.

The apparent angle of incidence \bar{i}_o of the recorded composite P wave is the arc-tangent of the ratio of the surface radial component to the surface vertical component of the recorded P wave. The true angle of incidence i_o of the P wave is obtained from the equation (Bullen, 1963, p. 129) where Poisson's ratio (σ) equals 0.25, expressed as:

$$2 \sin^2 i_o = 3 (1 - \cos \bar{i}_o) \quad (2)$$

Figure 3 illustrates this relation between \bar{i}_o and i_o .

Equations 3 and 4 (Bullen, 1963, p. 128-129) demonstrate the relation between ground particle displacements (horizontal in direction of propagation U, vertical W) and the P wave incident amplitude

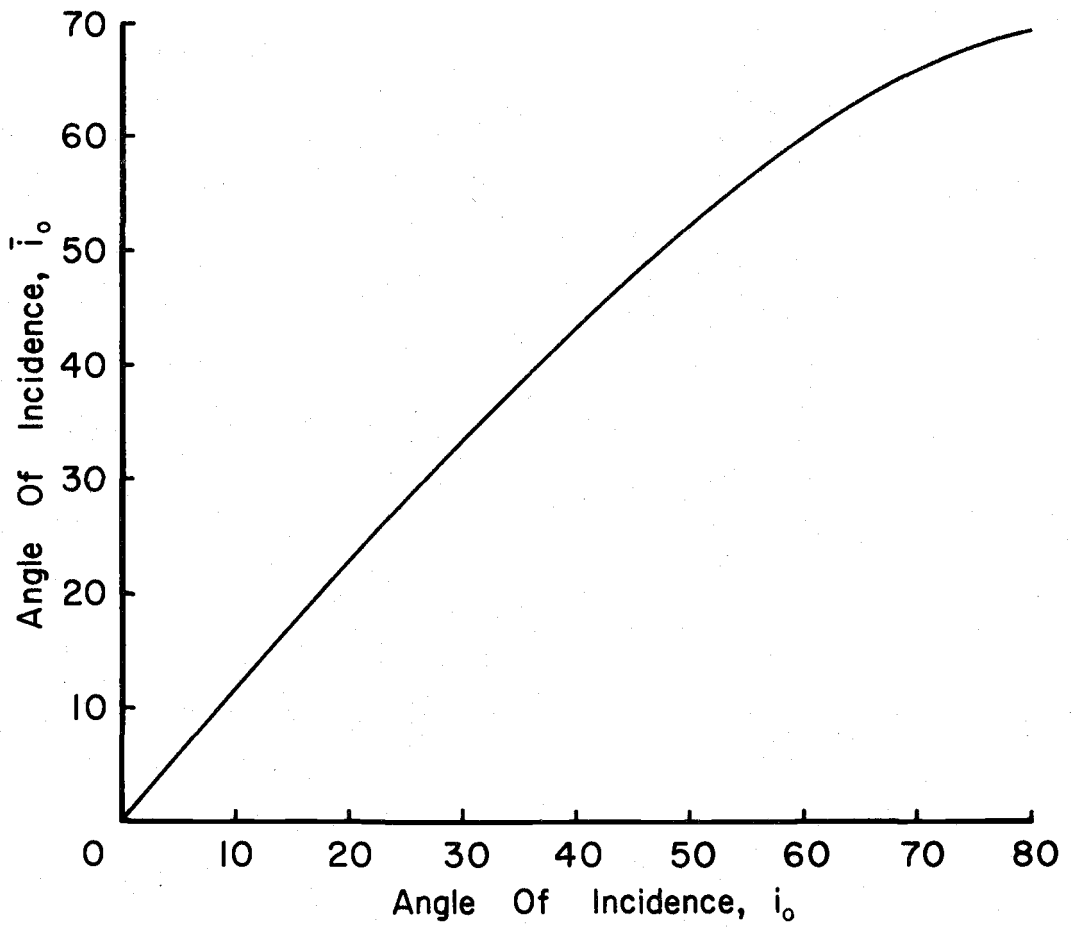


Figure 3. Apparent and true angles of incidence for a P wave at the surface of the earth.

A for any angle of incidence i_o . These relationships are shown in Figure 4.

$$\frac{U}{A} = \frac{12 \sin e \sec^2 e \tan f}{4 \tan e \tan f + (1 + 3 \tan^2 e)^2} \quad (3a)$$

$$\frac{W}{A} = \frac{6 \sin e \sec^2 e (1 + 3 \tan^2 e)}{4 \tan e \tan f + (1 + 3 \tan^2 e)^2} \quad (3b)$$

where:

$$e = \pi/2 - i_o$$

$f = \pi/2 - j_o$, j_o is the angle of incidence of the reflected SV wave.

to find j_o from i_o one uses

$$j_o = \arcsin(\beta/a \sin i_o)$$

For an S wave incident at the surface of the earth, the SH component is reflected only as an SH wave but the SV component is reflected as both SV and P waves.

An incident SH wave always gives ground displacements that are twice the incident amplitude regardless of the incidence angle. Therefore, the angle of incidence j_o of an S wave cannot be determined from its SH component. The angle j_o can be determined from the ground displacements of incident SV components provided the reflected SV and P waves are taken into account. The ground displacements of the SV wave are complicated when the angle i_o of

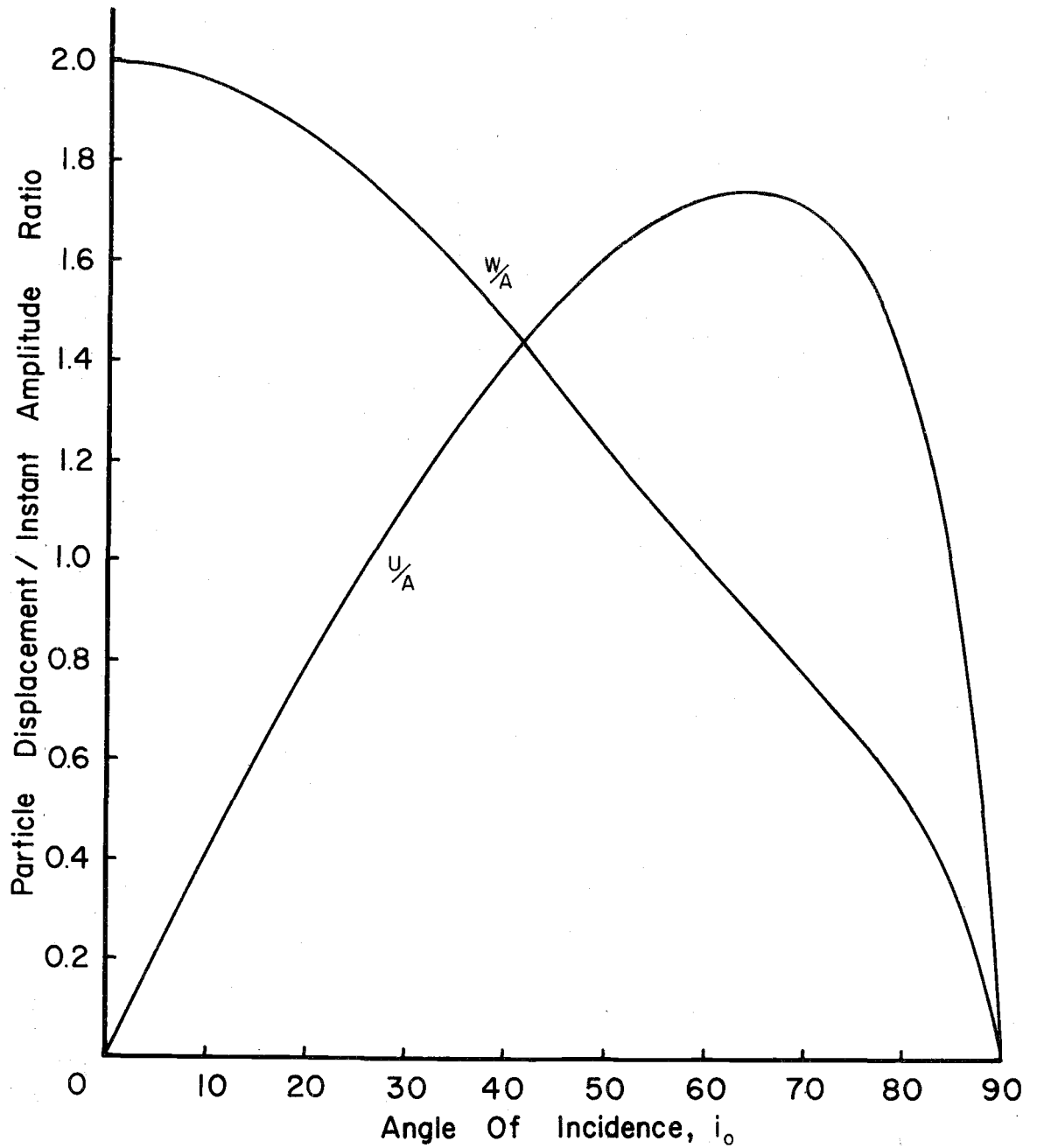


Figure 4. Horizontal (U) and vertical (W) ground displacement and incident amplitude (A) of a P wave at the surface of the earth (determined from Bullen equations, 1963).

the reflected P wave is 90° or greater. For that condition j_o is multiple valued.

The ground displacements of the S wave (Nuttli, 1961) for real value of i_o ($i_o < 90^\circ$) are:

$$\bar{U}_H = 2U_H \cos(wt) \quad (4a)$$

$$\bar{U}_R = U_V (\cos j_o - f_1 \cos j_o + f_2 \sin i_o) \cos(wt) \quad (4b)$$

$$\bar{U}_Z = U_V (\sin j_o + f_1 \sin j_o + f_2 \cos i_o) \cos(wt) \quad (4c)$$

where:

$$f_1 = \frac{-(\cos^2 2j_o - C^2 \sin 2j_o \sin 2i_o)}{\cos^2 2j_o + C^2 \sin 2j_o \sin 2i_o}$$

$$f_2 = \frac{2C \sin 2j_o \cos 2j_o}{\cos^2 2j_o + C^2 \sin 2j_o \sin 2i_o}$$

$C = \beta/a$, β is the velocity of the S wave, a is the velocity of the P wave.

U_H and U_V are the amplitudes of the incident SH and SV waves respectively.

\bar{U}_Z , \bar{U}_R , and \bar{U}_H are the ground displacements in the vertical, radial (the direction of the ray from the earthquake) and transverse (direction perpendicular to radial and parallel to earth) directions.

ω is the angular frequency in radians per second

t is the time in seconds

For imaginary values of i_o ($i_o > 90^\circ$)

$$\bar{U}_H = 2U_H \cos(\omega t) \quad (5a)$$

$$U_R = 2U_v \cos^2 2j_o [\cos^2 2j_o \cos j_o \cos \omega t + \frac{\sqrt{(\sin^2 j_o - C^2)} \sin^2 2j_o \sin \omega t}{\cos^4 2j_o + 4(\sin^2 j_o - C^2) \sin^2 2j_o \sin^2 j_o}] \quad (5b)$$

$$\bar{U}_Z = 2U_v \cdot \sqrt{(\sin^2 j_o - C^2)} \sin 2j_o [2\sqrt{(\sin^2 j_o - C^2)} \sin j_o \frac{\sin 2j_o \cos \omega t - \cos^2 2j_o \sin \omega t}{\cos^4 2j_o + 4(\sin^2 j_o - C^2) \sin^2 2j_o \sin^2 j_o}] \quad (5c)$$

A computer program (Appendix III) was developed in the present study to calculate the ratios \bar{U}_Z/\bar{U}_R , \bar{U}_Z/\bar{U}_H , and \bar{U}_H/\bar{U}_R for all values of j_o . In the case where i_o is imaginary the real value of the displacements was used and the phase relation between \bar{U}_Z and \bar{U}_R was calculated. All calculations were based on $\sigma = 1/4$ and are shown in Figure 5.

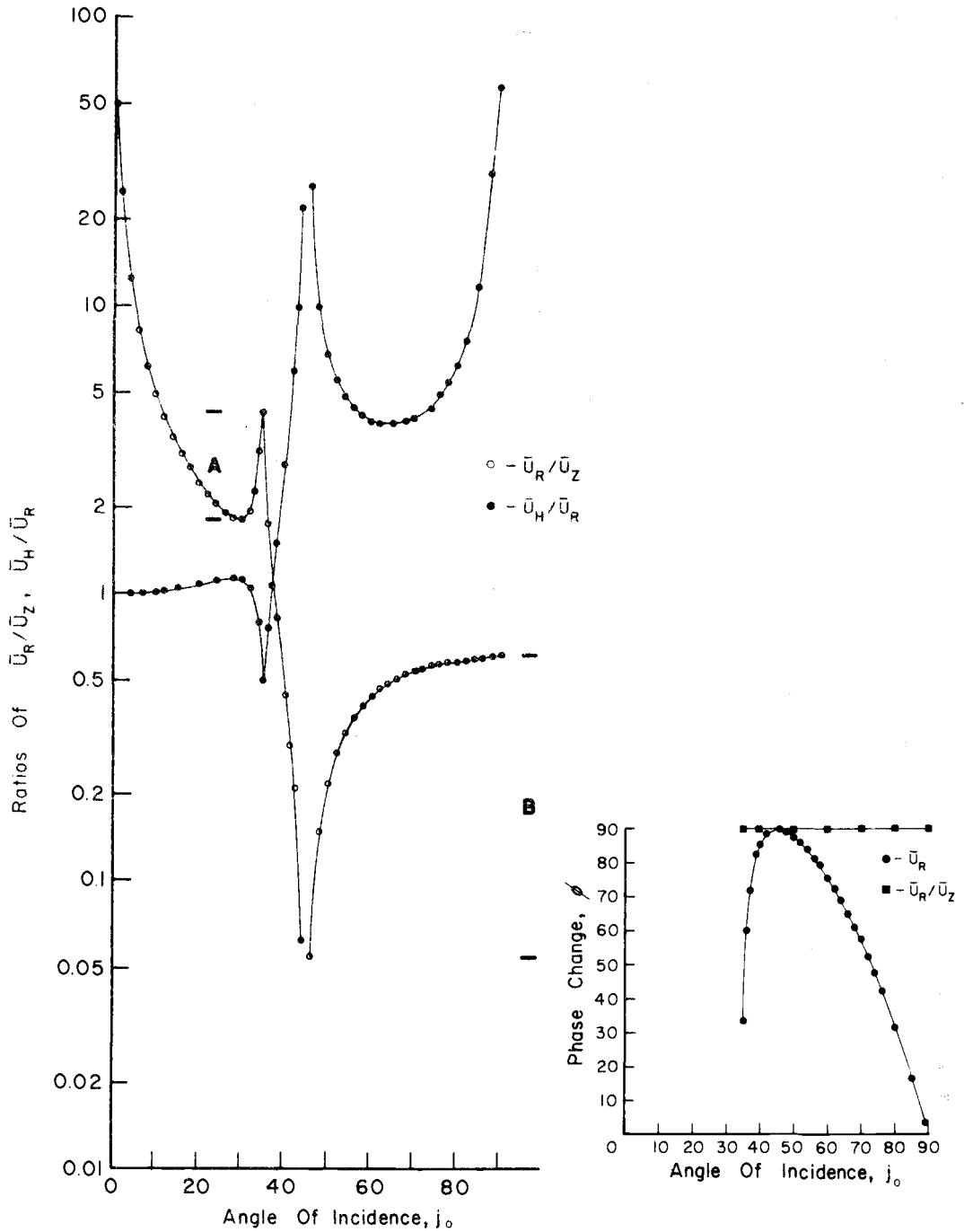


Figure 5. Ratios of the transverse, radial and vertical displacements of the S wave at the surface of the earth. Inset shows phase relationship between vertical and radial components (determined from Nuttli equations, 1961).

Amplitude Conversion Factors for the Effect of
the Crust and Upper Mantle

Conversion factors for removing the effects of geometrical spreading, partitioning of energy and wave attenuation may be made to the incident amplitude, provided ray paths and properties of traversed materials are known. All conversion factors calculated in the present study were made on the basis of a perfectly elastic medium. The amplitude conversion factors multiplied by the incident amplitude at the station give the earthquake source amplitude.

For the Pn wave, the amplitude conversion factors for the crust and mantle are incorporated (except for the effect of attenuation) in a mathematical derivation obtained by Heelan (1953).

Heelan (1953) derived particle displacement equations for Pn waves for a point type source in a two-layer medium by applying boundary conditions to the wave equation. A variation of wave types, including P and S head waves, was found. Heelan solved the integral equations of the particle displacement for the Pn wave using the method of steepest descents.

Brekhovskikh (1960) has described the general mathematical methods used to derive Heelan's (1953) integral equations. He derived Heelan's equations for the Pn wave with a slightly different mathematical procedure. Recently, Berry and West (1966) have generalized the methods to make them applicable to a multilayered

medium. The Heelan method was applied to incident P, SV and SH waves while the Berry-West (1966) method is applicable only to P and SV waves.

In the present study, it was necessary to ascertain the effects of a multilayered medium on the P and S waves for a point source. The equations for the P, SV and SH components of head waves were derived using the integral equations of Heelan and the methods described by Brekhovskikh (1960) and by Berry and West (see Appendix I).

The vertical and radial components of the P and SV waves incident at the surface of the earth (Appendix I) are:

$$U_{1,4} = \frac{A_{p,s} Q_{1P,1SV}}{r^{1/2} L^{3/2}} \quad (6a, b)$$

$$W_{1,4} = \frac{A_{p,s} Q_{2P,2SV}}{r^{1/2} L^{3/2}} \quad (7a, b)$$

and the horizontal component of the SH waves:

$$V_1 = \frac{A_{SH} Q_{SH}}{r^{1/2} L^{3/2}} \quad (8)$$

Where: $Q_{1,2P}$, $Q_{1,2SV}$, Q_{SH} include the head wave coefficients as described by Brekhovskikh (1960) and Berry and West (1966).

r is the radial distance on the surface of the earth traveled by a wave from the epicenter to the seismic station.

L is the distance the head wave is propagated just beneath the Moho.

A_p , A_s , A_{SH} , are the amplitudes of the P, SV and SH waves at the source.

The amplitudes of incident P and S waves can be corrected using these head wave equations, provided the focal depth and crustal structure are known.

Figure 2 illustrates earthquake sources at arbitrary depths above and beneath the Moho. It also shows ray paths of the p and P waves for crustal shocks and the ray paths of the P wave for sub-crustal shocks. The source amplitudes of these waves can be determined by a mathematical equation developed by DeBremaecker (1955) to convert incident wave amplitudes at stations to source amplitudes. The DeBremaecker method determines the effect of geometrical spreading and partitioning of energy at significant earth boundaries on the source wave amplitudes. The angle of incidence i_h of a ray leaving the source and the epicentral distance of the ray must be used in the equation.

In the present study a program (spherical model) was developed for a CDC 3300 computer, assuming a spherically layered earth, straight ray paths in the crust, and either curved or straight

ray paths in the mantle. By specifying a focal depth and velocity structure, the program determines the angle of incidence at each interface, the travel time and the epicentral distance for each ray leaving the source. The program also designates reflected and critically refracted ray paths for a focus in the crust (See Appendix III).

A modification of the DeBremaecker method was used in this investigation. Figure 6 shows the geometrical spreading as a spherical segment at the focus radiating into an expanded spherical segment at the surface of the earth. The areas of spherical segment at the focal sphere S_f and surface of the earth S_Δ can be defined as:

$$S_f = 2\pi r^2 (\cos i_2 - \cos i_1) \quad (9a)$$

$$S_\Delta = 2\pi r_e^2 (\cos \Delta_2 - \cos \Delta_1) \quad (9b)$$

Where:

- r is the radius of the focal sphere
- r_e is the radius of the earth
- i_2, i_1 are the angles of incidence i_h leaving the earthquake
- Δ_2, Δ_1 are the angular distances traveled by a seismic ray from source to station.

The flux of wave energy (total energy per unit area per unit time) leaving the earthquake source was equated with the energy flux at the surface of the earth. Terms that were equal in the equation

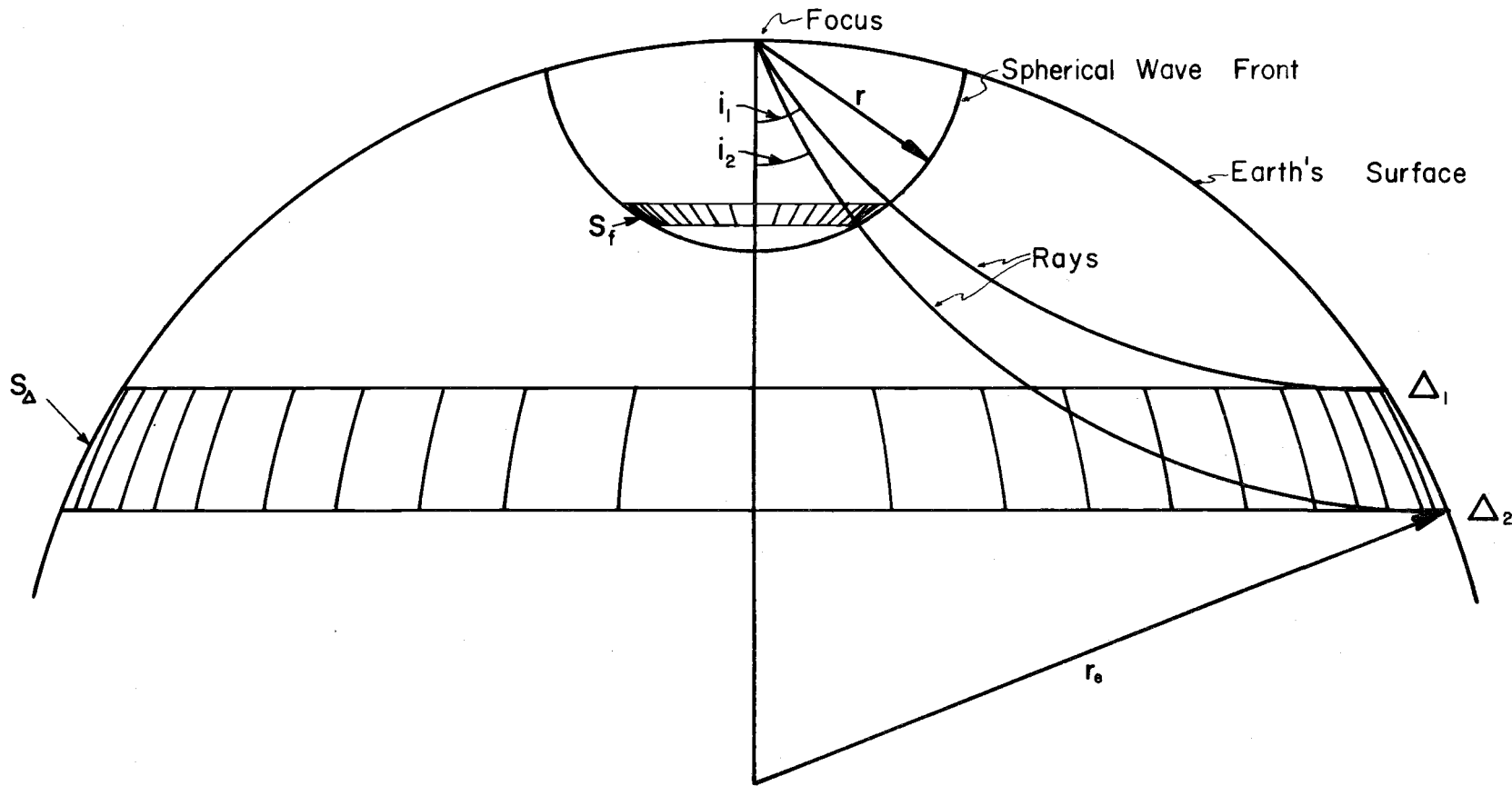


Figure 6. Geometrical spreading of the wave from focus to surface of the earth (after DeBremaecker, 1955).

were cancelled and the remaining terms were combined to give the ratio of source amplitude to the incident amplitude for a seismic station. The modified DeBremaecker (1955) equation, becomes:

$$\frac{A_f}{A_s} = \frac{r_e}{r} \cdot \left[\frac{(\cos \Delta_2 - \cos \Delta_1)}{(\cos i_2 - \cos i_1)} \right]^{1/2} \cdot \left\{ \frac{\rho_s V_s}{\rho_f V_f} \right\}^{1/2} \cdot \frac{1}{f_1 \cdot f_2} \cdot \frac{T_s}{T_f} \quad (10)$$

where: A_f is the amplitude of the wave leaving the source
 A_s is the incident amplitude of the wave at the station
 $\rho_f V_f$ is the acoustic impedance of the focal medium
 $\rho_s V_s$ is the acoustic impedance of the material at the station
 T_f, T_s are the periods of the wave at the focus and at the station, respectively
 f_1, f_2 are the partitioning energy ratios for a wave incident from above and beneath the Moho (for a sub-crustal shock $f_1 = 1.0$)

The amplitude ratio (equation 10) was converted into the ratio of spherical wave displacements at the source to the incident amplitude at the station (equation 14). These spherical displacements of P, SV or SH waves for an isotropic medium are as follows (Brekhovskikh, 1960):

For P wave, the vertical and horizontal displacements are:

$$U_p = \frac{F_1(\theta_o)}{R\alpha} \cdot w \cdot p(t - R/\alpha) \sin \theta_o \quad (11a)$$

$$W_p = \frac{-F_1(\theta_o)}{R\alpha} \cdot w \cdot p(t - R/\alpha) \cos \theta_o \quad (11b)$$

For SV wave, the vertical and horizontal displacements are:

$$U_{SV} = \frac{F_2(\theta_o)}{R\beta} \cdot w \cdot p(t - R/\beta) \cos \theta_o \quad (12a)$$

$$W_{SV} = \frac{F_2(\theta_o)}{R\beta} \cdot w \cdot p(t - R/\beta) \sin \theta_o \quad (12b)$$

and for SH, the horizontal component is

$$V_{SH} = \frac{K(\theta_o)}{R\beta} \cdot w \cdot S(t - R/\beta) \quad (13)$$

where: $F_1(\theta_o)$, $F_2(\theta_o)$, $K(\theta_o)$ are functions of the source.

R is the distance the wave has traveled from the source.

α is the velocity of the P wave and β is the velocity of the S wave.

θ_o is the angle of incidence at which the ray leaves the source.

$p(t - R/\alpha, \beta)$, $s(t - R/\beta)$ are the source functions.

Combining the derived spherical displacements with equation (10) gives, for $r = R$:

$$\frac{F_{1,2}(\theta_o) p(t - r/a, \beta), K(\theta_o) s(t - r/\beta)}{A_s} =$$

$$\frac{r_e}{2\pi} \cdot \frac{T_s}{T_f^2} \cdot \left[\frac{(\cos \Delta_2 - \cos \Delta_1)}{(\cos i_2 - \cos i_1)} \right]^{1/2} \cdot \left\{ \frac{V_s V_f \rho_s}{\rho_f} \right\}^{1/2} \frac{1}{f_1 f_2} \quad (14)$$

Equation (14) applies to both p and P waves from foci above the Moho and to P waves from foci beneath the Moho. It was used to determine the wave displacements at the earthquake source, corrected for the effects of geometrical spreading and partitioning of energy in the crust and upper mantle.

Correcting for Effects of Wave Attenuation

Attenuation of seismic waves in the present study will be restricted to absorption. Absorption can be removed by employing the equation of Asada and Takano (1963) and Gutenberg (1959) for a compressional wave.

$$\frac{A}{A_o} = \exp \left[\frac{-\pi f r}{Qv} \right] \quad (15)$$

where: A_o , A are the amplitudes at the source and seismic station

f is the frequency

$1/Q$ is the composite absorption factor for the wave path

r is the distance traveled by the ray

v is the composite velocity of propagation of the wave
through the earth

The equation can be rewritten with $t = r/v$ where t is the travel time from the source to receiver.

Method for Determining Fault-Plane Solutions

Wave displacements at the source can be used to determine fault-plane solutions by various methods. Most methods that have been used are based on first motions and/or amplitudes of incident P, SV and/or SH waves. The method used in this analysis is based only on the first motion and amplitude of the incident P wave.

Honda (1957) derived equations for particle displacements of Type I and Type II mechanisms (Figure 1) in an infinite elastic medium. The displacements at the earthquake source were expressed:

for Type I:

$$\begin{aligned}
 U_{pr} &= \frac{R_P}{T} \cdot (1/2) \sin 2\theta \cos \phi \\
 U_{s\theta} &= \frac{R_s}{T} \cdot \cos^2 \theta \cos \phi \\
 U_{s\phi} &= \frac{-R_s}{T} \cdot \cos \theta \sin \phi
 \end{aligned}
 \tag{16a, b, c}$$

and for Type II:

$$\begin{aligned}
 U_{pr} &= \frac{R'_p}{T} \sin 2\theta \cos \phi \\
 U_{s\theta} &= \frac{R'_s}{T} \cos 2\theta \cos \phi \\
 U_{s\phi} &= -\frac{R'_s}{T} \cos \theta \sin \phi
 \end{aligned}
 \tag{17a, b, c}$$

where: T is the period of the wave

R'_p , R'_s and R'_p , R'_s are expressions of the source functions in terms of λ , μ , α , β , w , R and wave amplitudes.

ϕ is the azimuth angle and θ is the polar angle as illustrated in Figure 7d.

Figure 7d depicts the y' axis as the polar axis, the angle ϕ measured in the z' , x' plane from the x' axis, and fault planes A and B in radiation of the P wave. A and B in Figure 7d represent an orientation as it is used in this study. Equations (16a) and (17a) indicate that the P amplitude patterns are identical for Type I and II sources.

As shown in Figure 7d, the radiation pattern for the P wave is fixed in the primed coordinate system, x' , y' , z' . Assuming a unit sphere at the origin of the primed system, the equations between the angles ϕ , θ and the primed system are

$$x' = \sin \theta \sin \phi$$

$$y' = \cos \theta$$

$$z' = \sin \theta \cos \phi$$

The origin of the unprimed coordinate system is fixed at the earthquake focus, such that x is to the north, y to the west and z up. The values x , y , and z are calculated from the azimuth and angle of incidence i_h . These values were used to calculate the P-wave radiation for any ray by rotating the primed system in relation to the unprimed system.

This rotation is accomplished by use of Euler Angles a, b, c (Goldstein, 1959) as defined and illustrated in Figure 7a, b, c. The three rotations about the $z, x',$ and z' axes can be represented by three matrices whose product is the matrix B :

$$\left[\begin{array}{ccc} \cos(c) \cdot \cos(a) - \cos(b) \cdot \sin(a) \cdot \sin(c), & \cos(c) \cdot \sin(a) + \cos(b) \cdot \cos(a) \cdot \sin(c), & \sin(c) \cdot \sin(b) \\ -\sin(c) \cdot \cos(a) - \cos(b) \cdot \sin(a) \cdot \cos(c), & -\sin(c) \cdot \sin(a) + \cos(b) \cdot \cos(a) \cdot \cos(c), & \cos(c) \cdot \sin(b) \\ \sin(b) \cdot \sin(a) & , & -\sin(b) \cos(a) & , & \cos(b) \end{array} \right]$$

The transformation from the unprimed system into the primed system is obtained from

$$X' = BX$$

where X' and X are the column matrices representing the two coordinate systems.

The computer program in Appendix III describes the rotation of Euler Angles a , b , and c in a progression of increments. An orientation is defined by these angular increments in the program. Each set of angles a , b , c , the angle i_h and the azimuth at a station give the angles ϕ , θ , for that station. The angles ϕ , θ were used to determine the source amplitudes at three seismic stations. These computer calculated amplitudes are placed in three sets of ratios and compared to three sets of observed ratios for each earthquake. The size of the angular increments determined the number of orientations required. All possible orientations of the P radiation pattern are obtained when the angles a , b , c are rotated through 180° .

The calculated amplitude ratios and direction of initial motion for each of the three stations were compared to the observed amplitude ratios and direction of initial motion for each station. The difference between the calculated and observed amplitude ratio, divided by the observed amplitude ratio, is the fractional deviation. The deviations, based on the three experimental amplitude ratios, are plotted for each orientation of the P-wave radiation. When each deviation is a minimum for an orientation and the total of minimum deviations is a minimum for all possible orientations, the fault-plane solution is assumed to be determined.

MATERIALS USED

Earthquakes and Stations

Thirty-three earthquakes located in the northwestern United States and adjacent areas were used in this study. Eight of these, located off British Columbia, had not been investigated previously. They were used to determine travel times, as shown in Appendix IV. The geographical locations of the thirty-three earthquakes are presented in Figure 8.

The location (latitude and longitude), origin time, magnitude, calculated focal depth and depth assumed are given in Table I for each of the earthquakes. Focal depths are denoted by symbols: gh, the focal depth determined by the Gutenberg-Hodgson technique; cg, focal depth determined by the U. S. Coast and Geodetic Survey; st, focal depth determined statistically. Most of the earthquakes analyzed in this study occurred at depths of less than 100 km.

Accurate determination of the focal depth is dependent upon several factors: wave arrivals observed, seismic stations available, and knowledge of earth structure in the vicinity of the focus and seismic station. The Gutenberg-Hodgson method may be used to determine foci, provided the Pn and p travel times and velocity structure are known. When numerous travel times are available, the uncertainty of focal depths for shallow earthquakes can be as low

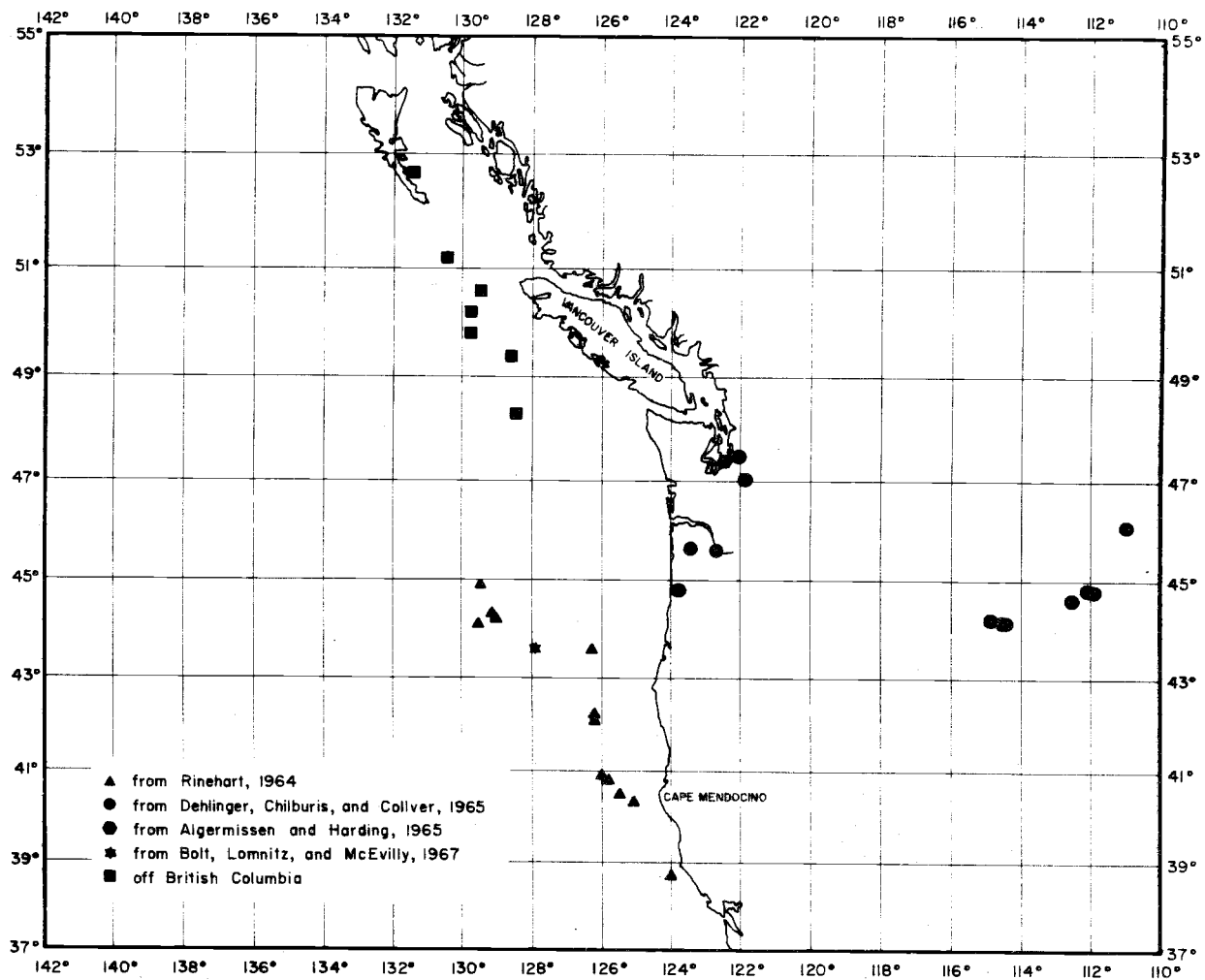


Figure 8. Locations of thirty-three earthquakes in the Pacific Northwest used in this investigation.

Table I. Data for Thirty-Three Earthquakes in the Pacific Northwest.

No.	Date	Origin Time	Lat. N.	Long. W.	Focal Depth (km)	Assumed Depth (km)	Mag. (C&G. S.)
1	April 29, 1965	15:28:43.6	47.3	122.2	59.0 cg	60.0	6.5
2	May 8, 1968	12:17:13.4	43.6	127.9	-- st	30.0	6.1
3	Aug. 22, 1963	09:27:07.3	42.1	126.2	-- st	30.0	5.6
4	Oct. 14, 1962	10:14:27.7	38.7	124.0	-- st	30.0	4.7*
5	Mar. 7, 1963	23:53:22.3	44.8	123.8	50.0 cg	44.0	4.6
6	April 19, 1967	18:12:24.6	52.7	131.4	-- st	60.0	4.6
7	April 29, 1967	00:04:41.8	51.2	130.4	6.0 cg	10.0	5.1
8	Mar. 30, 1966	12:40:01.0	49.8	129.7	-- st	30.0	5.3
9	May 20, 1966	23:58:51.7	50.2	129.7	37.0 cg	30.0	5.0
10	Nov. 4, 1966	20:30:13.3	49.4	128.6	-- st	30.0	4.2
11	June 25, 1963	08:26:21.7	44.2	129.0	31.0 cg	30.0	4.5
12	July 4, 1963	05:50:47.5	43.6	126.3	-- st	30.0	4.4
13	June 25, 1963	09:39:28.4	44.3	129.1	32.0 cg	30.0	4.5
14	Feb. 21, 1963	12:01:16.4	40.4	125.1	100.0*gh	60.0	3.7*
15	Nov. 6, 1962	03:36:43.0	45.6	122.7	44.0 cg	44.0	4.8*
16	Jan. 24, 1963	21:43:11.8	47.5	122.0	0.0*gh	10.0	N.
17	Sept. 26, 1962	05:07:11.2	44.6	112.5	-- st	40.0	N.
18	Feb. 16, 1963	03:01:37.8	46.1	110.9	-- st	40.0	N.
19	Oct. 18, 1962	18:03:14.0	44.2	114.9	40.0*gh	40.0	N.
20	Oct. 18, 1962	20:31:02.6	44.2	114.9	38.0*gh	40.0	N.
21	Jan. 6, 1963	18:07:42.9	44.9	112.1	-- st	40.0	N.
22	Feb. 24, 1963	15:24:51.8	44.8	111.9	-- st	40.0	N.
23	Sept. 2, 1965	18:01:19.4	48.3	128.4	-- st	Normal	4.9
24	Sept. 2, 1965	19:41:25.2	48.3	128.4	-- st	Normal	4.9
25	Oct. 11, 1965	15:47:55.4	50.6	129.4	-- st	Normal	4.8
26	July 8, 1963	04:19:08.4	40.8	125.8	-- st	30.0	4.7
27	Aug. 19, 1963	09:38:56.2	40.9	126.0	-- st	30.0	4.1
28	Feb. 1, 1963	16:38:55.8	44.2	114.5	30.0*gh	40.0	N.
29	Jan. 27, 1963	15:24:41.9	44.2	114.4	31.0 cg	40.0	N.

Continued on next page

Table I. Continued.

No.	Date	Origin Time	Lat. N.	Long. W.	Focal Depth (km)	Assumed Depth (km)	Mag. (C&G.S.)
30	Dec. 27, 1963	02:36:18.5	45.6	123.4	37.0 cg	44.0	N.
31	Dec. 31, 1962	20:49:34.4	47.0	121.9	20.0*gh	20.0	N.
32	Aug. 2, 1963	22:17:18.2	40.5	125.4	-- st	30.0	5.1
33	Aug. 27, 1963	05:51:34.1	44.1	129.5	-- st	30.0	4.2

*(In Magnitude) determined by University of California, Berkeley.

*(In Focal Depth) Depth calculated.

N (in Magnitude column) means no data available.

as five percent. However, errors in focal depth under generally favorable conditions can be large if the travel times are limited.

As the required data are insufficient for many earthquakes, statistical procedures can be effective in estimating focal depths. The statistical method used in this paper and in the Gutenberg-Hodgson method are discussed in Appendix II.

Seismic stations employed in the study, station abbreviations and locations are listed in Table II.

The seismograms used were available on film and on paper. Known magnification and response curves of both short-period and long-period instruments at each seismic station were used to determine ground amplitudes from measured seismogram amplitudes.

Assumed Crustal Sections

The crust is defined in the present paper as all material above the layer of the earth which has a seismic velocity greater than a 7.6 but less than 8.4 km/sec. Velocity structures of the crust and upper mantle of the earth were determined from gravity, seismic reflection and refraction, and travel-time data. Gravity surveys in conjunction with seismic refraction work were used to construct crustal sections (Dehlinger, Couch and Gemperle, 1968). The densities used in these sections were converted to P-wave velocities by applying the empirical curves of Nafe and Drake (1961).

Table II. Seismic Stations Used in Present Study.

Location	Type	Abbreviation	Lat. N.	Long. E.
Arcata, California		ARC	40.88	235.93
Big Bear, California		BBC	34.24	243.76
Boulder City, Nevada		BCN	35.97	245.16
Bellingham, Washington		BEL	48.74	237.52
Big Mountain, Alaska		BIG	59.39	204.78
Byerly, California		BKS	37.88	237.77
Bozeman, Montana	WWSSS	BOZ	45.60	248.37
Berkeley, California		BRK	37.87	237.74
Butte, Montana		BUT	46.01	247.44
Blue Mountain Obs., Oregon	Geneva	BMO	44.85	242.70
Cedar Spring, California		CED	34.28	242.67
Calistoga, California		CLS	38.64	237.42
Coppermine, Canada	WWSSS	CMC	67.83	244.92
Concord, California		CNC	37.97	237.93
College Outpost, Alaska	WWSSS	COL	64.90	212.21
Corvallis, Oregon	WWSSS	COR	44.59	236.70
Dugway, Utah	WWSSS	DUG	40.20	247.19
Edmonton, Canada		EDM	53.22	246.65
Eureka, California		EUR	39.48	244.03
Fallon, Nevada	LRSM	FAL	39.20	241.62
Frobisher Bay, Canada		FBC	63.73	191.53
Fresno, California		FRE	36.77	240.20
Fort St. James, Canada		FSJ	54.43	235.75
Golden, Colorado	WWSSS	GOL	39.70	254.63
Goldfield, Nevada	LRSM	GFD	37.92	242.80
Goldstone, California	WWSSS	GSC	35.30	243.19
Haiwee, California		HAI	36.14	242.05
Hailey, Idaho	LRSM	HLID	43.65	245.75
Hailey, Idaho	LRSM	HL2ID	43.56	245.58
Hungry Horse, Montana		HHM	48.35	245.97
Jameston, California		JAS	37.95	239.56
Klamath Falls, Oregon		KFO	42.27	238.25
LASA Center, Montana		LAO	46.69	253.78
Llanada, California		LLA	36.62	239.06
Longmire, Washington	WWSSS	LON	46.75	238.19
Lovelock, Nevada	LRSM	LOV	39.94	241.16
Mt. Hamilton, California		MHC	37.34	238.36
Mina, Nevada	LRSM	MNA	38.44	241.85
Mineral, California		MIN	40.54	238.40
Marysville, California	LRSM	MVCL	39.21	238.71
Mould Bay, Canada		MBC	76.23	240.67
Newport, Washington		NEW	48.26	242.88
Portland, Oregon		OMSI	45.51	237.28
Oroville, California		ORV	39.56	238.50
Ottawa, Canada		OTT	45.39	284.28
Palisades, New York		PAL	41.01	286.09

Continued on next page

Table II Continued

Location	Type	Abbreviation	Lat. N.	Long. E.
Palo Alto, California		PAC	37.42	237.82
Pedro Dome, Alaska		PJD	65.04	212.49
Port Hardy, Canada		PHC	50.70	232.57
Penticton, Canada		PNT	49.32	240.38
Pt. Reyes, California		PRC	38.08	237.13
Priest, California		PRI	36.14	239.34
Paraiso, California		PRS	36.33	238.63
Pendleton, Oregon	LRSM	PTOR	45.61	241.12
Rapid City, South Dakota	WSSS	RCD	44.08	256.79
Reno, Nevada		REN	39.54	240.19
Resolute, Canada		RES	74.69	265.10
San Andreas Geo. Obs., California		SAO	36.77	238.56
Santa Cruz, California		SCC	37.01	238.00
Scarborough, Canada		SCB	43.72	280.77
Schefferville, Canada		SCH	54.82	293.22
Sheep Creek Mt., Alaska		SCM	61.83	212.67
Seattle, Washington		SEA	47.66	237.69
San Francisco, California		SFC	37.78	237.55
Seligman, Arizona	LRSM	SGAZ	35.64	246.74
Shasta, California		SHS	40.70	237.61
Sitka, Alaska		SIT	57.06	224.68
San Luis Dam, California		SLD	37.07	238.78
Sunflower, Arizona	LRSM	SNAZ	33.86	248.31
St. Johns, Canada		STJ	45.57	307.27
Spokane, Washington		SPO	47.73	242.66
Seattle, Washington (Marshall)		STT	47.42	237.69
Stillwater, Nevada	LRSM	STW	39.44	241.42
Tonto Forest, Arizona		TFO	34.29	248.73
Tonasket, Washington	LRSM	TKWA	48.79	240.41
Tanana, Alaska		TNN	65.26	208.09
Tumwater, Washington		TUM	47.02	237.09
Vineyard, California		VIN	36.75	238.62
Vineyard, California	(Telemeter)	VIT	36.75	238.61
Ukiah, California		UKI	39.14	236.79
Victoria, Canada		VIC	48.52	236.58
Winnemucca, Nevada	LRSM	WINV	41.35	242.54
Yakima, Washington	LRSM	YAWA	46.50	240.08
Yellowknife Array, Canada		YKA	62.49	245.39

Ten crustal sections located near the earthquakes were used in the present investigation. These sections are illustrated in Figure 9. Depths of the sections are indicated in km and P-wave velocities in km/sec. The following crustal sections, as based on geophysical surveys, were used.

Crustal Sections

Number

1. Oceanic (off Oregon). Based on refraction survey (Shor, et al., 1968).
2. Continental margins (off Oregon). Based on refraction survey (Shor, et al., 1968).
3. On continental shelf near coast of Alaska. Based on refraction survey (Shor, 1962).
4. On oceanic abyssal plain (west of Queen Charlotte Islands). Based on refraction survey (Shor, 1962).
5. South of Puget Sound. Based on gravity section (Dehlinger, Couch, and Gemperle, 1968).
6. Eastern Oregon and western Idaho. Based on gravity section (Dehlinger, Couch, and Gemperle, 1968).
7. Central Idaho and southwest Montana. Based on refraction survey, No. 921 (McConnell and McTaggart-Cowan, 1963).

CRUST AND SUBCRUSTAL CROSS SECTIONS

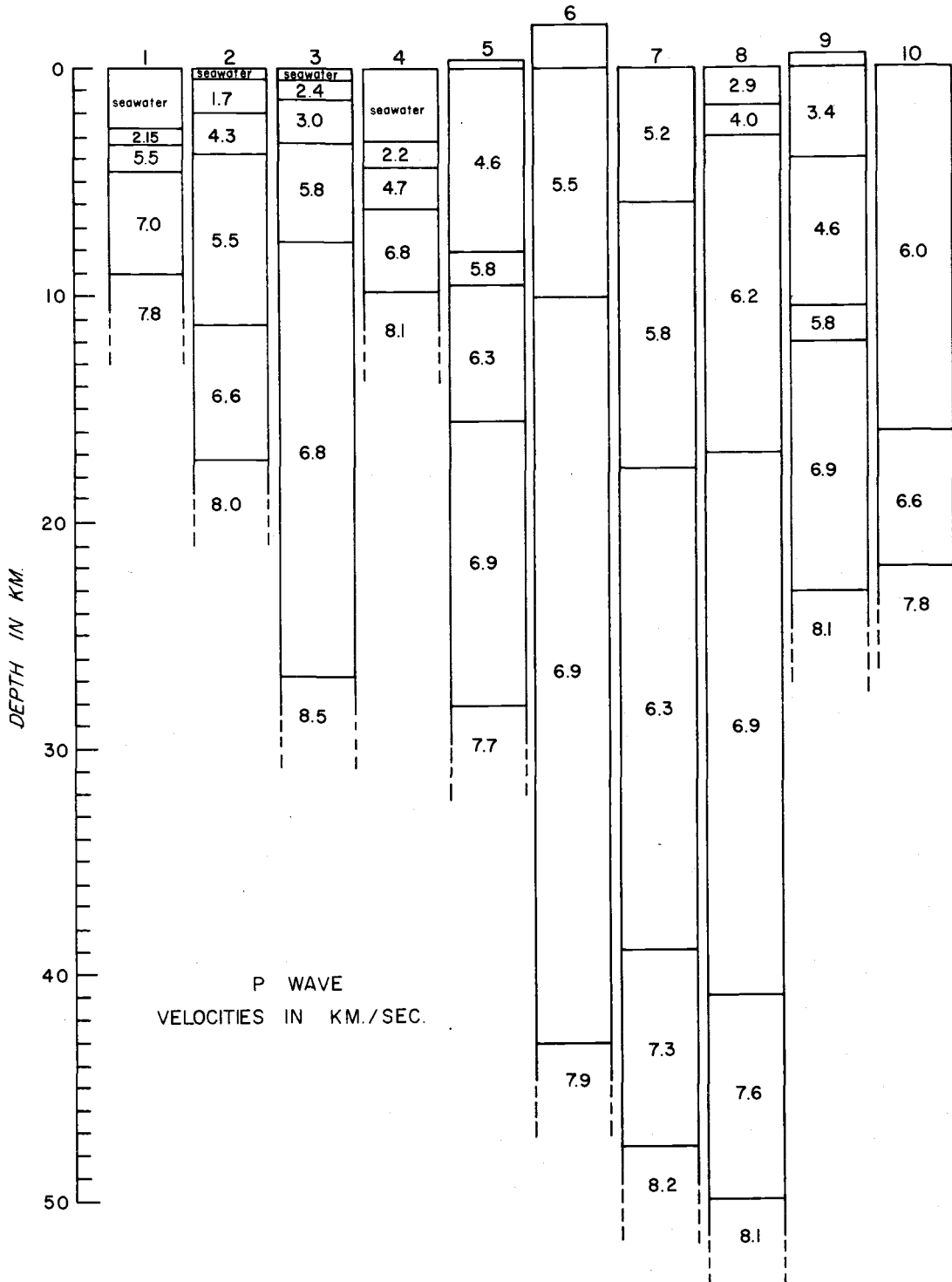


Figure 9. Ten crustal sections in the Pacific Northwest area based on analyses of gravity and seismic data.

Number

8. Southwest Montana. Based on refraction survey No. 909 (McConnell and McTaggart-Cowan, 1963).
9. Willamette Valley. Based on gravity section (Dehlinger, Couch, and Gemperle, 1968).
10. Central Nevada and California. Based on refraction survey (Eaton, 1963).

P velocities for all of these sections can be converted to S velocities using $\sigma = 1/4$.

Results of the Shor, et al. (1968) refraction survey off Oregon were used as a basis for crustal section No. 1. The velocities beneath the Moho varied from 7.3 km/sec to 8.4 km/sec. The low velocity of 7.3 km/sec was found below the Juan de Fuca Ridge. Rinehart (1964) found an 8.0 km/sec average velocity beneath the Moho for earthquakes off the coast of Oregon and northern California.

Crustal section No. 10 is based on a refraction line across California and Nevada as obtained by Eaton (1963). Eaton stated that the Moho deepens in Nevada from 22 to 32 km eastward from Carson-Sink. Pakiser (1963) also found that the Moho deepens from Nevada into western Idaho and stated that it may be related to an intermediate layer in the crust.

Crustal section Nos. 7 and 8 are based on refraction lines 921

and 909, respectively, from McConnell and McTaggart-Cowan (1963). Line 921 in northern Utah may not be representative of Central Idaho.

Calculation of Ground Velocities

The arrival times of first motions of P and S waves were compared to travel times developed by (1) Dehlinger, Chiburis, and Collver (1965) -

east of the Cascade Range:

$$\text{Pn: } (6.62 + \Delta/7.96) \pm 0.90$$

$$\text{Sn: } (10.87 + \Delta/4.46) \pm 2.38$$

and west of the Cascade Range:

$$\text{Pn: } (4.73 + \Delta/7.67) \pm 0.76$$

$$\text{Sn: } (8.17 + \Delta/4.37) \pm 2.62$$

and, (2) travel time curves developed in this study for earthquakes located off British Columbia for which curves previously had not been determined (see Appendix IV). All P and S-wave arrivals beyond an epicentral distance of 10^0 were compared to the Gutenberg-Richter travel-time curves. Directions of the first motions of the P arrivals, which were identified, were read from the short-period and long-period records.

Short-period P-wave amplitudes of first motions were measured for this study; long-period amplitudes were measured for

comparison. P-wave amplitudes on a seismogram were measured in millimeters from the peak to the line of rest in the first half-cycle. Gutenberg (1956) found that initial amplitudes are not substantially modified by ground effects at the station. Peak to peak amplitudes in the first cycle were also measured.

Wave periods were measured and used to determine the instrument response. When the wave period was difficult to read for a component, the average period of the other components was used.

The measured amplitudes were changed to ground velocities by dividing the amplitude by the wave period, instrument response, and instrument magnification.

The first motions of the S wave are extremely difficult to select at epicentral distances 5° to 12° due to possible lack of S energy, interference from other arriving waves, and the effects of resonance of alluvium beneath the seismic station.

Because of these difficulties, S waves were selected where:

- (1) the character of the waves changed frequency, and/or
- (2) the wave amplitudes increased.

The S wave was difficult to identify for foci above the Moho; it was more easily found for foci beneath the Moho.

The procedure for measuring P-wave amplitudes and determining the ground velocities was used for the S wave. However, the S-wave amplitudes for S polarization were selected at the

first motion when it was clear and impulsive; otherwise the amplitude of a wave closely following the first motion was selected.

PROCEDURE FOR DETERMINING FAULT-PLANE SOLUTIONS

Removing Surface Effects from Ground Motions

Three components of P wave motion--vertical, north-south and east-west--were used to determine ground motion particle velocities. The apparent angle of incidence \bar{i}_0 was obtained from these velocities. The square root of the sum of the squares of the horizontal velocities divided by the vertical velocity gave the tangent of the apparent angle. This method was applied to all seismic stations where all three P-wave components were available. The apparent angle of incidence of a P wave was converted to a true angle of incidence by using Figure 3.

The true angles of incidence for each seismic station were plotted relative to epicentral distances and periods. No relationships were found. Finally, the true angles of incidence for all earthquakes recorded at a seismic station from a given region were averaged. This average was used to determine the average deviation of the true angles of incidence for each station. Results of this analysis are shown in Figure 10.

The average value of the true angles of incidence for all earthquakes and seismic stations was 31.2° . The angles of incidence at western stations were generally smaller than at eastern stations.

The true angle of incidence i_0 must be known to determine the

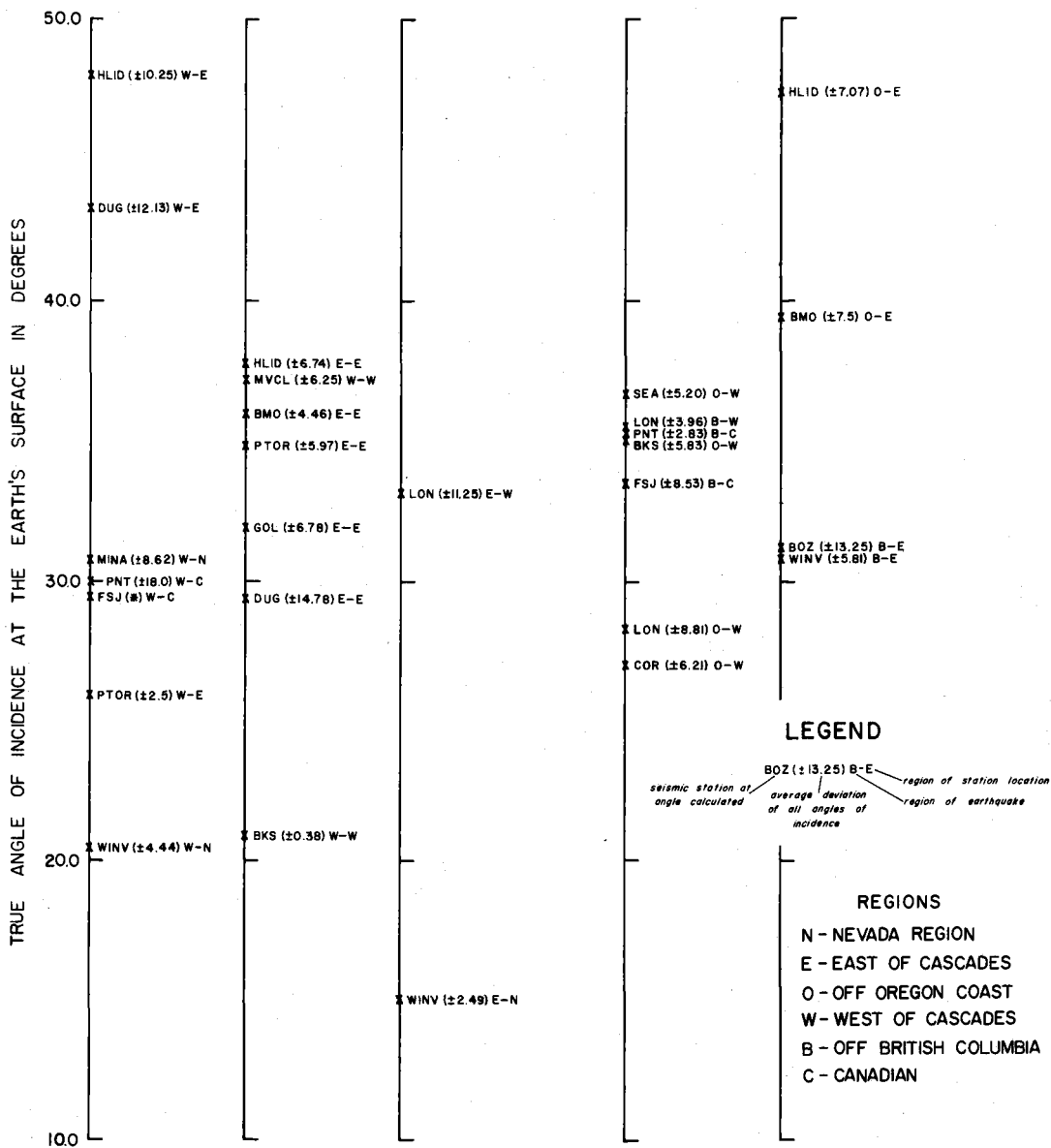


Figure 10. Calculated true angles of incidence at various seismic stations based on amplitudes of P waves.

incident amplitude at the surface of the earth from the recorded ground amplitude at a seismic station. It was possible to determine the angle at a station for an earthquake if the particle velocities were known; otherwise, the angle which was taken was the average at the station for all earthquakes in a region or the average for all of the earthquakes. In Figure 4, the relation between the angle of incidence i_0 and the ratio W/A (vertical component of ground amplitude divided by incident amplitude) is shown. Using this ratio, the incident amplitude of the P wave at the surface was determined.

The three components of S wave motion--vertical, north-south and east-west--were used to determine particle velocities. These particle velocities were converted to radial and transverse ground velocities, using the azimuth of the ray path at a station. Azimuths were calculated according to Bullen (1963). See Appendix III for a computer program of this calculation. The ratio of incident transverse velocities to radial ground velocities gives the polarization of the S wave. The incident polarization of the S wave can be determined from the recorded polarization when the angle of incidence j_0 at the surface of the earth is known. The angle of incidence can be determined using the ratio of the radial to vertical velocity components.

As shown in Figure 5, the ratio of vertical velocity to radial velocity has two regions in which multi-valued angles of incidence

are obtained. In region B, S-wave angles of incidence larger than P-wave angles of incidence should be questioned as both angles should be the same. Although the computed angles of incidence in region A are not constant, the polarization of the incident wave is nearly the same.

Removing Crust and Upper Mantle Effects

The effects of geometrical spreading and partitioning of energy in the crust and upper mantle can be determined when the ray path of the P wave and depth of focus have been established. An amplitude conversion factor (dimensionless factor) was determined from these effects, which was multiplied by the incident amplitude to obtain the source amplitude. For foci above the Moho, the amplitude conversion factor for the Pn wave was obtained by the theoretical equations originally derived by Heelan (1953), modified for purposes of the present study (Eq. 6a, b; 7a, b). The amplitude conversion factors for the p and P waves were determined by the DeBremaecker equation, which also was modified for this study (Eq. 14).

The amplitude conversion factors for the P and p waves were calculated in several steps. This required the determination of the angle of incidence i_h for the ray leaving the focus, the angle of incidence i_m for the ray incident at the Moho, and the epicentral distance the ray travels. The angle i_m incident from above and below

the Moho was used to determine the partitioning of energy (Gutenberg, 1944). Crustal sections assumed for the P and Pn wave calculations are numbered 5 and 7 in Figure 9.

Pn, SVn and SHn waves at focal depths of 10 km and 20 km in the Puget Sound region and depths of 15 and 40 km in Idaho were calculated with this procedure. The amplitude conversion curves are shown in Figures 11, 12 and 13.

The amplitude conversion factors for the p wave for foci above the Moho and for the P wave for foci beneath the Moho were computed. For each ray leaving the focus, the spherical model computer program calculated epicentral distance and the angle of incidence at each layer boundary. The program was applied to the crustal sections shown in Figure 9. Where the crustal section beneath the station was different from that near the focus, an average velocity beneath the Moho was calculated. The plots of i_h versus epicentral distances are shown in Figures 14 and 15. The angle of incidence at the Moho, i_m , was used to determine the partitioning of energy, using curves derived by Gutenberg (1944).

The angle of incidence i_h , partitioning of energy, and epicentral distance were used to determine amplitude conversion factors for the p and P waves (Eq. 14). Amplitude conversion factors are shown in Figures 16, 17 and 18.

Table III shows the crustal section and related variables used

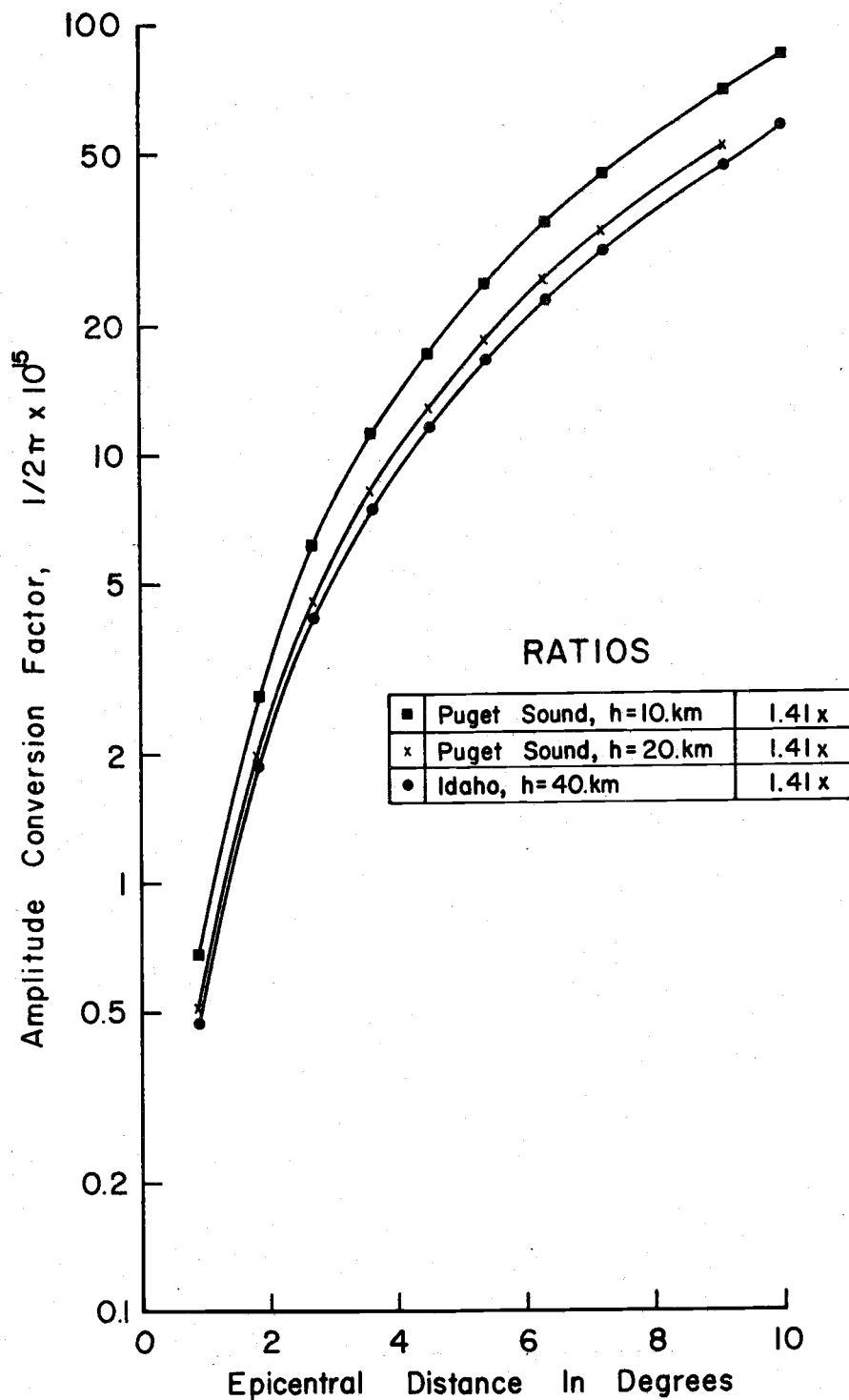


Figure 11. Amplitude conversion factor of the Pn wave as a function of epicentral distance for different crustal sections and focal depths (use of ratio gives resultant displacement).

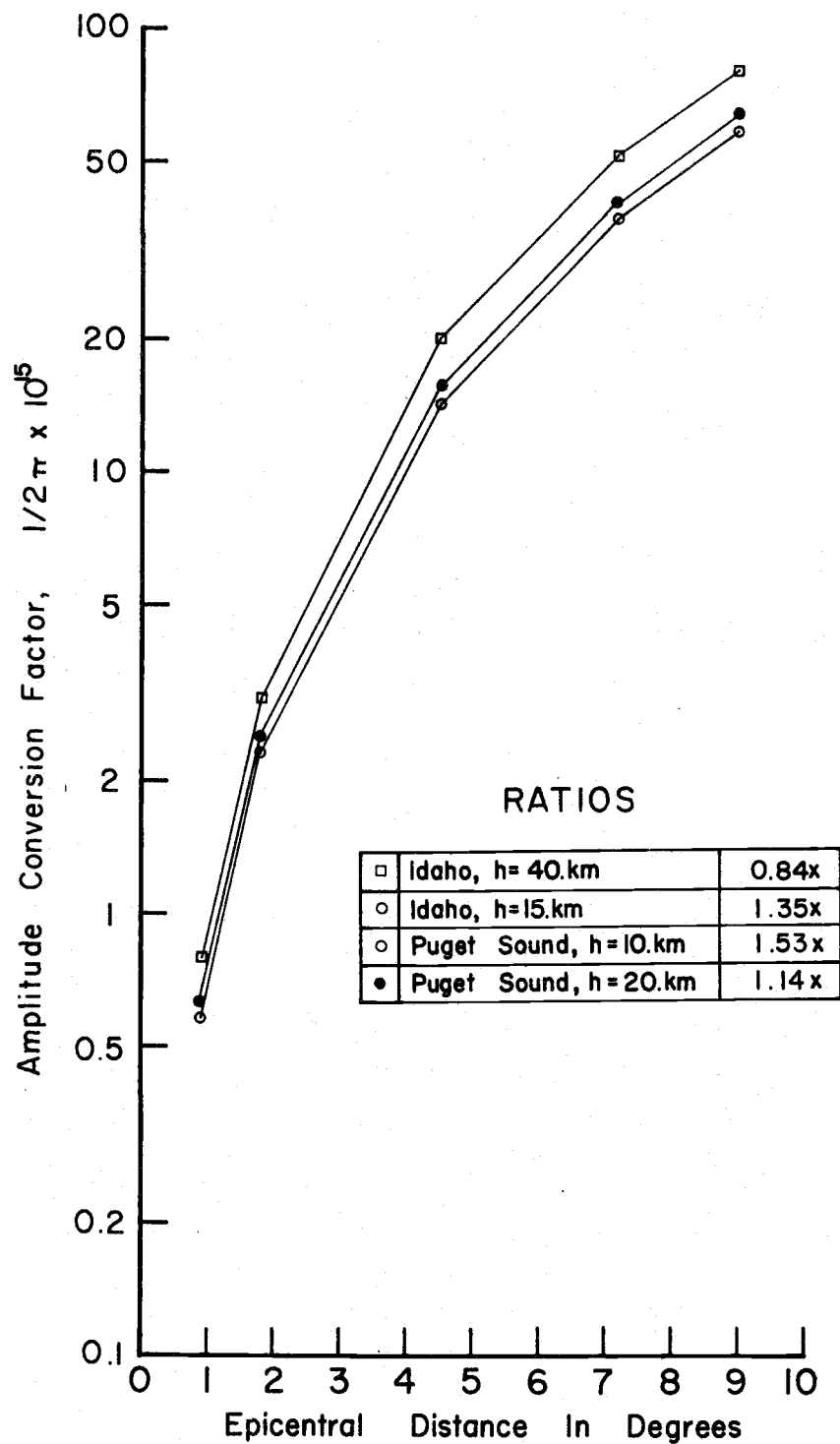


Figure 12. Amplitude conversion factor of the SV_n wave as a function of epicentral distance for different crustal sections and focal depths (use of ratio gives resultant displacement).

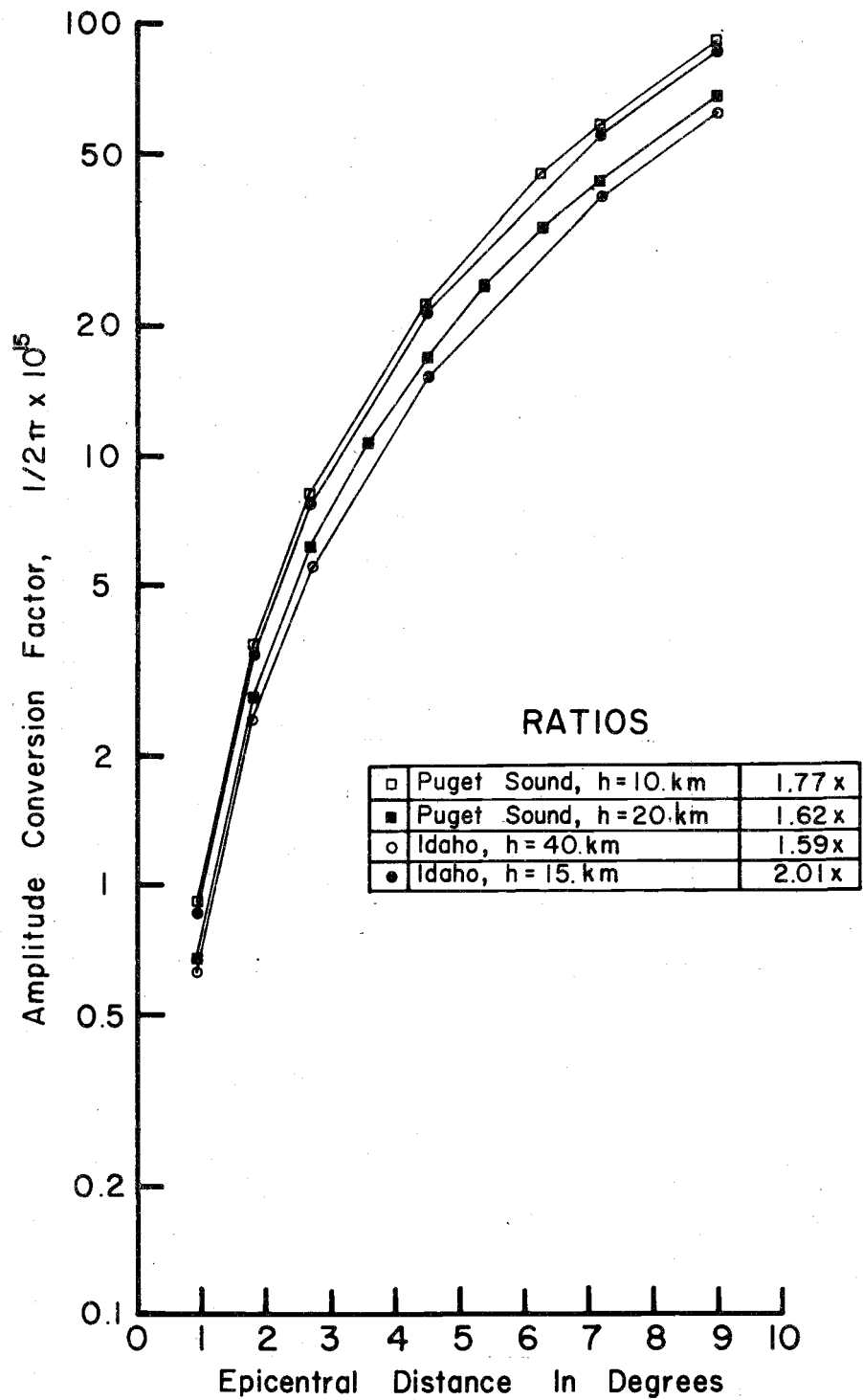


Figure 13. Amplitude conversion factor of the SH_n wave as a function of epicentral distance for different crustal sections and focal depths (use of ratio gives resultant displacement).

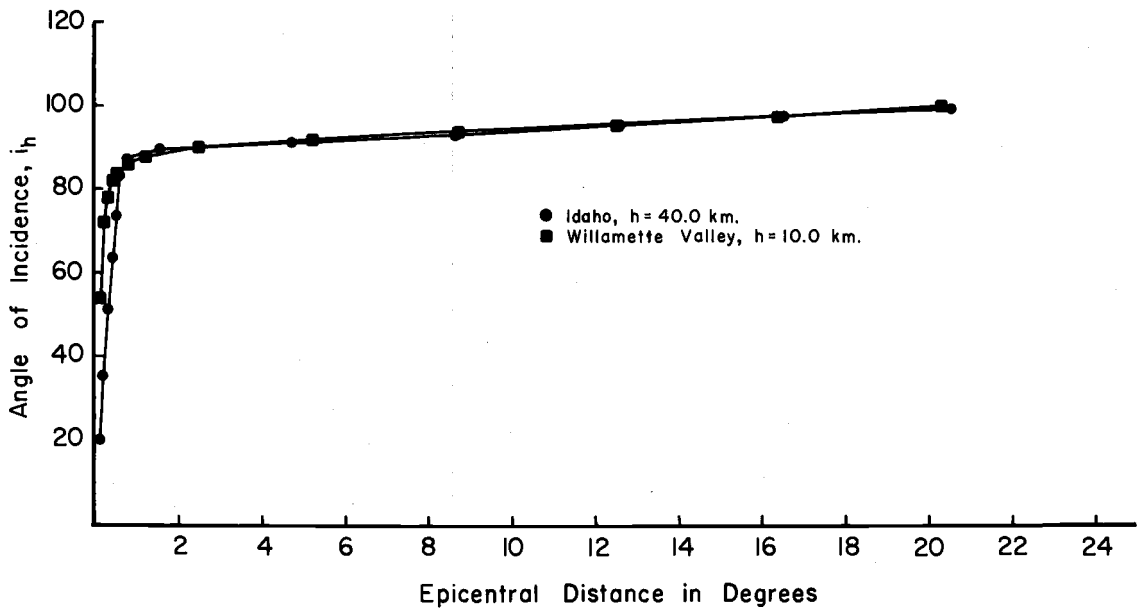
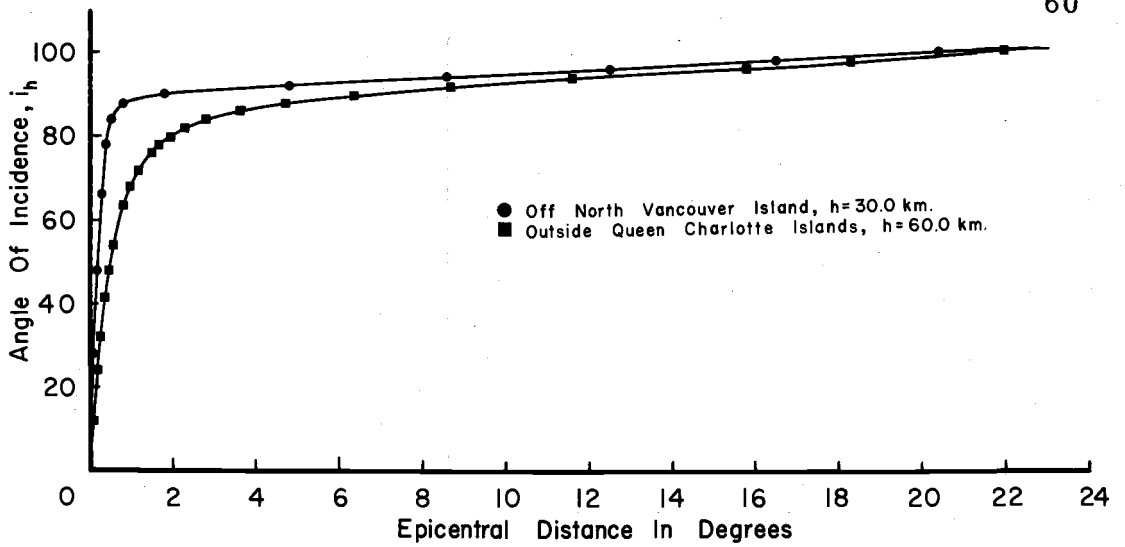


Figure 14. Variation of the angle of incidence i_h with epicentral distance for different focal depths and selected crustal sections.

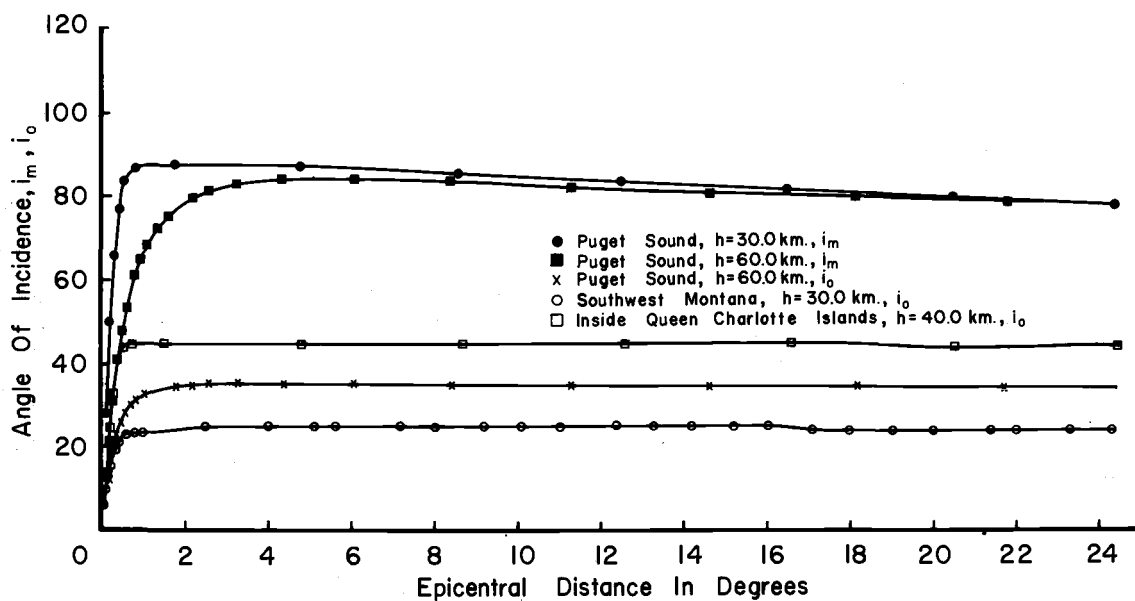
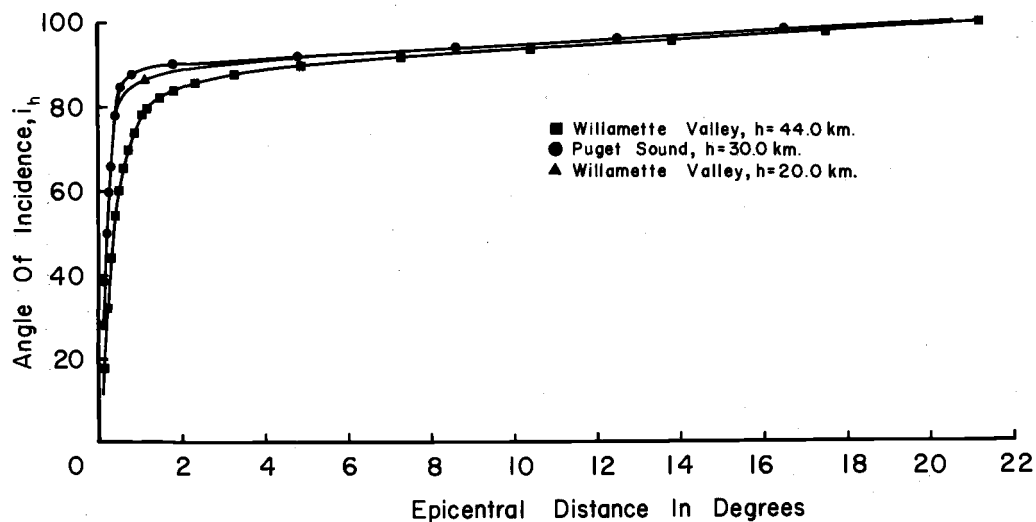


Figure 15. Variation of the incidence angle (a) beneath the Moho, i_m , at the surface of earth i_o and (b) at the source i_h with epicentral distance for different focal depths and selected crustal sections.

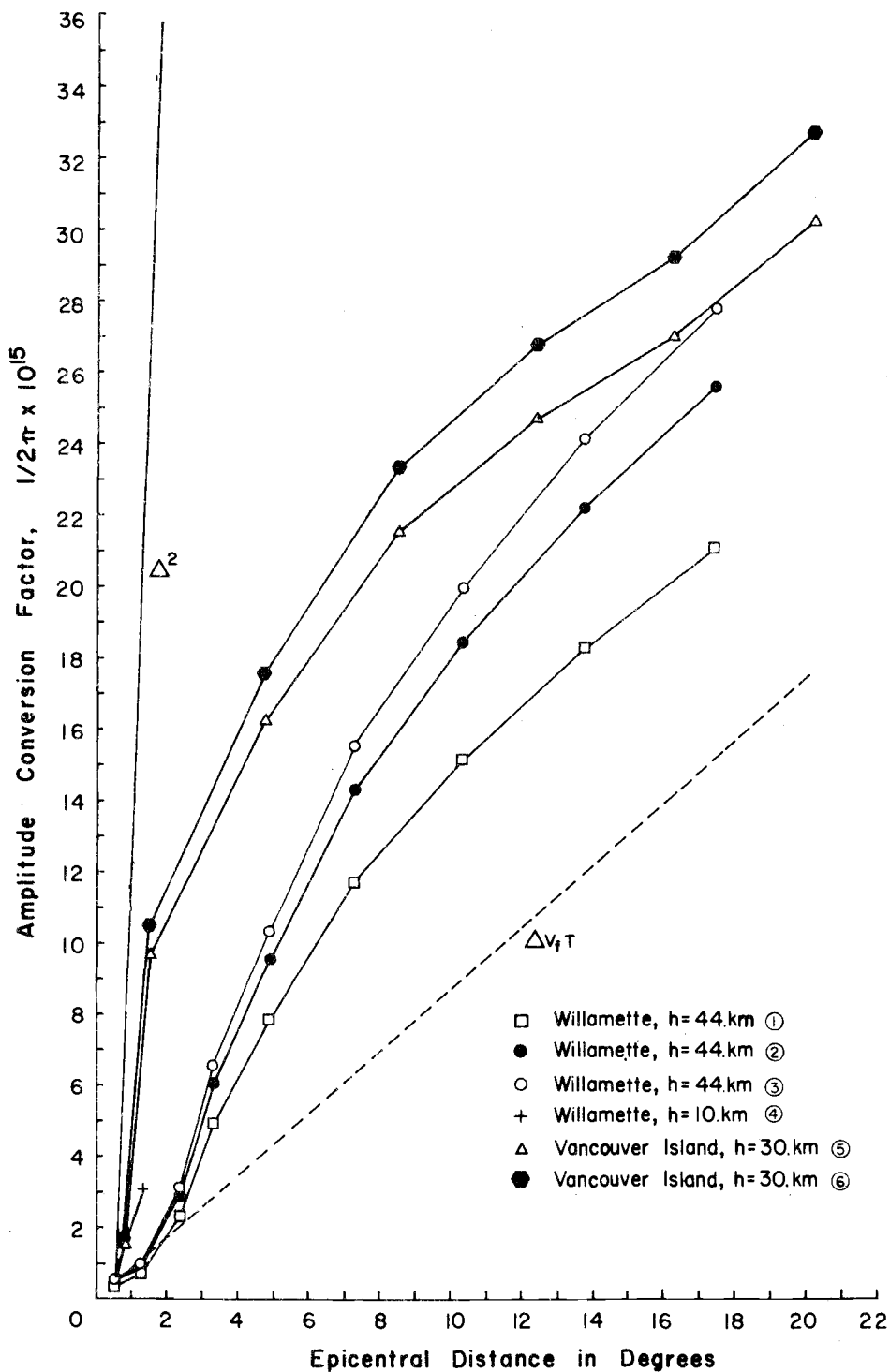


Figure 16. Amplitude conversion factors of P and p waves as a function of epicentral distance for different crustal sections and focal depths.

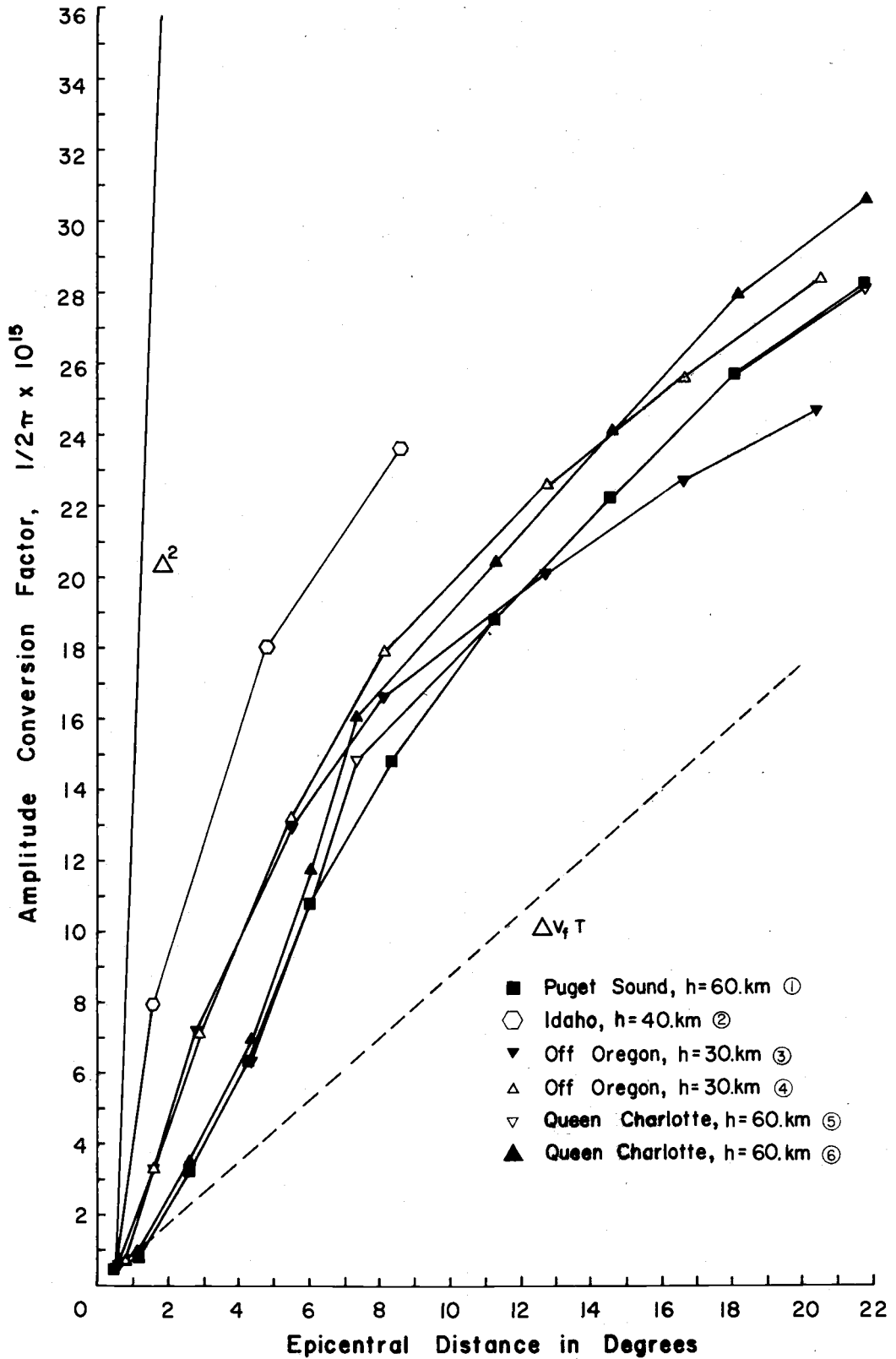


Figure 17. Amplitude conversion factors of P and p waves as a function of epicentral distance for different crustal sections and focal depths.

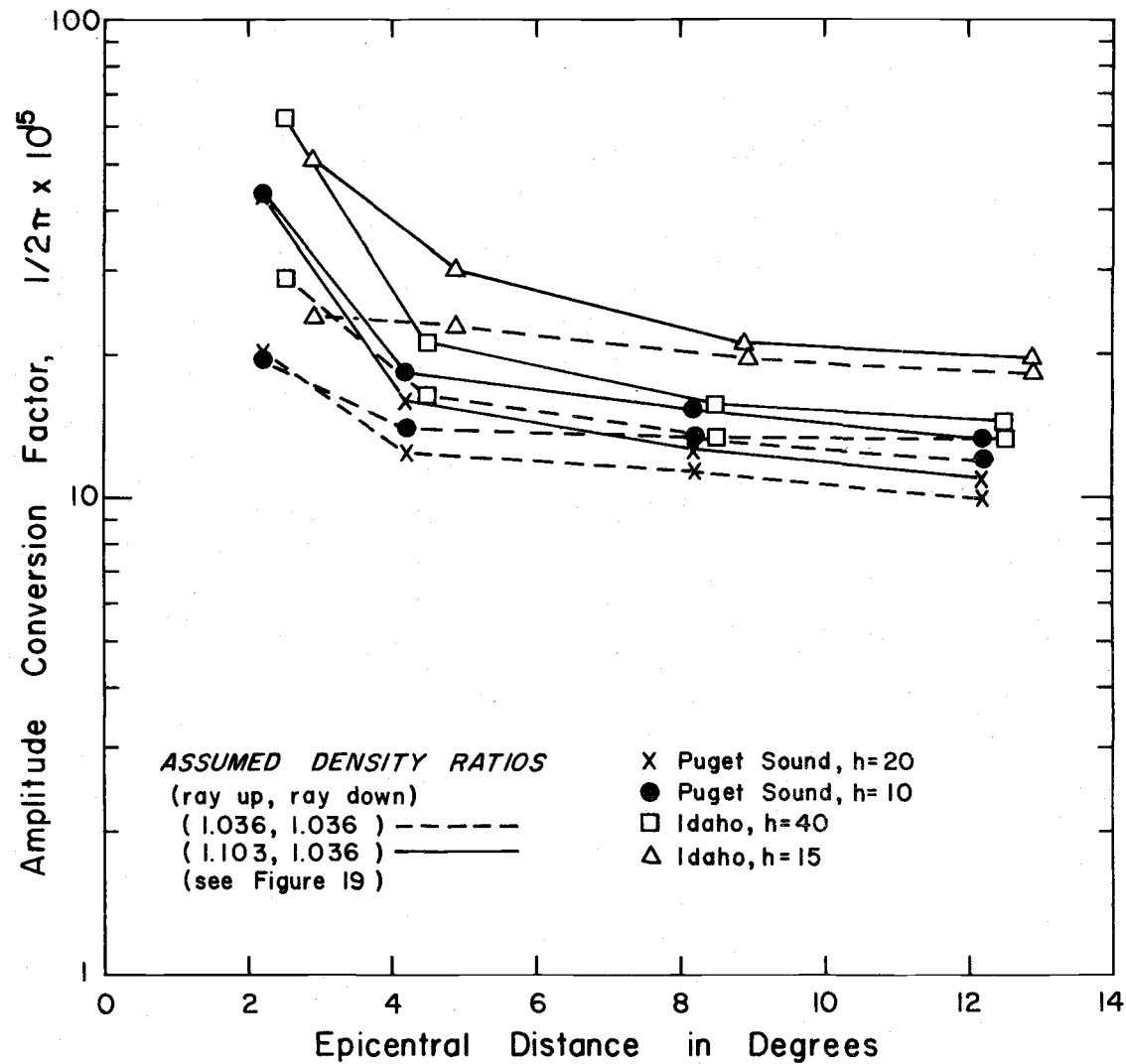


Figure 18. Amplitude conversion factors of the P wave as a function of epicentral distance for different crustal sections and focal depths above the Moho.

Table III. Tabulations for Amplitude Conversion Factors.

Figure	Crustal Section	Focal Depth km	Velocity at Focus km/sec	Density at Focus g/cc	Velocity at Surface km/sec	Surface Density g/cc	Density Ratio Used
16							
1	Willamette Valley	44.0	8.10	3.40	3.38	2.30	1.036
2	Willamette Valley	44.0	7.90	3.32	4.60	2.50	1.036
3	Willamette Valley	44.0	7.90	3.32	5.20	2.60	1.036
4	Willamette Valley	10.0	4.60	2.50	3.38	2.30	1.103
5	Vancouver Island (Puget Sound)	30.0	7.90	3.32	4.60	2.50	1.103
6	Vancouver Island (Puget Sound)	30.0	7.90	3.32	5.20	2.60	1.103
17							
1	Puget Sound	60.0	7.90	3.32	4.60	2.50	1.036
5	Queen Charlotte (Puget Sound)	60.0	8.13	3.41	4.60	2.50	1.036
6	Queen Charlotte (Puget Sound)	60.0	8.13	3.41	5.20	2.60	1.036
2	Idaho	40.0	7.30	3.16	5.20	2.60	1.103
3	Off Oregon (Willamette Valley)	30.0	7.80	3.29	3.38	2.30	1.103
4	Off Oregon (Willamette Valley)	30.0	7.80	3.29	4.60	2.50	1.036

for each amplitude conversion curve in Figures 16 and 17. Densities in the tables were determined from P-wave velocities using Nafe and Drake (1961) curves. Density ratios correspond to assumed densities above and beneath the Moho.

Figures 16 and 17 also illustrate the relation between the amplitude conversion factors in this study and conversion factors that are commonly made for head waves and body waves. Amplitudes for body waves in the earth generally are assumed to be proportional to $(\Delta V_f T)^{-1}$ and head waves to $(\Delta^2)^{-1}$, where Δ is the epicentral distance, V_f is the velocity at the focus (assumed 8.0 km/sec), and T is the period of the waves (assumed one second).

Figure 18 presents the amplitude conversion curves for a P wave originating in the crust in Idaho or the Puget Sound region.

Gutenberg curves (1944), 1 and 4 in Figure 19, were used in the present study to determine the partitioning of energy across the Moho in crustal sections. Assuming the Nafe-Drake curves (Nafe and Drake, 1961) can be used to determine actual densities for basic and ultra-basic rocks, curves 2 and 3 in Figure 19 represent the partitioning of energy for actual impedances across the Moho.

The source amplitudes of the waves were obtained from the incident amplitudes recorded at the seismic stations, using the calculated amplitude conversion curves. The amplitudes have not been corrected for wave attenuation. This effect will be examined in

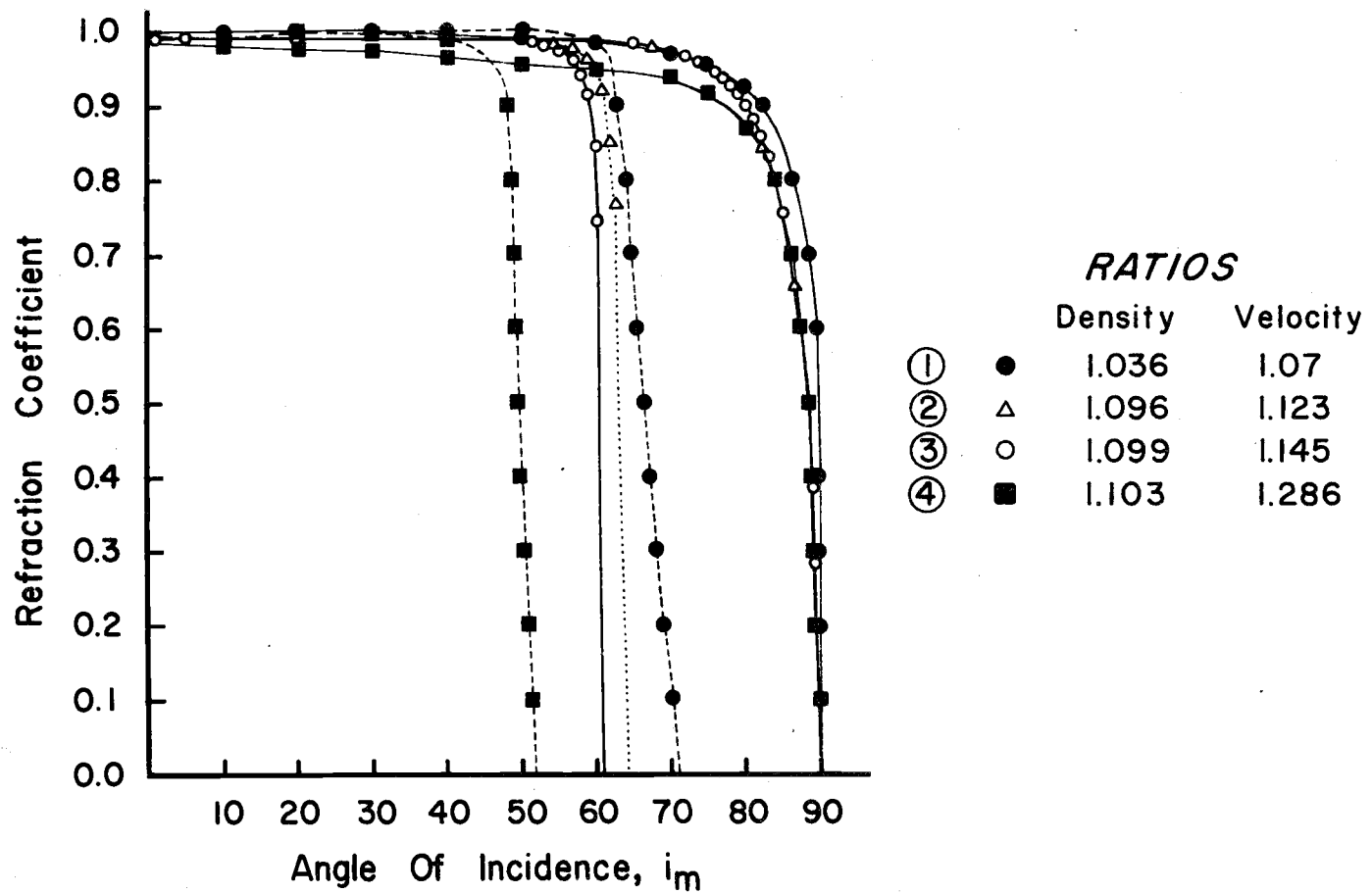


Figure 19. Partitioning of energy curves: 1 and 4 after Gutenberg (1944); 2 and 3 computed in present study.

Discussion of Results.

Calculation of the Fault-Plane Solution

The direction of first motions of the P wave recorded at different seismic stations were plotted on a stereographic projection of the focal sphere. The stereographic projection uses the epicenter as the pole of projection. The position of each seismic station on the projection was found by using the azimuth of the seismic station in relation to the epicenter and the angle i_h .

For each earthquake any three seismic stations were selected which recorded an amplitude of the P wave. The stations were selected according to the following criteria: (1) the greatest range in azimuth; (2) the clearness of recorded amplitudes; (3) P wave arrival time consistent with travel-times. Background noise on seismograms caused the greatest difficulties in selecting adequate stations. While arrival times were reliable in most cases, some deviations from the travel-time curves could be due to (1) inaccuracies in the travel-time curves; (2) crustal effects; and/or (3) earthquake source phenomena. The source amplitudes determined at the three stations were placed in three amplitude ratios for the experimental purposes.

A computer program was used to calculate the theoretical amplitude and direction of P-wave first motions at each station,

using the angle i_h and azimuth. The program placed the theoretical amplitudes in ratios and compared them with the observed ratios in terms of fractional deviations.

The computer program for obtaining orientations of fault planes used first motions and amplitudes at the three stations.

This procedure follows:

- (1) The theoretical directions of P-wave first motions were computed and compared to observed directions for two stations. If they were inconsistent, the orientation was rejected.
- (2) If the directions agreed, then the theoretical amplitude ratio for the two stations was compared with the ratio of observed source amplitudes. If the fractional deviation in the amplitude ratios was greater than 1.00, the orientation was rejected.
- (3) If the fractional deviation was less than 1.00, the direction of first motion of the P wave at the third station was checked in similar manner.
- (4) When the directions of the P-wave first motions agreed and the fractional deviations in P-wave amplitudes at all three stations were less than 1.00, the orientation was printed by the computer. The orientation computed shows the possible attitudes of the two fault planes.

This procedure was followed for over 6000 orientations of fault planes.

The sum of the fractional deviations for each orientation was made. Sums having least deviations were chosen as indicative of the probable orientations. These orientations were then compared with the directions of first motions of the P wave recorded for the earthquake at other stations. The orientation best fitting these first motions was called the preferred fault-plane solution.

The analysis of the S wave to determine force orientations of the earthquakes would be similar to the analysis of the P wave. The S-wave analysis has not been attempted because identification of the Sn wave was usually unreliable or the phase was not recorded. Consequently, only a few recorded polarizations of the S wave could be determined from the seismograms. The incident polarizations were calculated from those polarizations which were recorded (See curves in Figure 5). These incident polarizations are plotted on the stereographic projection in this study.

Data used in determining the fault-plane solution of each earthquake is in Appendix VI.

DISCUSSION OF RESULTS

The results of this study are presented in the following order: comparison of the Byerly Method and the present method; the present method applied to earthquakes in northwestern North America; reliability of the fault-plane solutions; and the general tectonic forces in western North America.

Comparison of Byerly Method and Present Method

A comparison was made of fault-plane solutions for five earthquakes determined by both the Byerly method and the present method. (Data of present study in Table IV.)

The April 29, 1965 earthquake with a magnitude of 6.5 at Tacoma, Washington was analyzed by Algermissen and Harding (1965). They used recorded P and PKP waves to determine a fault-plane solution, using the Byerly method. This solution is given in Table V. The present study found the fault planes determined by Algermissen and Harding (1965) improperly constrained approximately 5° in strike and/or dip.

The present investigation included determination of a fault-plane solution under the Byerly method. The solution was based on recordings at epicentral distances of less than 20° (Appendix V). The procedure in the present method showed that a limited number

Table IV. Summary of Fault-Plane Solutions Obtained in Present Study.

No.	Date	Region of Earthquake	Crustal Section Used	Seismic Stations	Plane A	Dip	Plane B	Dip	Assumed Focal Depth (km)
1	April 29, 1965	Tacoma, Washington	Puget Sound	FSJ, DUG, BKS	N27°W	32SW	N04°W	61E	60.0
2	May 8, 1968	Blanco Fracture	Off Oregon	COR, UBO, BKS	N52°W	41NE	N30°W	50SW	30.0
3	Aug. 22, 1963	Gorda Ridge	Off Oregon	WINV, HLID, BKS	N45°E	84SE	N92°E	08N	30.0
4	Oct. 14, 1962	Pt. Arena, Calif.	Off Oregon	PTOR, WINV, BKS	N12°W	56E	N42°E	50NW	20.0
5a	Mar. 7, 1963	N.W. of Corvallis, Oregon	Willamette Valley	PNT, HLID, MNA	N41°W	35S	N82°W	61NE	44.0
5b	Mar. 7, 1963	N.W. of Corvallis, Oregon	Willamette Valley	PNT, HLID, MNA	N50°E	32SE	N54°W	80NE	20.0
6	April 19, 1967	East of Moresby Island	Queen Charlotte Island	PNT, LON, COL	N12°W	14E	N32°E	80W	60.0
7	April 29, 1967	In Queen Charlotte Sound	Queen Charlotte Island	FSJ, COL, LON	N 0°E	60E	N90°E	90	10.0
8	May 20, 1966	West of north Vancouver Island	Off north Vancouver Island	VIC, LON, COR	N07°W	80W	N54°W	14NE	30.0
9	Mar. 30, 1966	West of north Vancouver Island	Off north Vancouver Island	COR, PNT, FSJ	N42°E	54SE	N74°W	62NE	30.0
10	Nov. 4, 1966	West of north Vancouver Island	Off north Vancouver Island	LON, PNT, FSJ	N32°E	80SE	N64°W	62NE	30.0
11	June 25, 1963	Blanco Fracture	Off Oregon	HLID, PTOR, WINV	N69°W	80SW	N69°W	10NE	30.0
12	July 4, 1963	Blanco Fracture	Off Oregon	PTOR, WINV, COR	N80°W	80S	N80°W	10N	30.0
13	June 25, 1963	Blanco Fracture	Off Oregon	HLID, LON, WINV	N09°W	81W	N09°W	10E	30.0

Continued on next page

Table IV Continued.

No.	Date	Region of Earthquake	Crustal Section Used	Seismic Stations	Plane A	Dip	Plane B	Dip	Assumed Focal Depth (km)
14	Feb. 21, 1963	Near Cape Mendocino, California	Puget Sound	COR, WINV, HLID	N27°E	14SE	N71°E	79N	60.0
15	Nov. 6, 1962	Portland, Oregon	Willamette Valley	LON, DUG, COR	N12°W	22SW	N54°E	80SE	44.0
16	Jan. 24, 1963	East of Seattle, Washington	Puget Sound	PNT, PTOR, MVCL	N74°E	80N	N10°E	22E	10.0
17	Sept. 26, 1962	Near Lima, Montana	Idaho	HLID, BMO, PTOR	N57°E	74NW	N50°W	44SW	40.0
18	Feb. 16, 1963	Near Hatfield Mtn., Montana	Idaho	BMO, WINV, DUG	N06°E	66NW	N83°E	60S	40.0
19	Oct. 18, 1962	N. W. of Hailey, Idaho	Idaho	PTOR, WINV, DUG	N50°E	50SE	N40°W	90	40.0
20	Oct. 18, 1962	N. W. of Hailey, Idaho	Idaho	PTOR, WINV, DUG	N28°E	64NW	N78°W	62S	40.0
21	Jan. 6, 1963	N. E. of Lodge Peak, Montana	Idaho	LON, HLID, GOL	N30°E	66NW	N82°W	48S	40.0
22	Feb. 24, 1963	S. of Black Butte in Travelly Range, Mont.	Idaho	WINV, HLID, PTOR	N40°E	70NW	N40°E	20SE	40.0

Data for each earthquake found--Appendix VI.

of fault-plane orientations could be obtained when the stations had the greatest separation on the focal sphere. Two fault-plane solutions were obtained from orientations having minimum fractional deviations, as shown in Figure 20. Solutions obtained with the present method compared favorably with the solutions obtained with the Byerly method. This was remarkable, as fault-plane orientations were calculated at ten degree increments in this study.

Fault-plane solutions were obtained for the earthquake of May 8, 1968, in the Blanco fracture zone off the coast of Oregon. Four groups of three seismic stations were employed. Two of the groups resulted in three preferred solutions, illustrated in Figure 22. The solutions could fit the direction of P-wave first motions with only slight fault-plane adjustments (excluding the station BEL, at Bellingham, Washington). A fault-plane solution for this earthquake was obtained also by Bolt, Lomnitz and McEvelly (1969), using the Byerly method. The focal depth for the earthquake was assumed to be beneath the Moho in this study and above the Moho by Bolt, Lomnitz, and McEvelly (1969). The solutions of the two studies were not in agreement.

A fault-plane solution obtained for the earthquake of August 22, 1963 in the Gorda Ridge off northern California is illustrated in Figure 21. This solution was obtained after 12,000 orientations had been tested. The calculation involved a 5° increment in the

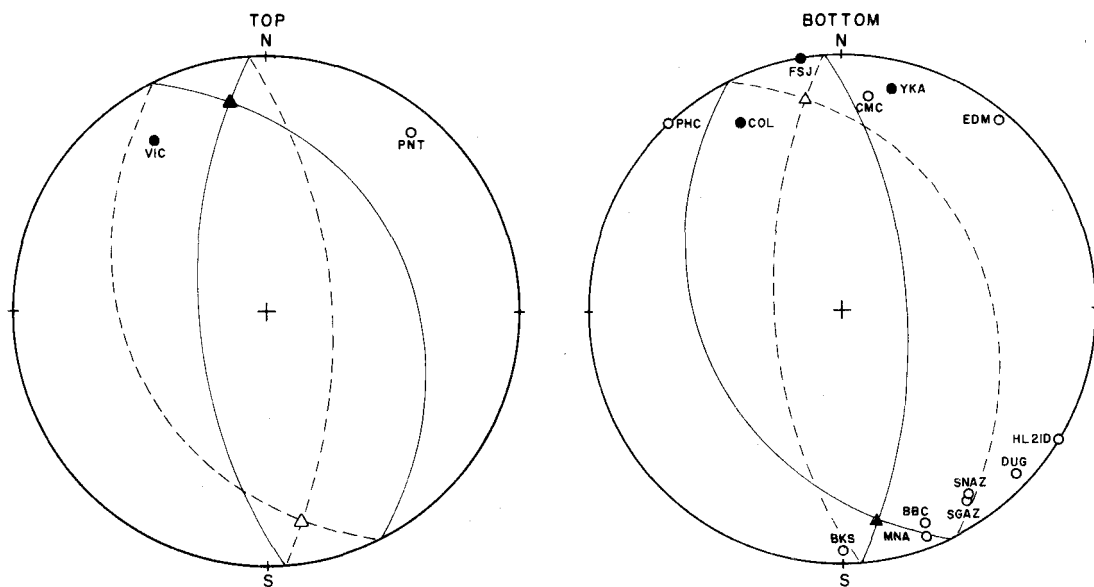


Figure 20. Fault-plane solutions for earthquake of April 29, 1965 projected on top and bottom half of focal sphere.

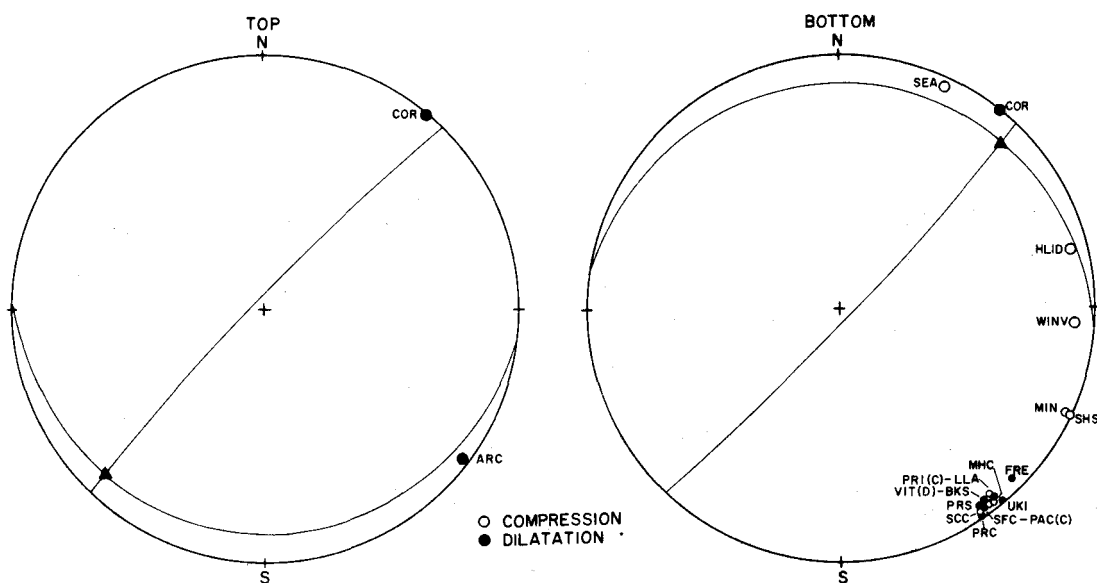


Figure 21. Fault-plane solution for earthquake of August 22, 1963 projected on top and bottom half of focal sphere.

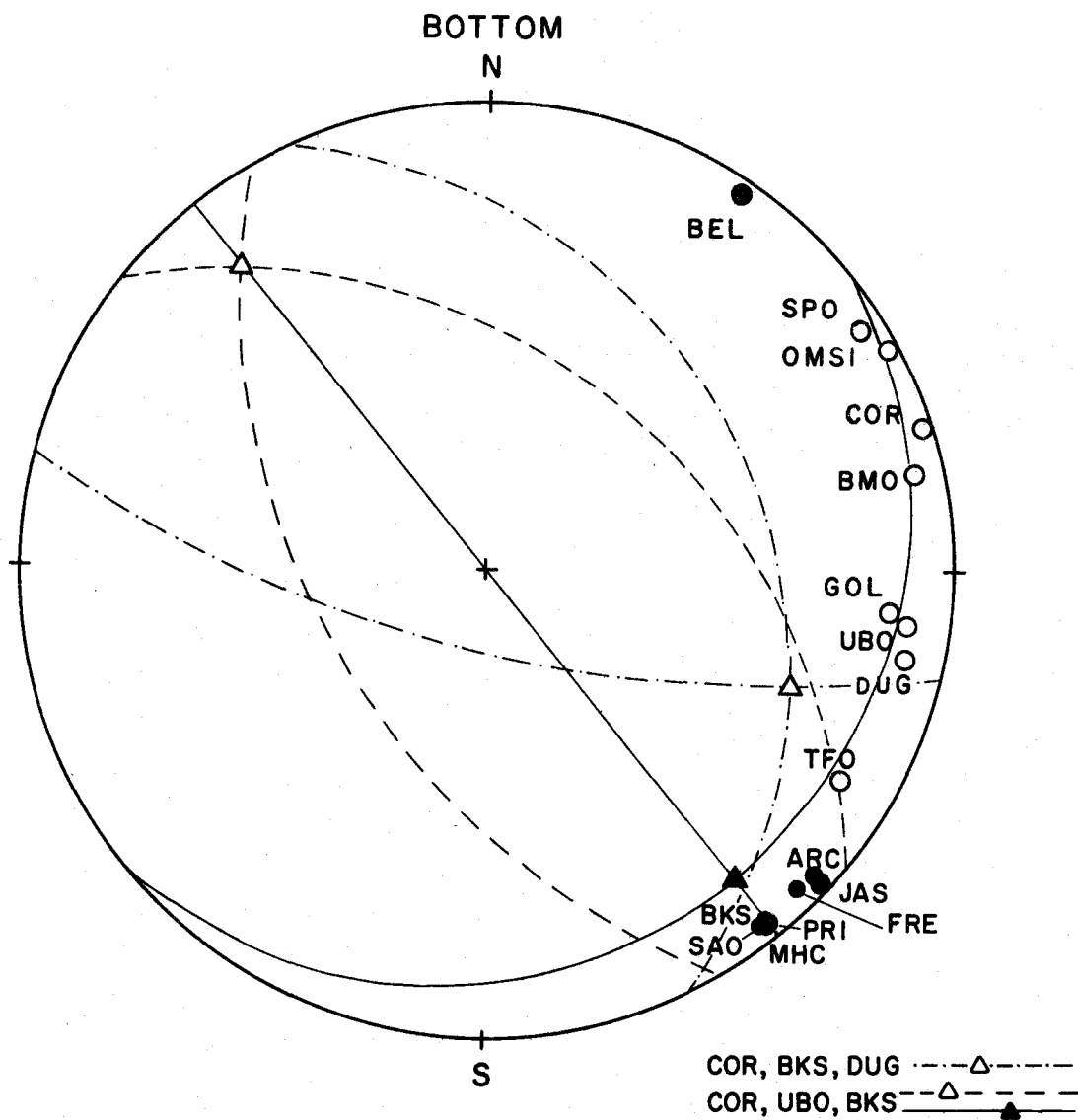


Figure 22. Fault-plane solution for earthquake of May 8, 1968 projected on bottom half of focal sphere.

computer program instead of the normal 10° . The density of the orientations for the 5° and 10° increments are illustrated in Figure 23. A fault-plane solution for this earthquake was determined by Tobin and Sykes (1968), using the Byerly method (Table V). The strike and dip of Plane A for the two solutions are similar in the tables while they are different in Plane B. Tobin and Sykes (1968) concluded that Plane B is defined by minimum amplitudes; Plane B in the present method is constrained by amplitude ratios.

The earthquake of October 14, 1962 was located near Point Arena off the coast of northern California. Fault-plane solutions for this earthquake obtained by the present method are illustrated in Figure 24. A solution was calculated for a focus beneath the Moho which did not fit the direction of first motions of the P wave. Another solution, based on a focus above the Moho, appeared to fit the first motions. These solutions were compared with the solution obtained by Bolt, Lomnitz and McEvelly (1969), who used the Byerly method (Table V). The solutions were found nearly in agreement.

Two fault-plane solutions were determined for the March 7, 1963 earthquake located northwest of Corvallis, Oregon. The solutions for foci above and beneath the Moho are illustrated in Figure 25. The two solutions show normal faults with fault planes that tend to rotate about the null line when focal depths change. A fault-plane solution of the earthquake was obtained based on the Byerly method

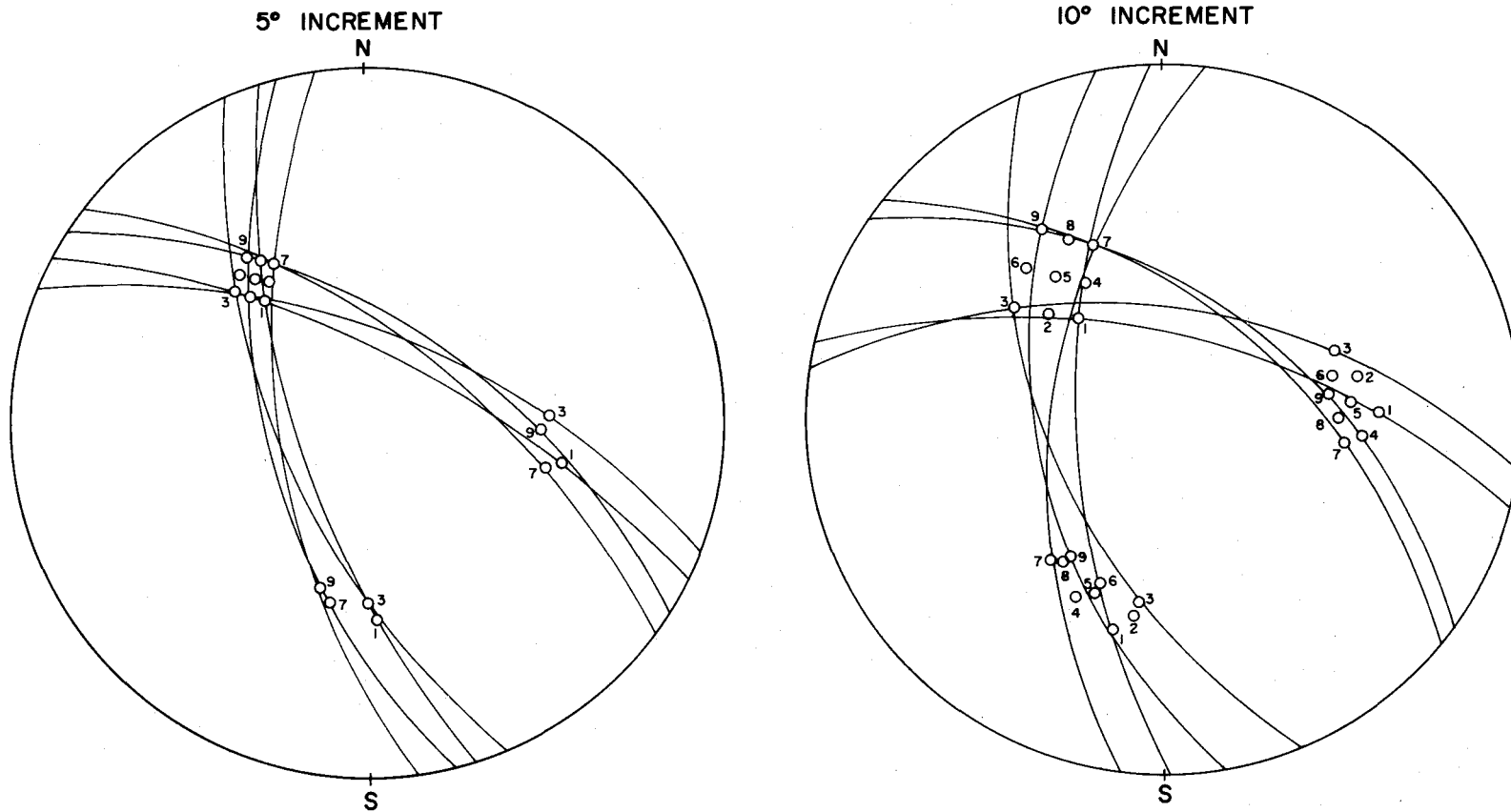


Figure 23. Reliability of fault-plane solution based on 5° and 10° increments of Euler Angles.

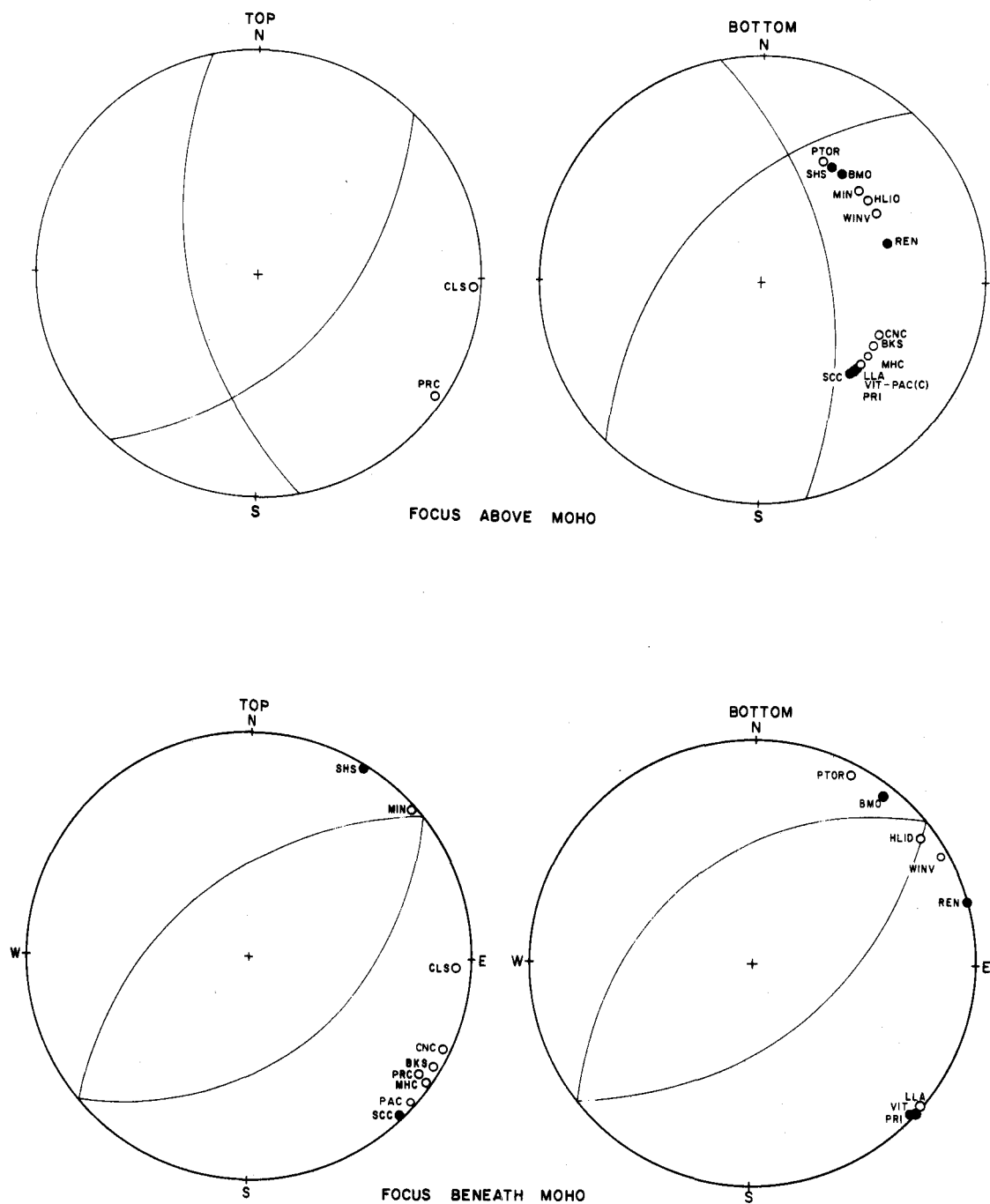


Figure 24. Fault-plane solutions for earthquake of October 14, 1962 projected on top and bottom half of focal sphere.

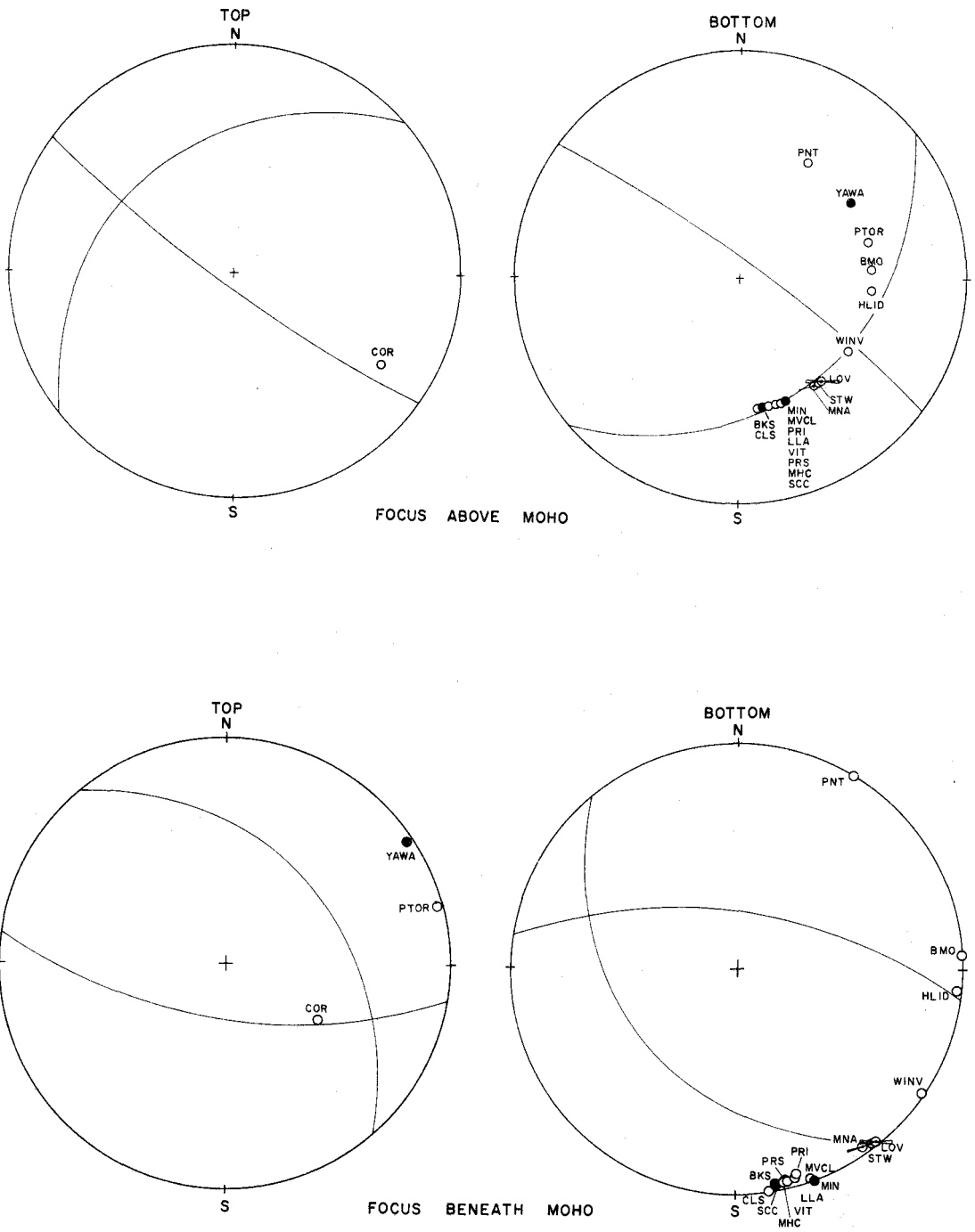


Figure 25. Fault-plane solutions for earthquake of March 7, 1963 projected on top and bottom half of focal sphere.

Table V. Summary of Fault Plane Solutions Found by Other Investigators Using Byerly Method.

No.	Date	Lat. N.	Long. W.	Plane A	Dip	Plane B	Dip	Motion *	Null Line	Dip	Reference
1	Sept. 16, 1965	40.4	125.8	N18E	90	N108E	90	S	N 0 E	90	Tobin & Sykes, 1968
2	July 6, 1934	41.4	125.4	N50E	64E	N40W	84E	S	S60E	62.5	Byerly, 1938
3	April 18, 1965	41.5	127.2	N33W	65E	N18E	35W	D	N21W	24	Tobin & Sykes, 1968
4	Aug. 22, 1963	42.1	126.2	N53E	90	N143E	90	S	N 0 E	90	Tobin & Sykes, 1968
5	June 20, 1965	42.9	126.3	N24E	80E	N108E	60N	D	N43E	59	Tobin & Sykes, 1968
6	July 7, 1964	43.4	127.7	N33E	90	N123E	90	S	N 0 E	90	Tobin & Sykes, 1968
7	April 13, 1949	47.0	122.6	N49E	83W	N76W	12S	S	S47.5W	9.7	Hodgson & Storey, 1954
8	April 29, 1965	47.4	122.3	N18W	69E	N53W	35W	S	N154E	18 ^a	Algermissen & Harding, 1965
9	June 23, 1946	49.9	124.9	N01E	33W	N23W	60E	S	N17W	11.9	Hodgson & Milne, 1951
10	Mar. 31, 1964	50.8	130.1	N15W	90	N75E	90	D	N 0 E	90	Tobin & Sykes, 1968
11	Dec. 30, 1948	51.0	131.0	N56E	67E	N65W	39E	D	N69E	29.6	Hodgson & Storey, 1954

Continued on next page

Table V Continued.

No.	Date	Lat. N.	Long. W.	Plane A	Dip	Plane B	Dip	Motion *	Null Line	Dip	Reference
12	Aug. 22, 1949	54.1	132.6	N64E	72E	N29W	77E	S	S63.5E	67.8	Hodgson & Milne, 1951
13	July 21, 1952	35.0	119.0	N50E	63SE	N90E	36N	S	N59E	19	Fara, 1964
14	June 28, 1925	46.4	111.2	N26E	87SE	N65W	83NE	D	N51E	81.8	Fara, 1964
15	Oct. 24, 1927	57.6	137.1	N30W	82NE	N63E	77SE	D	S62E	74	Fara, 1964
16	July 6, 1954	39.5	118.5	N56E	51NW	N24W	78NE	S	N10W	48	Tocher, 1955
17	Aug. 24, 1954	39.5	118.5	N45E	51NW	N05W	51NE	S	N20E	27.7	Tocher, 1955
18	Dec. 16, 1954	39.5N	118.0	N66E	66NW	N11W	62NE	S	N31E	52.0	Romney, 1957
19	Feb. 9, 1956	31.5	116.	N19E	85SE	N72W	72NE	S	N35E	70.9	Hodgson & Stevens, 1958
20	April 29, 1954	28.5	113.	N46E	88SE	N45W	68NE	S	N50E	68	Hodgson & Cock, 1957
21	July 10, 1958	58.3	136.9	N68E	82SE	N25W	72E	S	N90E	70	William Stauder, 1960a
22	June 28, 1966	37.	120.5	N33W	90	N57E	70NW	D	N34W	72	McEvilly, 1966

Continued on next page

Table V Continued.

No.	Date	Lat. N.	Long.W.	Plane A	Dip	Plane B	Dip	Motion *	Null Line	Dip	Reference
23	May 8, 1968	43.6	127.9	N66W	90	N24E	90	D	N 0 E	90	Bolt, Lomnitz, McEvelly, 1969
24	May 24, 1966	39.8	121.8	N30W	65NE	N68E	74SE	D	S84E	60	Lomnitz & Bolt, 1967
25	Nov. 16, 1954	37.1	121.7	N54W	70NE	N36E	90	S	N36E	71	McEvelly, 1967
26	Sept. 14, 1963	36.9	121.6	N54W	60NE	N36E	90	D	N36E	60	Udias A. 1965
27	Oct. 14, 1962	38.7	124.	N47W	90?	N43E?	25NW?	D	N47W	25	Bolt, Lomnitz, McEvelly, 1969
28	Mar. 7, 1963	44.9	123.7	N42W	90	N48E	90	D	N 0 E	90	Bolt, Lomnitz, McEvelly, 1969

* indicates movement along plane A, where: D = dextral, S = sinistral.

by Bolt, Lomnitz, and McEvelly (1969). See Table V. The solutions differed, possibly due to the limited number of first motions available and/or the inconsistencies of these first motions.

Present Method Applied in Northwestern North America

The four earthquake regions in the present study were: (1) off the coast of British Columbia; (2) off the coast of Oregon and northern California; (3) west of the Cascade Mountains; (4) east of the Cascade Mountains. These earthquakes are numbered in Table IV.

Each area has different crustal structures and are possibly subjected to different tectonic forces. Seismic station distributions vary in each area.

Either one of the planes in the fault-plane solutions obtained for a region could be a fault plane. The plane best fitting structural characteristics of a region was selected as the fault plane. Each fault plane was given a classification based on the dip and direction of movement of the fault plane. The fault-plane solutions for each geographical region also were compared to solutions determined by the Byerly method.

Off the Coast of British Columbia

Locations of five earthquakes studied in this region (as listed

in Table IV) were: No. 6, east of Moresby Island; No. 7, south of Moresby Island; Nos. 8, 9 and 10, west of Vancouver Island. The earthquake of August 22, 1949, located at the northern edge of Graham Island, and earthquakes of December 30, 1948 and March 31, 1964, located south of Morseby Island, were analyzed by other investigators using the Byerly method (Table V).

Tectonic features in this region have been represented as faults, trenches, ridges and gravity lows. A fault, based on lineation of epicenters, is traceable along the edge of the continental shelf from Cape Spencer to northern Vancouver Island. The Explorer Trench and the Juan de Fuca Ridge strike southward off the coast of northern Vancouver Island. A gravity survey by Couch (1969) has shown that gravity anomaly minima extend northward from Queen Charlotte Sound into Hecate Strait and that a graben-like structure with an asymmetrical gravity minimum exists west of northern Vancouver Island.

Earthquake No. 6 in Table IV presents a normal fault; No. 7, a right lateral strike-slip; No. 8, a normal fault (Figures 26, 27, 29). All of the faults strike in a northerly direction and may be related to the trend of gravity lows in Hecate Strait. The March 31, 1964 earthquake (Byerly method) is a strike-slip fault also in this direction. The December 30, 1948 earthquake (Byerly method) does not follow the northerly trend. Earthquake Nos. 9 and 10 (Figures

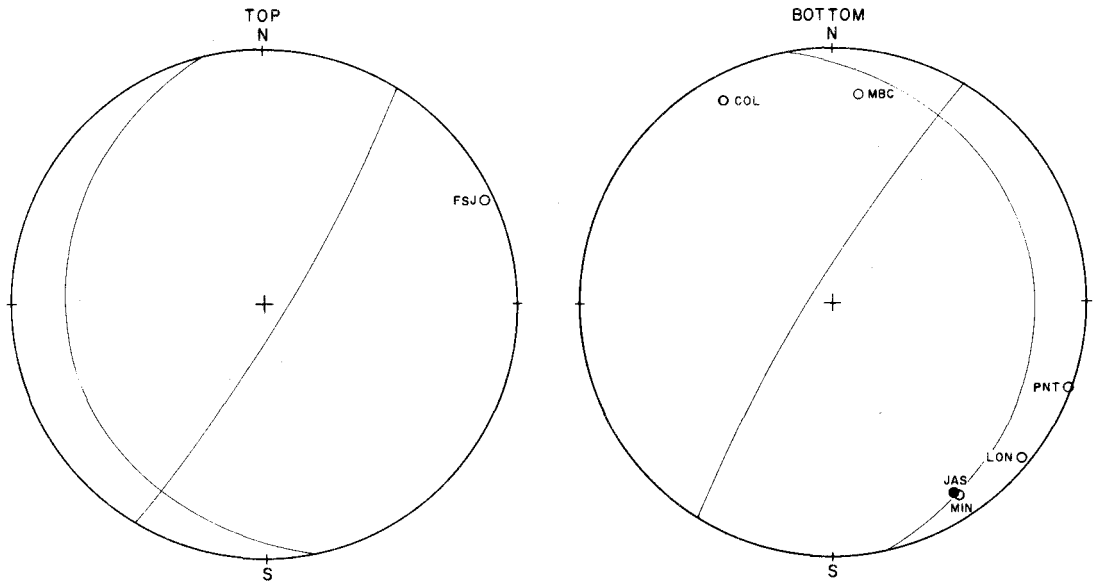


Figure 26. Fault-plane solutions for earthquake of April 19, 1967 projected on top and bottom half of focal sphere.

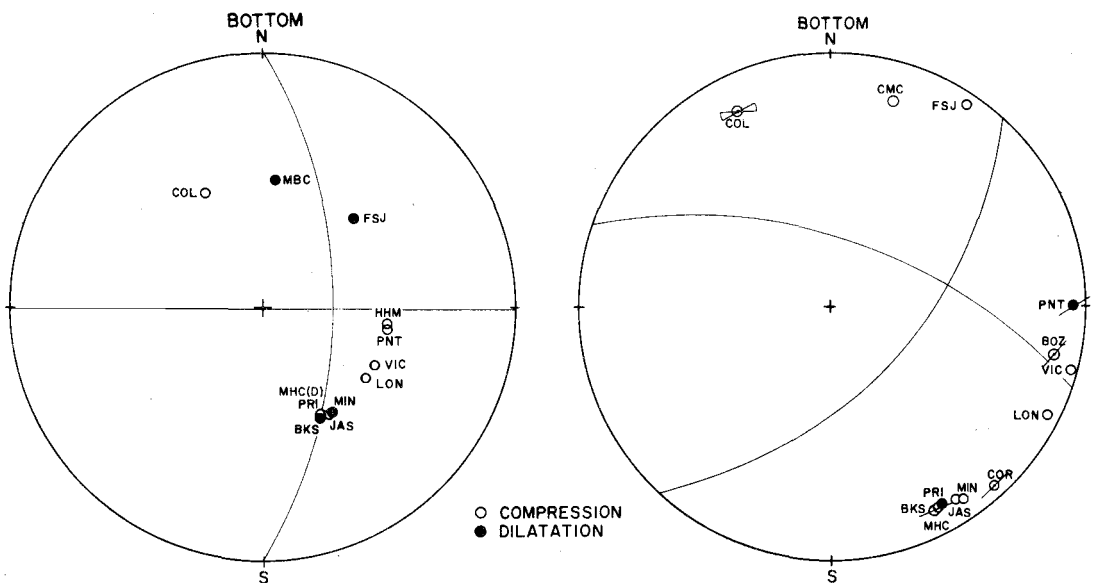


Figure 27. Fault-plane solution for earthquake of April 29, 1967 projected on bottom half of focal sphere.

Figure 28. Fault-plane solution for earthquake of March 30, 1966 projected on bottom half of focal sphere.

28, 30) have right lateral strike-slip faults trending in a northeasterly direction similar to the direction of the Explorer Trench.

Off the Coast of Oregon and Northern California

Earthquakes Nos. 2, 11, 12 and 13 (Figures 22, 31, 32 and 33) located along the Blanco Fracture Zone; No. 3 east of the Gorda Ridge (Figure 21); No. 14, on the Mendocino Escarpment (Figure 34); and No. 4, off Point Arena, were examined by the present method (Figure 24). Fault-plane solutions for earthquakes in this region also have been determined by Tobin and Sykes (1968) and Bolt, Lomnitz and McEvilly (1969). Seismic activity is known to exist in each of these geologic features.

In Table IV, earthquakes Nos. 2 and 12 had normal faults; No. 11, a thrust fault. These faults had a northwesterly direction similar to the Blanco Fracture Zone. No. 13 had a normal fault, striking in a northerly direction. No. 3 gives a normal fault striking along the Gorda Ridge and No. 14, a normal fault striking close to the direction of the Mendocino Escarpment. Earthquake No. 4 exhibits right lateral strike-slip motion similar to that of the San Andreas fault.

West of the Cascade Mountains

Earthquakes Nos. 1, 5, 15 and 16 are located west of the

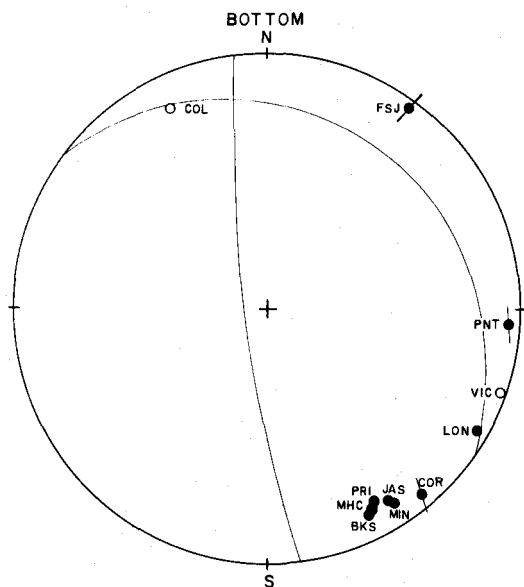


Figure 29. Fault-plane solution for earthquake of May 20, 1966 projected on bottom half of focal sphere.

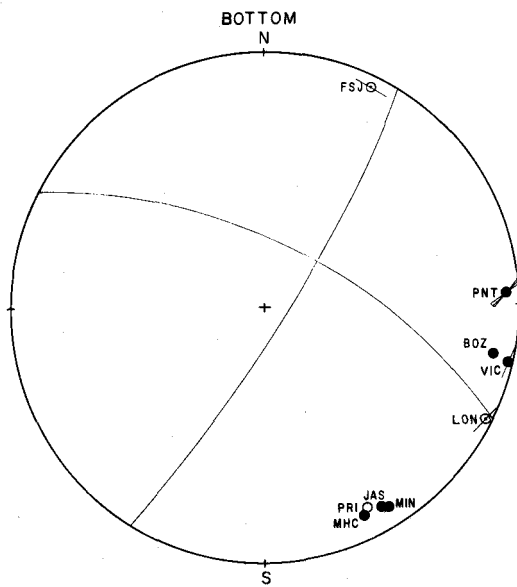


Figure 30. Fault-plane solution for earthquake of November 4, 1966 projected on bottom half of focal sphere.

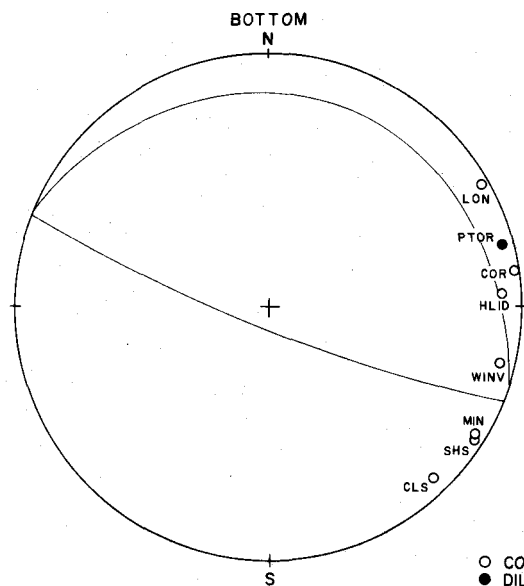


Figure 31. Fault-plane solution for earthquake of June 25, 1963 (08:26:21.7) projected on bottom half of focal sphere.

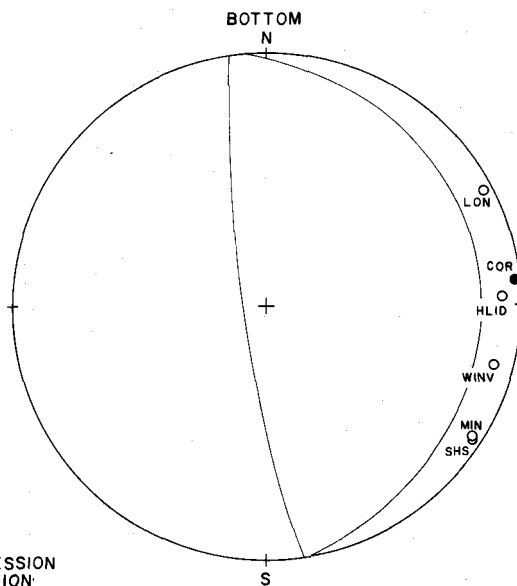


Figure 32. Fault-plane solution for earthquake of June 25, 1963 (09:39:27.7) projected on bottom half of focal sphere.

○ COMPRESSION
● DILATATION

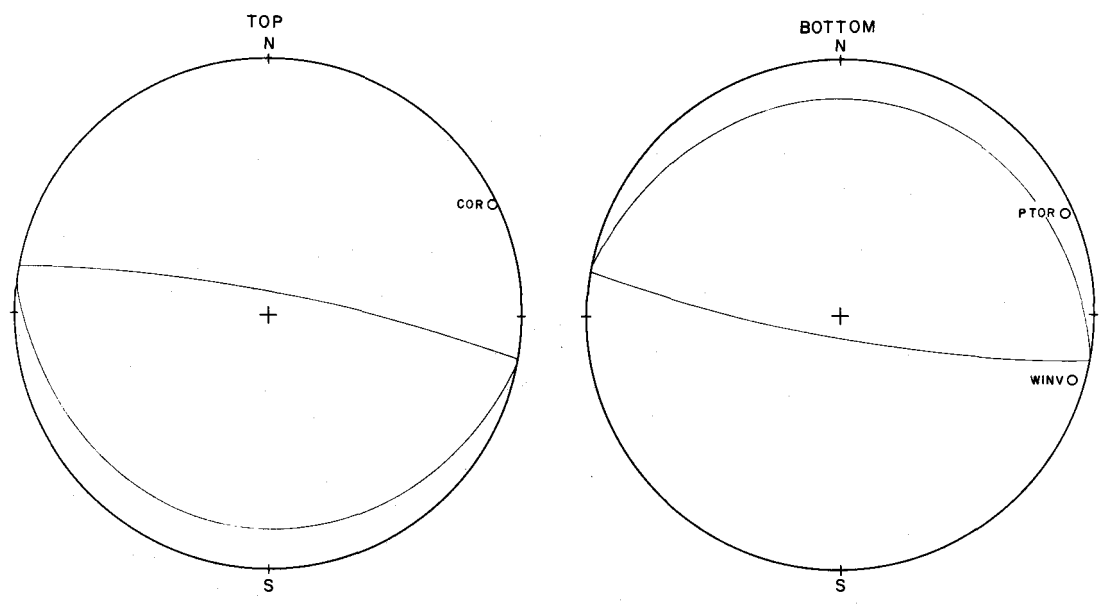


Figure 33. Fault-plane solution for earthquake of July 4, 1963 projected on top and bottom half of focal sphere.

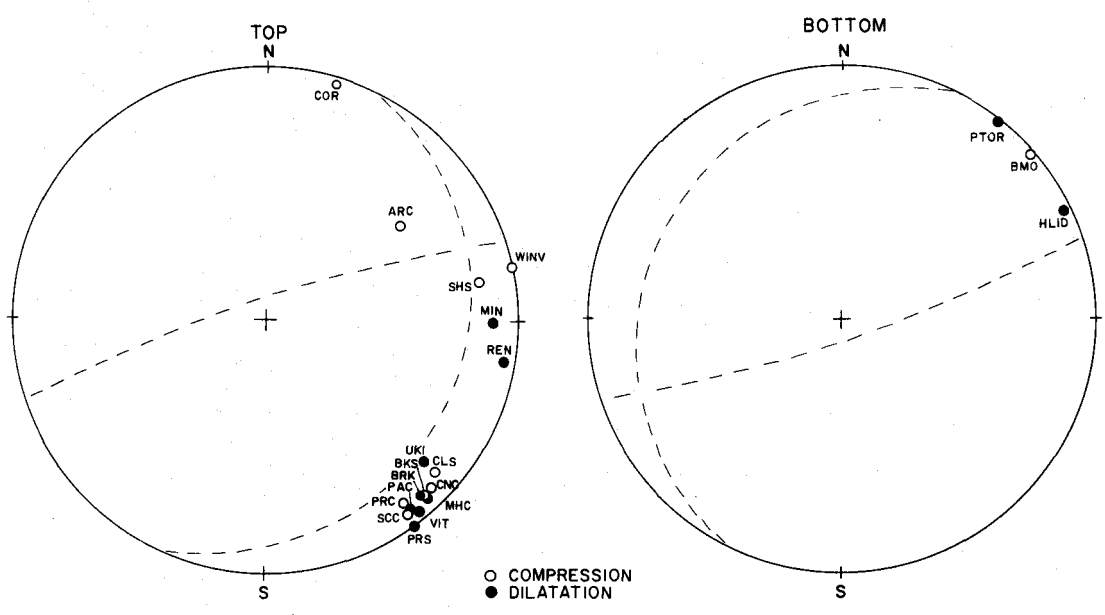


Figure 34. Fault-plane solution for earthquake of February 21, 1963 projected on top and bottom half of focal sphere.

Cascade Mountains (Figures 20, 25, 35 and 36). Seismic activity in the region is small compared to regions off the Pacific Coast. No. 5, southwest of Valsetz, Oregon, showed a normal fault striking northwesterly, or a right lateral strike-slip trending northeast. No. 15, north of Portland, Oregon, was due to normal faulting, trending northeast; No. 1, south of Seattle, Washington, was a normal fault; No. 16, southeast of Seattle, showed a thrust fault. Faults mapped in northwest Oregon generally strike northeasterly (Oregon. Dept. of Geology and Mineral Industries, 1961). Earthquake No. 5 may be related to such a fault near Valsetz. No. 15 has no fault nearby.

East of the Cascade Mountains

The locations of earthquakes Nos. 17, 18, 19, 20, 21 and 22 are in Idaho and Montana (Figures 37-42). Two earthquakes are northwest of Hailey, Idaho; No. 20, a right lateral strike-slip fault, striking northeast; and No. 19, a right lateral fault, striking northwesterly. The faulting in Idaho generally strikes from N. 50° E. to N. 50° W. around and in the Idaho Batholith (Ross and Savage, 1967). Four earthquakes were in Montana: No. 17, east of Lima, exhibits right lateral fault striking northeasterly; No. 18, northeast of Hatfield Mountain, a left lateral strike-slip fault trending northerly; No. 21, northeast of Lodge Peak, a right lateral fault striking northeast; and No. 22, south of Black Butte in the Travelly

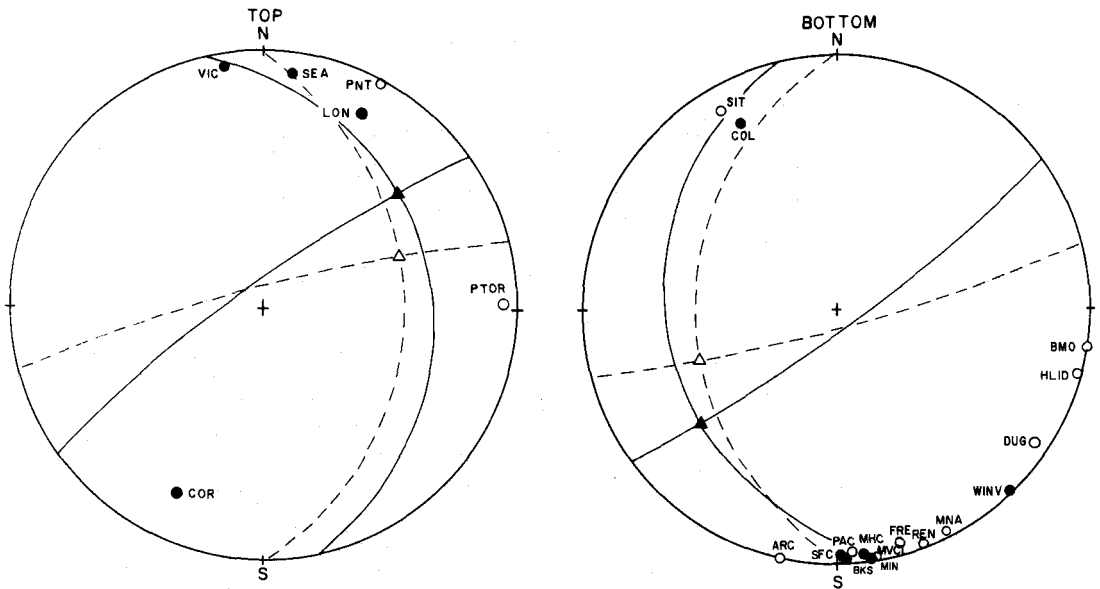


Figure 35. Fault-plane solution for earthquake of November 6, 1962 projected on top and bottom half of focal sphere.

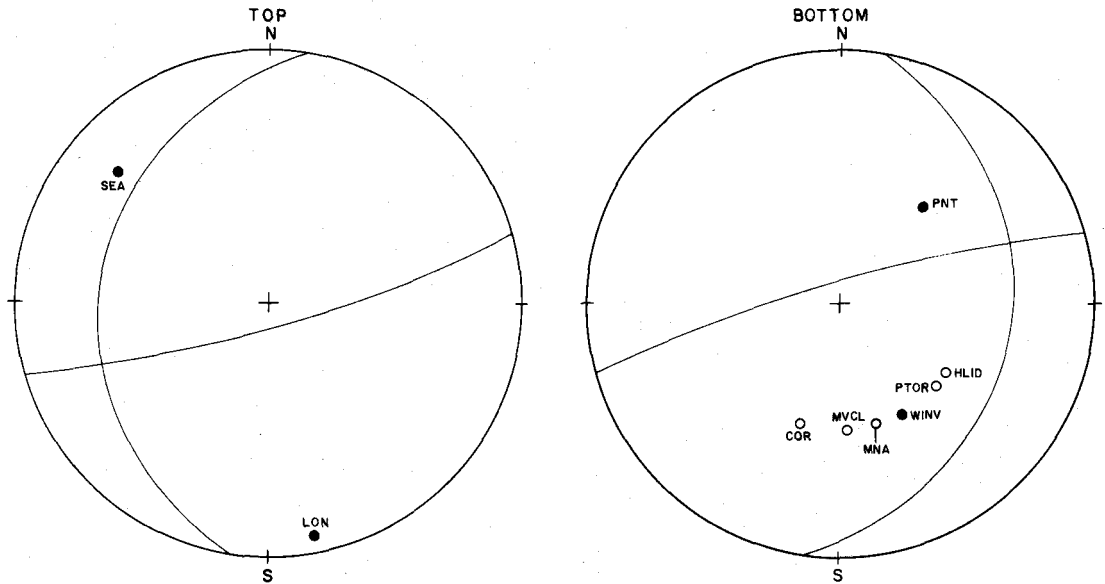


Figure 36. Fault-plane solution for earthquake of January 24, 1963 projected on top and bottom half of focal sphere.

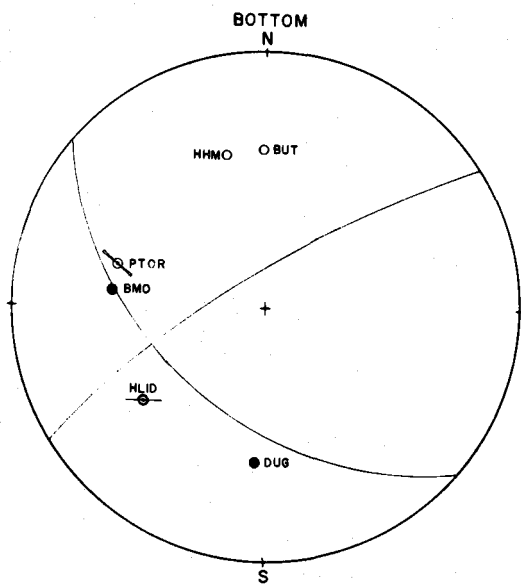


Figure 37. Fault-plane solution for earthquake of September 26, 1962 projected on bottom half of focal sphere.

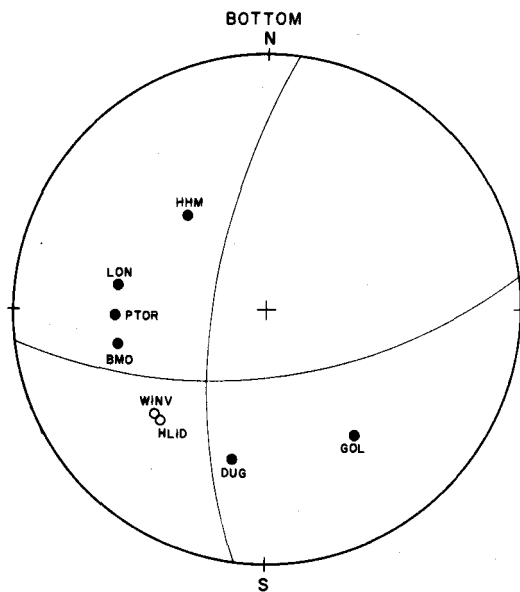


Figure 38. Fault-plane solution for earthquake of February 16, 1963 projected on bottom half of focal sphere.

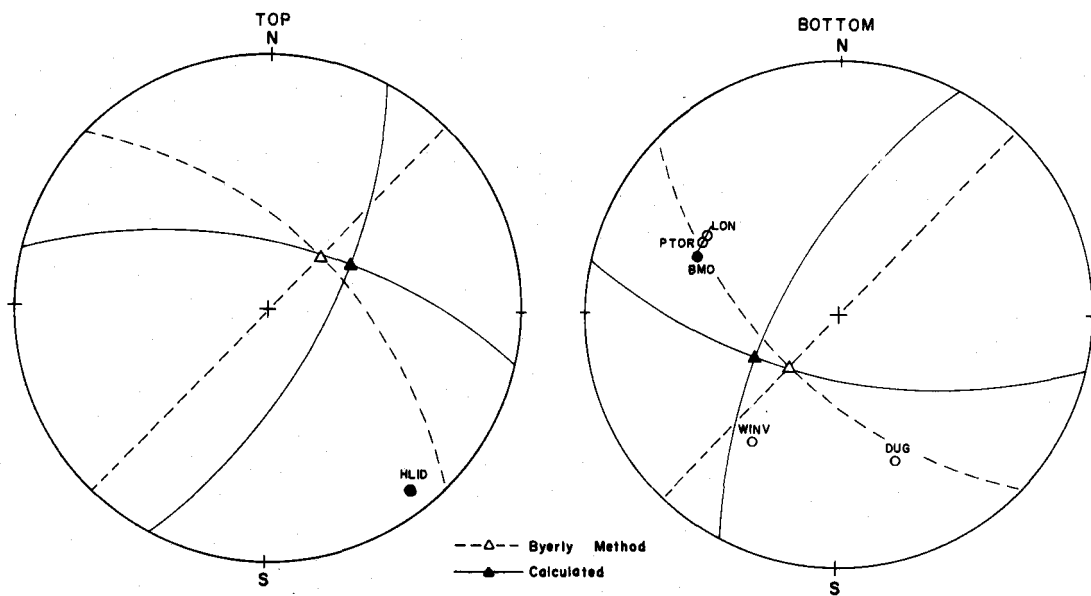


Figure 39. Fault-plane solution for earthquake of October 18, 1962 (20:31:02.6) projected on top and bottom half of focal sphere.

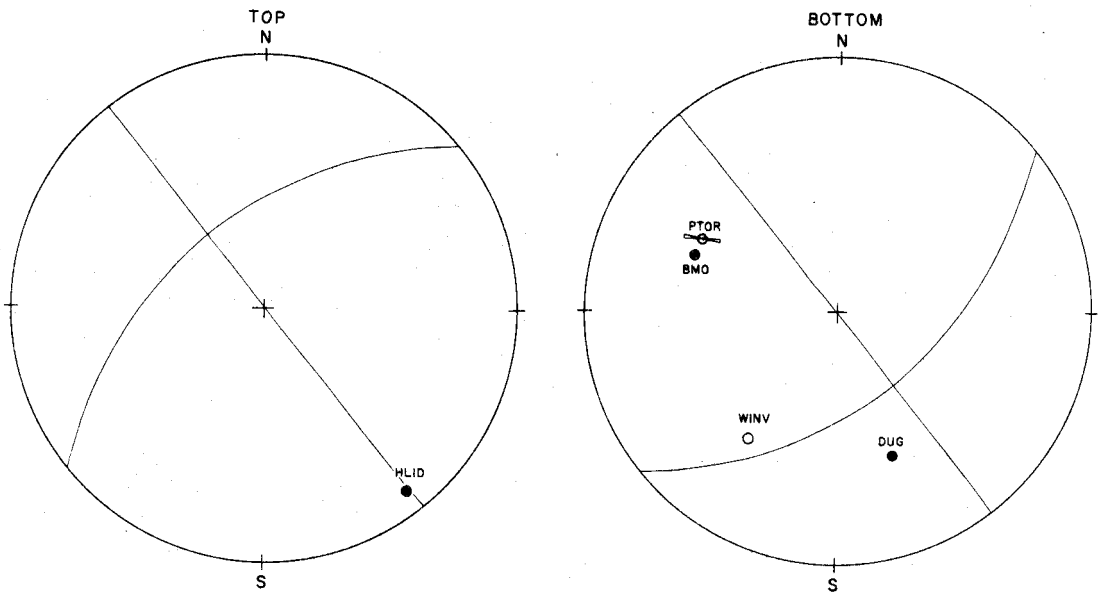


Figure 40. Fault-plane solution for earthquake of October 18, 1962 (18:03:14.0) projected on top and bottom half of focal sphere.

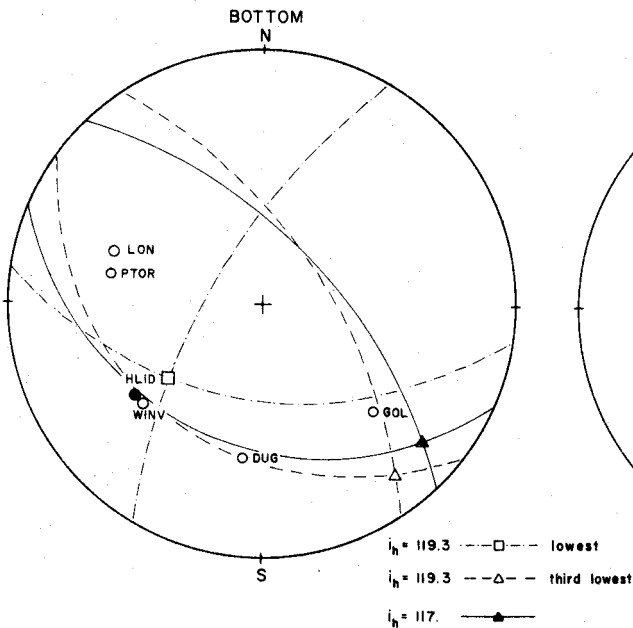


Figure 41. Fault-plane solution for earthquake of January 6, 1963 projected on bottom half of focal sphere.

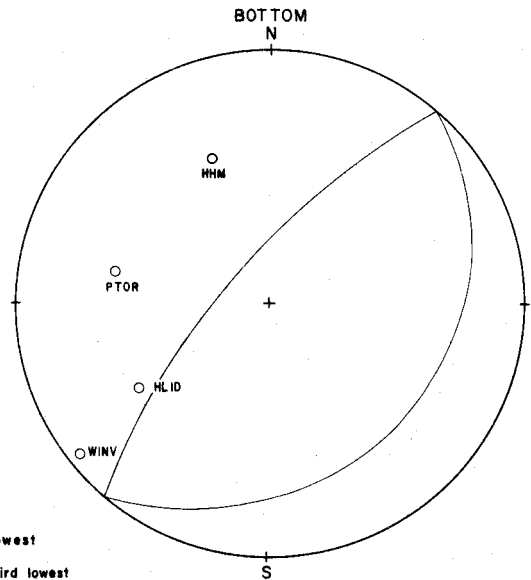


Figure 42. Fault-plane solution for earthquake of February 24, 1963 projected on bottom half of focal sphere.

Range, a normal fault trending northeast. Faults near the earthquakes (Ross, Andrews, Witkind, 1955) trended NW, N, or E.

Two minimum solutions were found for earthquake No. 20, one computed with the present method and one determined by the Byerly technique. Three minimum orientations of fault attitudes were computed for No. 21, a crustal earthquake, two using $i_h = 119.3^\circ$ and one using $i_h = 117^\circ$ for the Pn wave. The solution for No. 22 was the only one which was calculated by using both p and Pn wave amplitudes.

Reliability of the Fault-Plane Solutions

Accuracy of First-Motion Directions

Inconsistency of direction of P wave first motions recorded at a seismic station often occurs because of instrument malfunction and/or reading errors. Such inaccuracies cannot be evaluated correctly without a large distribution of closely spaced stations. Therefore, the inconsistency of seismograms traced by individual stations has not been examined statistically in the present study.

Possible Measurement Errors

An estimate of the possible errors is: in amplitude 5%; in period 10%; in response curves 10%; and in magnification 10%.

The total percentage of error in the calculation of the particle velocity is calculated at 18%. Not taking into account possible errors in crustal structure and amplitude conversion factors, the largest percentage error for particle velocity ratios is expected to be 25%.

Variations of the Angles i_h and Amplitude Conversion Factors

The most important factor in the calculation of the angle of incidence i_h (at the focus) was the focal depth. Figures 14 and 15 illustrate the variation of the angle i_h with epicentral distance for different focal depths and crustal sections. These figures show an inflection of the curves at $i_h = 90^\circ$ at epicentral distances of 0.5° to 1.0° . This inflection moves to greater epicentral distances with greater focal depths. Little effect in these curves occurs with changes in crustal structure. Small variations in these curves have considerable effect on the source amplitudes.

For the relation between the angle i_h and epicentral distances Δ , the present study assumed straight rays, while the Hodgson-Storey (1953) technique assumed curved rays. Figure 43 illustrates the plotting of the (i_h, Δ) data obtained by Hodgson and Storey (1953) for focal depths of 0 and 60 km and the data for 60 km obtained in the present study. Differences in the two 60 km curves may be due to (1) curved rays versus straight rays and (2) difference in velocity structure.

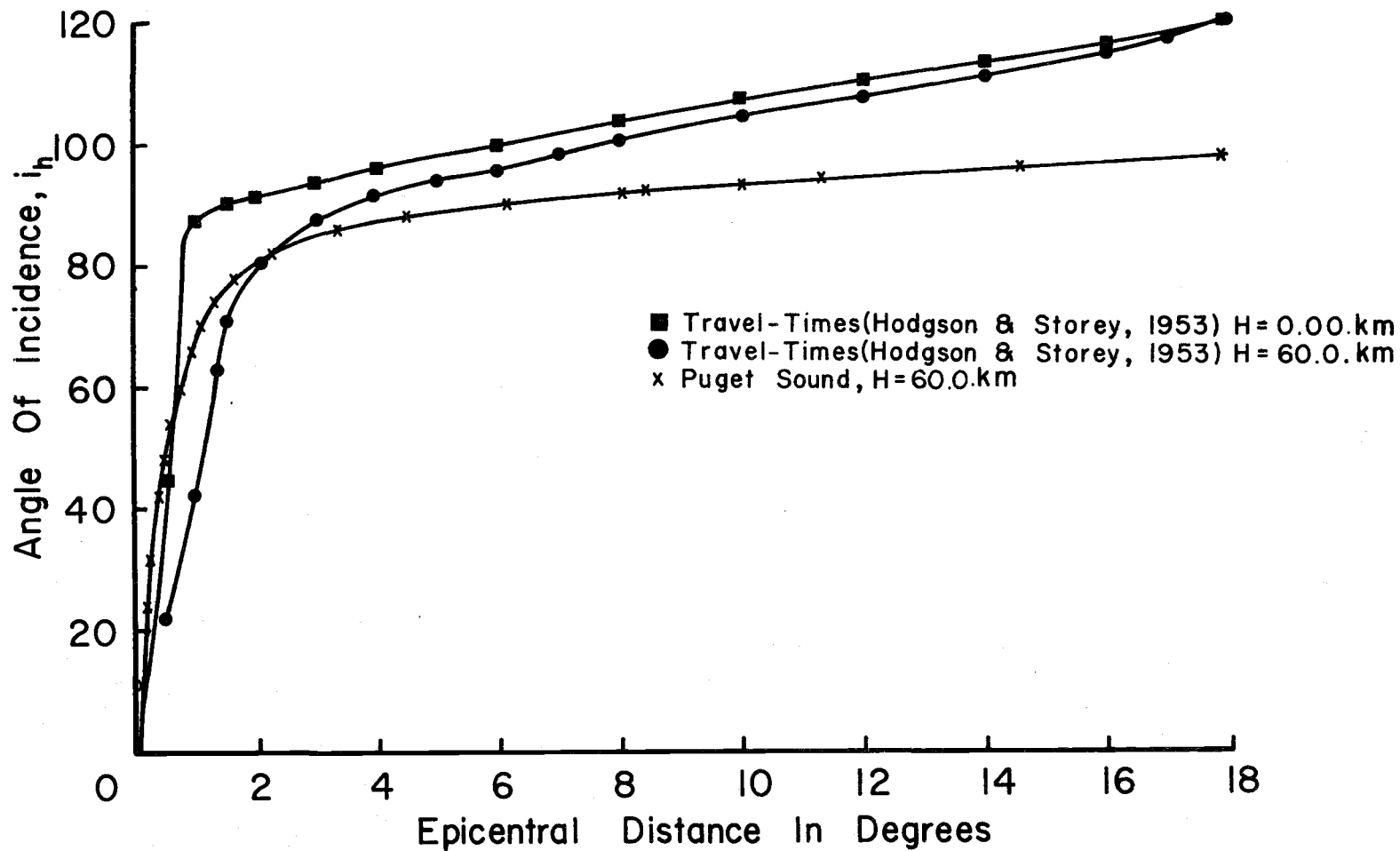


Figure 43. Comparison of the effects of straight and curved ray paths on calculated source incidence angles.

Accuracy of Orientations for Obtaining Fault-Plane Solutions

Because the Euler Angles at 10° increments were used to calculate fault-plane orientations, the most accurate orientations could be overlooked. As no orientations were computed for obtaining solutions at 10° increments for several earthquakes, these were again studied with 5° increments. Only one orientation for an earthquake was obtained. Subsequently, a 2° error in the angle of incidence i_h was found for some of these earthquakes. When the data for these earthquakes was rerun with the 2° correction, several fault-plane orientations for each earthquake were obtained. At present, it appears that the determination of angle i_h , or the focal depth, has a profound effect on the orientations and that 10° increments are sufficient to give accurate fault-plane solutions.

Effect of Amplitude Deviations on Orientations

Errors existing in experimental source amplitudes can cause changes in fault-plane orientations. Such changes are difficult to measure unless the relation of each fault plane to the seismic station is known.

Errors in experimental source amplitudes can be expressed in terms of theoretical amplitudes. The equation of the theoretical radiation pattern for the P wave is

$$A = A_o \sin 2\theta \cos\phi \quad (18)$$

The fractional error in the theoretical amplitudes is

$$\left[\frac{\delta A}{A} \right]_{\theta} = \left(\frac{\sin 2p}{\sin 2\theta} - 1 \right) \quad (19a)$$

$$\left[\frac{\delta A}{A} \right]_{\phi} = \left(\frac{\cos p}{\cos \phi} - 1 \right) \quad (19b)$$

Where θ and ϕ define the relative position of the theoretical amplitude to the fault plane and p defines the relative position of the corrected theoretical amplitude to the fault plane.

Assuming various values in Equations (19a) and (19b) it becomes apparent amplitude errors may cause small changes in dip for seismic stations in the vicinity of a fault or auxiliary plane and large changes in dip for stations midway between the planes.

Effect of Wave Attenuation on Orientations

The evidence for establishing values of $1/Q$, the absorption factor, is very limited. Asada and Takano (1963) have ascertained the values of Q for the frequency range 1 to 7 cps in earthquake studies. They determined Q values as 600 to 1200 for foci above the Moho at epicentral distances 9° to 25° and Q values as 400 to 2400 for foci beneath the Moho at epicentral distances 9°

to 19° .

Sarmah (1967), analyzing P waves from nuclear explosions, found that a composite Q value was between 100 to 400 in the frequency range 0.7 to 1.0 cps at epicentral distances of 9° to 20° .

Variability of Q values for different regions, focal depths and seismic sources is evident in these studies. Attenuation corrections in the present study were applied only to four earthquakes. While no absorption ($Q = \infty$) was assumed previously, $Q = 200$ and 400 was assumed for the four earthquakes. These Q values are illustrated in Figure 44, as a function of travel times. Table VI shows source amplitudes of the P wave calculated from Q values for each earthquake.

For the Tacoma earthquake of April 29, 1965, new orientations were attempted on the basis of the 200 and 400 Q values. No orientations were obtained for determining fault-plane solutions indicating that the Q values had increased relative errors (i. e., fractional deviations) between the theoretical and observed amplitude ratios.

For the Montana earthquake of February 16, 1963 the orientations, calculated for the Q values, deviated only slightly from the initial solutions which assumed $Q = \infty$. These slight deviations could be due to the Q correction of the source amplitude at each seismic station appearing almost equivalent. All of these solutions are shown in Figure 45.

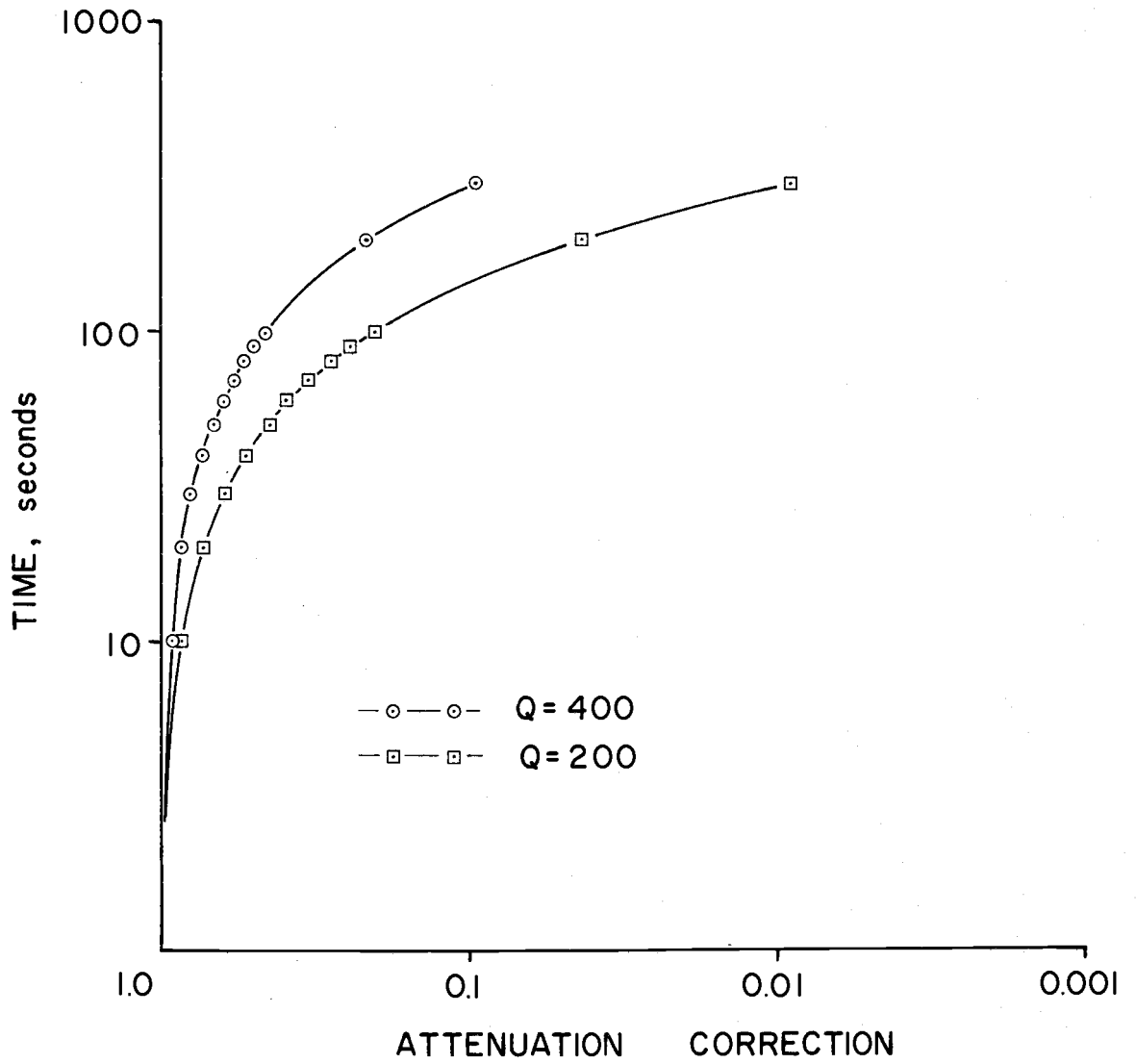


Figure 44. Attenuation for $Q = 200$ and $Q = 400$ in relation to travel time for waves of one cps.

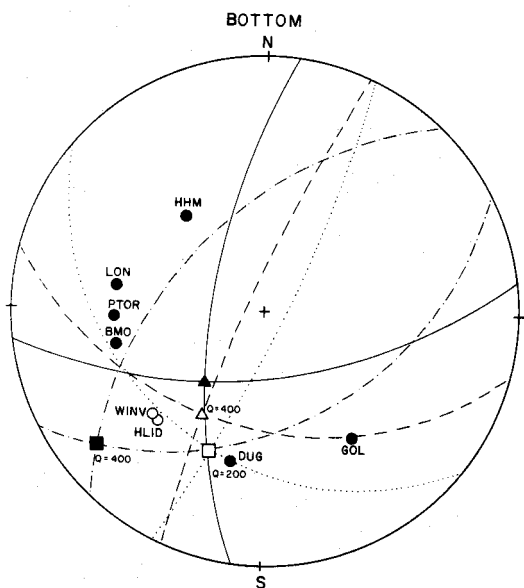


Figure 45. Fault-plane solutions for earthquake of February 16, 1963 using $Q = \infty$, $Q=200$, and $Q = 400$.

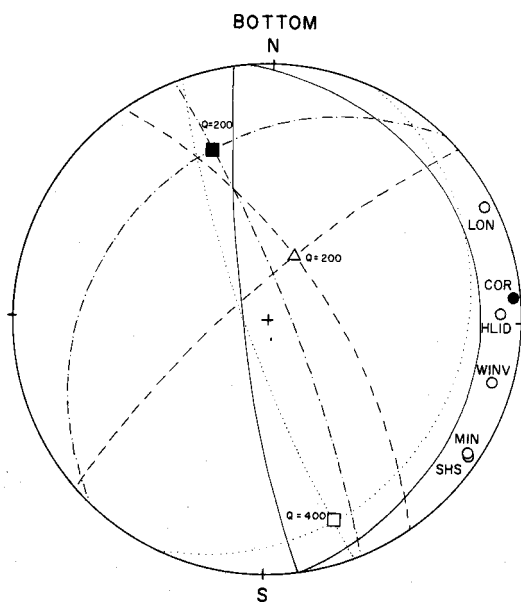
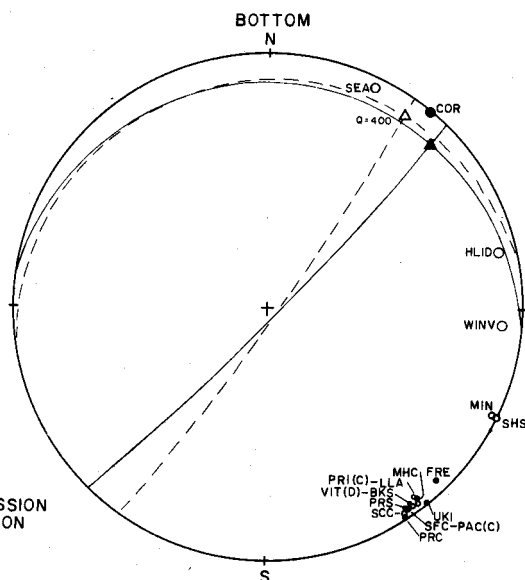
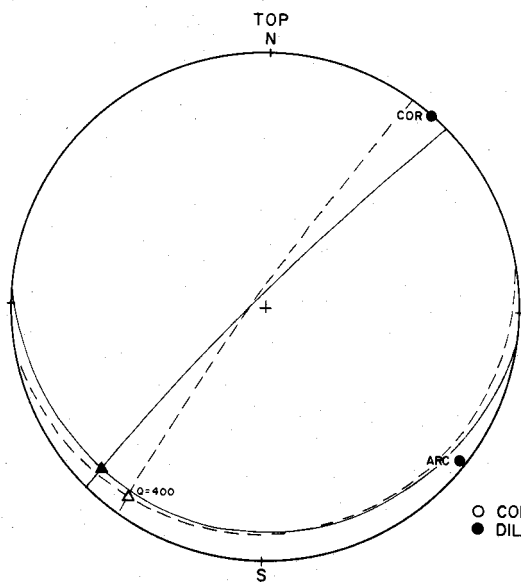


Figure 46. Fault-plane solutions for earthquake of June 25, 1963 (09:39:27.7) using $Q = \infty$, $Q = 200$, and $Q = 400$.



○ COMPRESSION
● DILATATION

Figure 47. Fault-plane solutions for earthquake of August 22, 1963 using $Q = \infty$ and $Q = 400$.

Table VI. Effect of Q Values on Source Amplitudes.

Earthquakes	Station	Amp.	Q ₁	Amp. Q ₁	Amp. % Increase	New Amp. Ratio	Q ₂	Amp. Q ₂	Amp. % Increase	New Amp. Ratio	Travel Time
April 29, 1965	FSJ	35.4	0.2	196.6	455%	0.0	0.4	80.4	127%	0.1	104.8
	DUG	511.4	0.1	7306.2	1328%	11.0	0.3	1763.6	245%	8.6	151.1
	BKS	66.4	0.1	664.4	900%	3.4	0.3	204.4	203%	2.5	137.1
Aug. 22, 1963	WINV	6.0	0.2	28.4	377%	0.6	0.5	12.7	113%	0.9	99.0
	HLID	5.3	0.1	47.7	810%	0.3	0.4	15.0	186%	0.2	130.2
	BKS	53.8	0.3	188.8	250%	6.7	0.5	99.6	85%	7.9	79.0
June 25, 1963	HLID	3.6	0.1	45.0	1240%	2.0	0.3	13.3	269%	1.1	158.1
	LON	6.5	0.3	24.9	285%	0.5	0.5	12.4	92%	0.8	85.2
	WINV	4.9	0.1	48.8	900%	1.0	0.3	15.3	213%	1.2	134.7
Feb. 16, 1963	BMO	3.7	0.3	11.3	203%	0.7	0.6	6.5	72%	0.9	70.3
	WINV	3.3	0.2	15.8	655%	0.2	0.5	7.2	117%	0.2	100.0
	LON	13.6	0.2	84.8	525%	7.5	0.4	33.1	144%	5.1	111.0

Q₁ = 200

Q₂ = 400

For the August 22, 1963 shock off the coast of northern California, the Q value of 200 increased relative errors, so that no orientation was found to compare with the first motions of the earthquake. Taking a Q value of 400, an orientation was calculated which compared favorably with the initial solution assuming $Q = \infty$ (Figure 47).

For the June 25, 1963 earthquake off the coast of Oregon, the newly calculated orientations showed marked decreases in relative errors. Specifically, an orientation for $Q = 400$ was close to the initial solution; while the orientation with minimum error for $Q = 200$ agreed with the attitude of one plane in the initial solution and disagreed 90° in dip with the attitude of the other plane. However, an orientation of attitudes differing only .05 in deviation from the orientation with the minimum error nearly coincided with the initial solution. The first motion data of the P wave were not sufficient to distinguish between the initial solution and the two orientations obtained for $Q = 200$ (Figure 46).

The attenuation analysis of these orientations, except that of the June 25, 1963 earthquake, would indicate that the effective Q is larger than 400, and that changes as large as 100% in the source amplitudes may have little effect on fault-plane solutions.

General Tectonic Forces in Western America

The geographical locations of earthquakes for which fault-plane solutions were obtained in this and other studies are shown in Figure 48.

The fault planes for each earthquake are useful in interpreting stress distribution just prior to the shock. The relation between the directions of the maximum, intermediate and minimum principal stresses and the fault planes is established by the Mohr-Coulomb theory (Clark, 1966; Jacobs, Russel and Wilson, 1959). The theory establishes that fracture occurs along planes less than 45° from the direction of maximum principal stress. Rock experiments have shown that fracture occurs on the average at 30° . Using 30° , two maximum and minimum principal stresses and an intermediate principal stress can be determined from two possible fault planes. The five directions for the stresses have been determined from fault-plane solutions listed in Table V. These solutions were determined with the Byerly method for earthquakes in western North America. The five stresses for each solution are presented in Figure 49. The directions of stresses for earthquakes attained in the present study are plotted in Figure 50. These maximum stresses tend to be vertical while the minimum stresses are random. Solutions using the Byerly method show the minimum stresses in

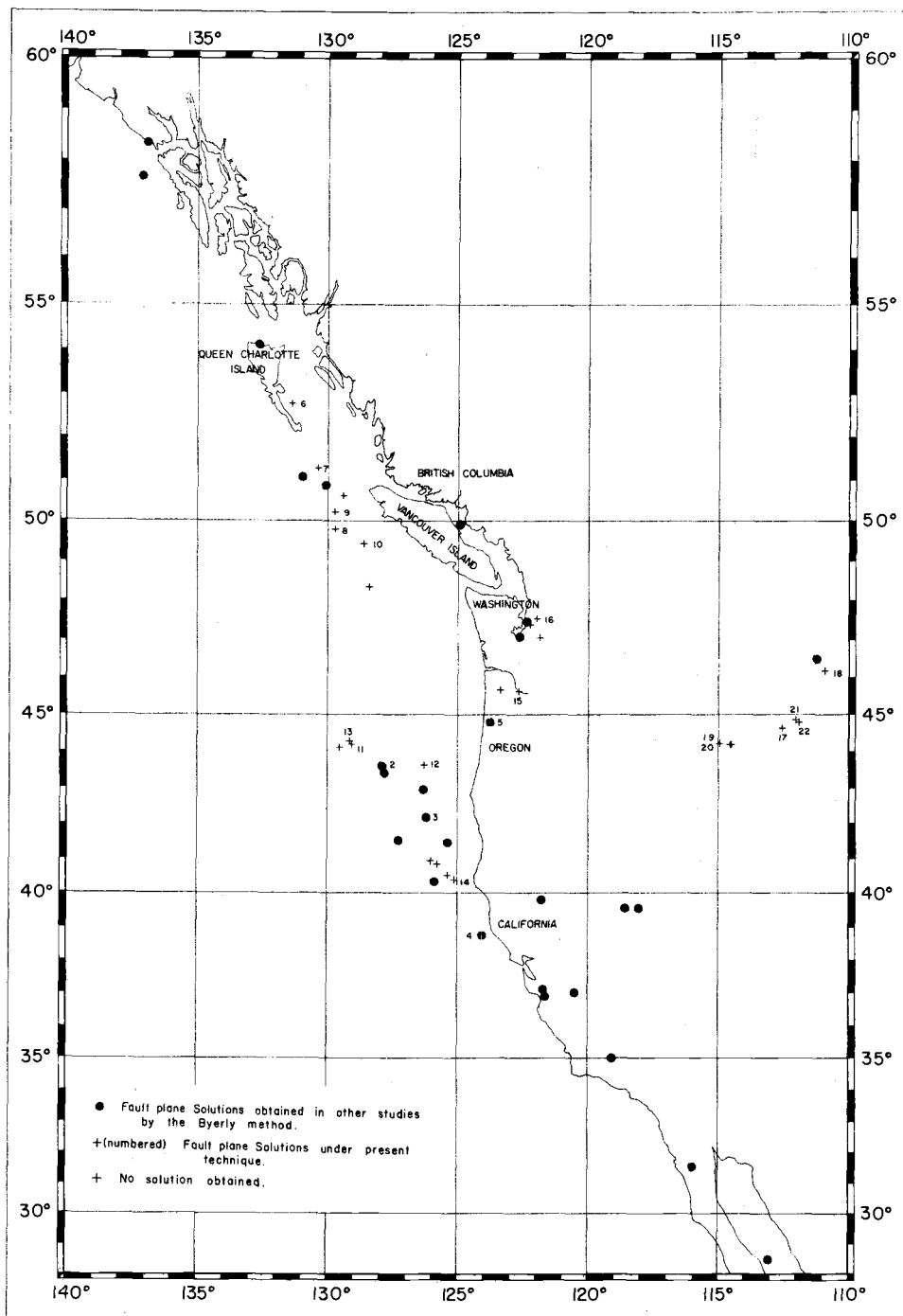


Figure 48. Location of earthquakes used in the present investigation.

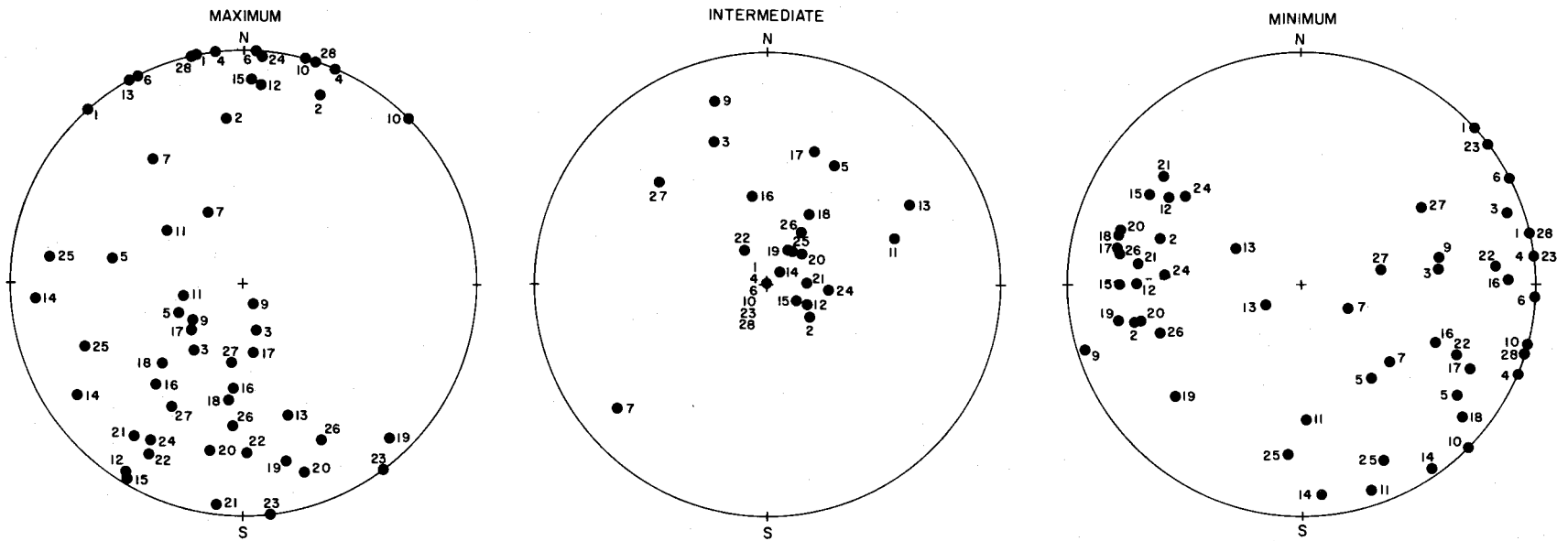


Figure 49. Direction of maximum, intermediate, and minimum principal stresses found from fault-plane solutions determined by the Byerly method. Numbered earthquakes listed in Table V.

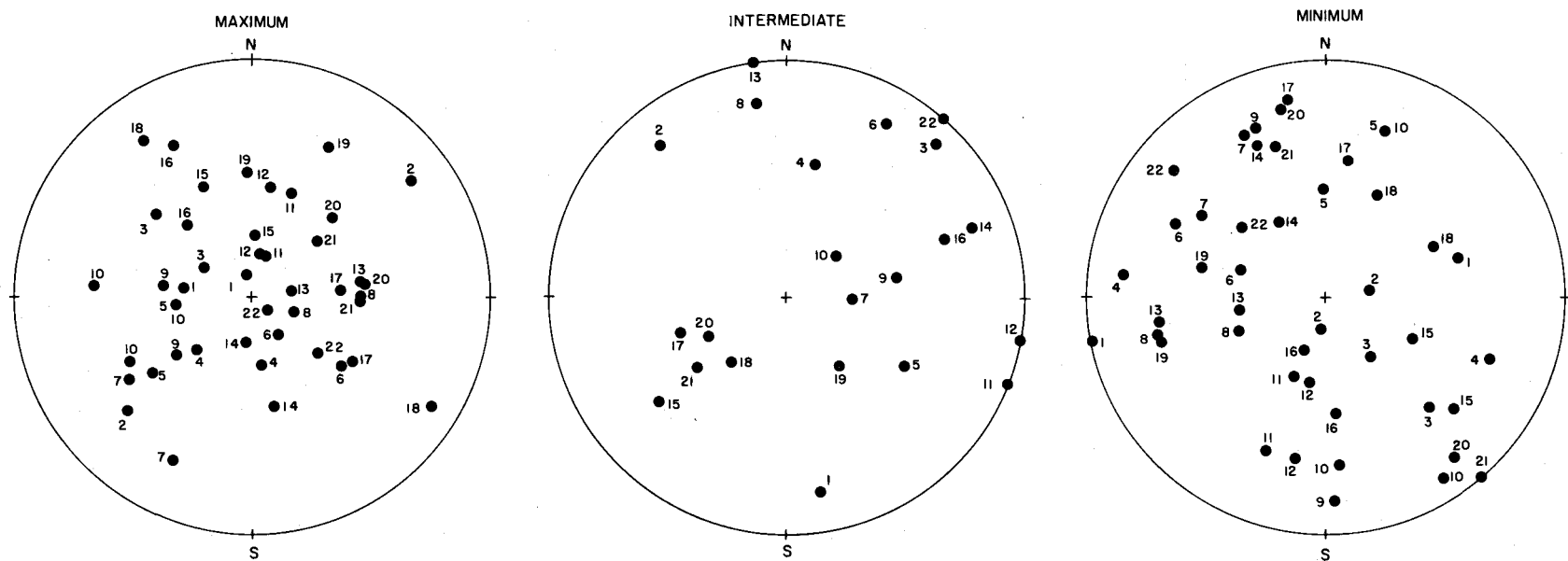


Figure 50. Direction of maximum, intermediate, and minimum principal stresses found from fault-plane solutions determined by the present method. Numbered earthquakes listed in Table IV.

east-west direction while the maximum stresses are in other directions. The intermediate directions of stresses have similar patterns in Figures 49 and 50.

Two hypotheses on the interpretation of the tectonic forces can be proposed:

Stress system A. Large earthquakes in the upper crust occur in areas where the minimum principal stress is in an east-west direction. Small earthquakes in the lower part of the crust or in the upper mantle occur where the maximum principal stress is vertical.

Stress system B. Large earthquakes occur where the minimum principal stress is in an east-west direction. Small earthquakes occur along planes of weakness created by an east-west minimum principal stress in areas where the maximum stress is vertical.

Difference between A and B. In stress system A fault planes of small earthquakes can strike in any direction, while in B, strikes of fault planes in small earthquakes are restricted by the east-west minimum principal stress.

Before either of these hypotheses can be pursued, a careful analysis of focal depths must be made. A change in focal depth for an earthquake can change the fault-plane solution which indicates normal or thrust fault to a strike-slip fault or vice versa. This could affect the stress patterns.

CONCLUSIONS

1. The new technique showed that the first motions of a short-period P wave for small earthquakes at three local stations can determine a fault-plane solution. The fault-plane orientation, obtained from the direction and amplitude of first motions, compared favorably with directions from other stations. The calculated orientation usually fitted the first motion data for the earthquake when seismic stations were selected on two criteria: (1) high signal to noise ratios; (2) large angular separations on the focal sphere.
2. Some fault-plane solutions obtained in the present study compared favorably with solutions reached by other investigators using the Byerly method. When disagreement occurred, Byerly fault-plane solutions were not constrained with first motions or a difference was assumed in focal depths. The fault-plane solutions and geologic structures for the regions showed reasonable agreement. These comparisons tend to confirm that the radiation pattern of the short-period P wave for Type I and II mechanisms is valid in determining fault-plane solutions.
3. As P-wave radiation patterns were established, the study showed that source amplitudes can be determined correctly from the amplitude conversion factors used. However, a reliability study

of the radiation patterns revealed that, when errors occurred in determining source amplitudes, the fault planes could change position. Conversion factors incorporating small Q wave attenuation caused great inaccuracies in fractional deviations, although inaccuracies as low as 100% in source amplitudes produced little change in fault-plane orientations.

4. Straight rays, changes in focal depth and in velocity structures determined variations in the angle of incidence i_h . Angles of incidence i_h were employed in calculation of amplitude conversion factors. Abrupt changes in these values occurred when the focal depth shifted from above to beneath the Moho. This analysis showed that for foci beneath the Moho, i_h varies little for focal depth at epicentral distances greater than 2° , and radically for focal depth at epicentral distances less than 2° . The effect of i_h variation is small when compared with the velocity structure. As a change in focal depth radically affects the position of the fault plane, the deduced stress pattern also can be affected radically. Therefore, an accurate determination of the focal depth of an earthquake should precede stress studies.
5. Angles of incidence at the surface of the earth were determined for the short-period P wave to obtain the incident amplitudes from the recorded amplitudes. These angles appeared to show local velocity structures and/or dips of lower boundaries,

especially of the Moho. Most P angles of incidence were lower than the critical angle of incidence for the S wave. For $\sigma = 1/4$ this means that the polarization of S waves can be found at epicentral distances less than 20° . A study of S waves revealed that multiple angles of incidence can be determined; however, comparable S-wave polarizations can be calculated from these angles of incidence.

6. The fault-plane solutions resulted largely in dip-slip components. A stress comparison of these solutions with fault planes determined by investigators using the Byerly method was made. As a result of this comparison, two stress systems for western North America are proposed.
7. The technique developed can be applied to weak and active earthquake regions with a minimum of local stations. Fault planes can be determined with ease for such seismic systems, once the amplitude conversion factors and i_h, Δ curves have been calculated. The following considerations should be taken into account in applying this technique: (1) the success of the technique may be related to the use of amplitude ratios. These ratios can remove the effects of source size, velocity structure and wave attenuation when they are the same at seismic stations; (2) a knowledge of crust and upper mantle is not a requirement although accurate determination of focal depth is

necessary; (3) statistical correlations of the minimum orientations may be helpful when studying micro-earthquakes; (4) a CDC 3300 or comparable computer should be available to determine the fault-plane solutions (cost about \$7 per solution).

BIBLIOGRAPHY

- Adams, W. M. 1958. A study of earthquake mechanisms using S wave data. *Bulletin of the Seismological Society of America* 48:201-220.
- Algermissen, S. T. and Samuel T. Harding. 1965. The Puget Sound, Washington, earthquake of April 29, 1965. Washington, D. C., U. S. Department of Commerce, Coast and Geodetic Survey. 51 p.
- Asada, Toshi, and Kei Takano. 1963. Attenuation of short period P waves in the mantle. *Journal of Physics of the Earth* 11:25-34.
- Ben-Menahem, Ari. 1967. Source studies from isolated seismic signals. In: *Proceedings of the Vesiac conference on the current status and future prognosis for understanding the source mechanism of shallow seismic events in the 3 to 5 magnitude range*. Vesiac report. Ann Arbor, University of Michigan, Willow Run Laboratories. 312 p.
- Berry, M. J. and G. F. West. 1966. Reflected and head wave amplitudes in a medium of several layers. In: *The earth beneath the continents*, ed. by John S. Steinhart and T. Jefferson Smith. Washington, D. C., American Geophysical Union. 663 p.
- Bolt, B. A., C. Lomnitz and T. V. McEvelly. 1969. Seismological evidence on the tectonics of central and northern California and the Mendocino escarpment. *Bulletin of the Seismological Society of America*. (In press)
- Brekhovskikh, Leonid M. 1960. *Waves in layered medium*. New York, Academic. 561 p.
- Bullen, K. E. 1963. *An introduction to the theory of seismology*. 3d ed. Cambridge, Cambridge University. 381 p.
- Byerly, Perry. 1926. The Montana earthquake of June 28, 1925. G. M. C. T. *Bulletin of the Seismological Society of America* 16:209-265.
-
1928. The nature of the first motion in the Chilean

earthquake of November 11, 1922. American Journal of Science, 5th Ser., 16:232-236.

Byerly, Perry. 1938. The earthquake of July 6, 1934 amplitude and first motion. Bulletin of the Seismological Society of America 28:1-14.

1955. Nature of faulting as deduced from seismograms. New York, Geological Society of America. (Special Paper no. 62) 75-86.

Byerly, Perry, and William V. Stauder. 1957. Motion at the source of an earthquake. Publications of the Dominion Observatory (Ottawa) 20:255-261.

Chiburis, E. F., Peter Dehlinger and W. S. French. 1965. The Tacoma earthquake of April 29, 1965. The Ore Bin 27:99-100.

Clark, Sydney P., Jr. (ed.) 1966. Handbook of physical constants. New York. 587 p. (Geological Society of America. Memoir 97)

Couch, Richard W. 1969. Gravity and structures of the crust and subcrust in the northeast Pacific Ocean west of Washington and British Columbia. Ph.D. thesis. Corvallis, Oregon State University. (In preparation)

DeBremaecker, J. Cl. 1955. Use of amplitudes. Part I; Pn from 3° to 23° . Bulletin of the Seismological Society of America 45: 219-244.

Dehlinger, Peter. 1952. Shear-wave vibrational directions and related fault movements in southern California earthquakes. Bulletin of the Seismological Society of America 42:155-174.

Dehlinger, Peter, E. F. Chiburis and M. M. Collver. 1965. Local travel-time curves and their geologic implications for the Pacific northwest states. Bulletin of the Seismological Society of America 55:587-607.

Dehlinger, P., R. W. Couch, and M. Gemperle. 1968. Continental and oceanic structure from the Oregon coast westward across the Juan de Fuca Ridge. Canadian Journal of Earth Sciences 5:1079-1090.

- Douglas, A. 1967. P-signal complexity and source radiation patterns. In: Proceedings of the Vesiac Conference on the current status and future prognosis for understanding the source mechanism of shallow seismic events in the 3 to 5 magnitude range. Vesiac report. Ann Arbor, University of Michigan, Willow Run Laboratories. 312 p.
- Eaton, Jerry P. 1963. Crustal structure from San Francisco, California, to Eureka, Nevada, from seismic-refraction measurements. *Journal of Geophysical Research* 68:5789-5806.
- Engdahl, Eric R. and Robert H. Gunst. 1966. Use of a high speed computer for the preliminary determination of earthquake hypocenters. *Bulletin of the Seismological Society of America* 56:325-336.
- Fara, H. D. 1964. A new catalogue of earthquake fault plane solutions. *Bulletin of the Seismological Society of America* 54:1491-1517.
- Galitzin, B. 1914. *Verlesungen über Seismometrie*, ed. by O. Hecker. Leipzig, Tuebner. p. 437-443. (Cited in: Stauder, William, S. J. 1960. S waves and focal mechanisms; the state of the question. *Bulletin of the Seismological Society of America* 50:341.)
- Goldstein, Herbert. 1959. *Classical mechanics*. Readings, Massachusetts, Addison-Wesley. 399 p.
- Gutenberg, B. 1944. Energy ratio of reflected and refracted seismic waves. *Bulletin of the Seismological Society of America* 34:85-102.
- _____ 1952. SV and SH. *Transactions of the American Geophysical Union* 33:573-584.
- _____ 1956. Effects of ground on shaking in earthquakes. *Transactions of the American Geophysical Union* 37:757-760.
- _____ 1959. *Physics of the earth's interior*. New York, Academic. 240 p.
- Heelan, Patrick A. 1953. On the theory of head waves. *Geophysics* 18:871-893.

Hodgson, John H. and W. G. Milne. 1951. Direction of faulting in certain earthquakes of the North Pacific. *Bulletin of the Seismological Society of America* 41:221-242.

Hodgson, John H. and R. S. Storey. 1953. Tables extending Byerly's fault-plane techniques to earthquakes of any focal depth. *Bulletin of the Seismological Society of America* 43:49-62.

_____ 1954. Direction of faulting in some of the larger earthquakes of 1949. *Bulletin of the Seismological Society of America* 44:57-84.

Hodgson, John H. 1957a. Nature of faulting in large earthquakes. *Bulletin of the Geological Society of America* 68:611-644.

_____ 1957b. The null vector as a guide to regional tectonic patterns. *Publications of the Dominion Observatory (Ottawa)* 20:369-384.

Hodgson, John H. and J. I. Cock. 1957. Direction of faulting in the larger earthquakes of 1954-1955. *Publications of the Dominion Observatory (Ottawa)* 19:221-258. (Cited in: Hodgson, John H., 1957. The null vector as a guide to regional tectonic patterns. *Publications of the Dominion Observatory (Ottawa)* 20:372.)

Hodgson, John H. and W. M. Adams. 1958. A study of the inconsistent observations in the fault-plane project. *Bulletin of the Seismological Society of America* 48:17-32.

Hodgson, John H. and A. E. Stevens. 1958. Directions of faulting in the larger earthquakes of 1955-1956. *Publications of the Dominion Observatory (Ottawa)* 19:281-317. (Cited in: Hodgson, John H., 1957. The null vector as a guide to regional tectonic patterns. *Publications of the Dominion Observatory (Ottawa)* 20:372.)

Honda, H. A., A. Masotsuka and K. Emura. 1956. On the mechanism of earthquakes and the stresses producing them in Japan and vicinity. (Second paper). *Science Reports (Sendai, Japan), Ser. 5, Geophysics*, 8:186-205. (Cited in: Honda, Hirokichi. 1957. The mechanisms of the earthquakes. *Publications of the Dominion Observatory (Ottawa)* 20:296.)

- Honda, Hirokichi. 1957. The mechanism of the earthquakes. Publications of the Dominion Observatory (Ottawa) 20:295-340.
- Jacobs, J. A., R. D. Russel and J. Tuzo Wilson. 1959. Physics and geology. New York, McGraw-Hill. 424 p.
- Kasahara, Keichi. 1963. Computer program for a fault-plane solution. Bulletin of the Seismological Society of America 53:1-13.
- Keylis-Borok, V. I. 1957. The study of earthquake mechanisms. Publications of the Dominion Observatory (Ottawa) 20:279-294.
- Knopoff, L. 1960. Analytical calculation of the fault-plane problem. Publications of the Dominion Observatory (Ottawa) 24:309-316.
- Lomnitz, C. and Bruce A. Bolt. 1967. Evidence on crustal structure in California from Chase V explosion and the Chico earthquake of May 24, 1966. Bulletin of the Seismological Society of America 57:1093-1114.
- McConnell, Robert K., Jr. and Gillian H. McTaggart-Cowan. 1963. Crustal seismic refraction profiles: A compilation. Toronto, University of Toronto. 54 p. (Scientific Report no. 8 on Contract no. AF 19 (628)-22)
- Macelwane, J. B. 1932. Introduction to theoretical seismology. Saint Louis, St. Louis University. 366 p.
- McEvelly, T. V. 1966. Preliminary Seismic Data. June-July 1966. Parkfield earthquakes of June 27-29, 1966, Monterey and San Luis Obispo Counties, California-Preliminary Report. Bulletin of the Seismological Society of America 56:967-971.
-
1967. Detailed study of the November, 1964, earthquake sequence near Corralitos, California. In: Proceedings of the Vesiac conference on the current status and future prognosis for understanding the source mechanism of shallow seismic events in the 3 to 5 magnitude range. Vesiac report. Ann Arbor, University of Michigan, Willow Run Laboratories. 312 p.
- Mikumo, Taheshi. 1962. Mechanism of local earthquakes in Kwanto region, Japan, derived from amplitude relation of P and S

- waves. Bulletin of the Earthquake Research Institute 40:399-424.
- Monachov, F. I. 1950. Some questions concerning the polarization of transverse seismic waves (In Russian) Izvestia Akademii Nauk SSR, Ser. Geographiceskaya and Geophyzicheskaya, 14: 501-513. (Cited in: Stauder, William. 1960. S waves and focal mechanisms: the state of the question. Bulletin of the Seismological Society of America 50:341.)
- Nafe, J. E. and C. L. Drake. 1961. Physical properties of marine sediments. New York. (Columbia University. Lamont Geological Observatory. Technical Report 2. CU-3-61, June) (Cited in: Dehlinger, P., R. W. Couch and M. Gemperle. 1968. Continental oceanic structure from the Oregon coast westward across the Juan de Fuca Ridge. Canadian Journal of Earth Sciences 5:1084.)
- Nakano, H. 1923. Notes on the nature of the forces which give rise to the earthquake motions. Seismological Bulletin Center Meteorological Observatory, Japan 1:92-120. (Cited in: Honda, Hirokichi. 1957. The mechanism of the earthquakes. Publications of the Dominion Observatory (Ottawa) 20:296.)
- Neumann, Frank. 1930. An analysis of the S wave. Bulletin of the Seismological Society of America 20:15-32.
- Nuttli, Otto. 1961. The effect of the earth's surface on the S wave particle motion. Bulletin of the Seismological Society of America 51:237-246.
- Oregon. Department of Geology and Mineral Industries. 1961. Geological map of Oregon west of the 121st meridian. 1 sheet. Portland, (Miscellaneous Geologic Investigations I-325)
- Pakiser, L. C. 1963. Structure of the crust and upper mantle in the western United States. Journal of Geophysical Research 68: 5747-5756.
- Pakiser, L. C. and D. P. Hill. 1963. Crustal structure in Nevada and southern Idaho from nuclear explosions. Journal of Geophysical Research 68:5757-5766.
- Richter, Charles F. 1958. Elementary seismology. San Francisco, Freeman. 768 p.

- Rinehart, Verril J. 1964. Investigation of twelve earthquakes off the Oregon and northern California coasts. Master's thesis. Corvallis, Oregon State University. 41 numb. leaves.
- Ritsema, A. R. 1962. P and S amplitudes of two earthquakes of the single force couple type. Bulletin of the Seismological Society of America 52:723-746.
-
1967. Problematics of small shallow earthquake mechanisms. In: Proceedings of the Vesiac conference on the current status and future prognosis for understanding the source mechanism of shallow seismic events in the 3 to 5 magnitude range. Vesiac report. Ann Arbor, University of Michigan, Willow Run Laboratories. 312 p.
- Romney, C. 1957. The Dixie Valley-Fairview Peak, Nevada, earthquakes of December 16, 1954. Seismic waves. Bulletin of the Seismological Society of America 47:301-320.
- Ross, Clyde P., David A. Andrews and Irving J. Witkind. 1955. Geologic map of Montana. Butte, Montana. Bureau of Mines and Geology. 2 sheets. (MR-4111)
- Ross, Sylvia H. and Carl N. Savage. 1967. Idaho earth science. Moscow, Idaho Bureau of Mines and Geology. 271 p.
- Sarmah, Suryya Kanta. 1967. Attenuation of compressional waves in the earth's mantle. Ph.D. thesis. Corvallis, Oregon State University. 1967. 80 numb. leaves.
- Scheidegger, Adrian E. 1957. The geometrical representation of fault-plane solutions of earthquakes. Bulletin of the Seismological Society of America 47:89-110.
- Shor, G. G., Jr. 1962. Seismic refraction studies off the coast of Alaska; 1956-1957. Bulletin of the Seismological Society of America 52:37-58.
- Shor, G. G., Jr., P. Dehlinger, H. K. Kirk and W. S. French. 1968. Seismic refraction studies off Oregon and northern California. Journal of Geophysical Research 73:2175-2194.
- Stauder, William. 1960a. The Alaska earthquake of July 10, 1958-- seismic studies. Bulletin of the Seismological Society of America 50:293-322.

- Stauder, William. 1960b. An application of S waves to focal mechanism studies. Publications of the Dominion Observatory (Ottawa) 24: 343-353.
-
- _____ 1960c. S waves and focal mechanisms: the state of the question. Bulletin of the Seismological Society of America 50: 333-346.
- Stevens, Anne E. 1967. S-wave earthquake mechanism equations. Bulletin of the Seismological Society of America 57: 99-112.
- Sutton, George H. and Eduard Berg. 1958. Direction of faulting from first-motion studies. Bulletin of the Seismological Society of America 48: 117-128.
- Tobin, Don G. and Lynn R. Sykes. 1968. Seismicity and tectonics of the northeast Pacific Ocean. Journal of Geophysical Research 73: 3821-3845.
- Tocher, D. 1955. Seismic velocities and structure in northern California and Nevada. Ph.D. thesis. University of California. (Cited in: Hodgson, John H., 1957. The null vector as a guide to regional tectonic patterns. Publications of the Dominion Observatory (Ottawa) 20: 372.)
- Udias, Agustin. 1965. A study of the aftershocks and focal mechanism of the Salinas-Watsonville earthquakes of August 31 and September 14, 1963. Bulletin of the Seismological Society of America 55: 85-106.

APPENDICES

APPENDIX I

THEORETICAL DEVELOPMENT OF THE HEAD WAVE EQUATION

Brekhovskikh (1960) determined the incident wave u , v , w in the directions r , θ , z for a pulsed (point type) source in a cylindrical cavity. The displacements were expressed in terms of cylindrical functions. The equations for the source functions of the P, SV and SH waves determined at large distances were:

$$f_o = iP_1(K) \left(2 \frac{\beta^2}{a^2} \cos^2 \theta - 1 \right) \frac{K \Delta}{8\pi\mu}$$

$$g_o = P_1(K) \cos \theta \frac{\Delta \beta^2}{4\pi\mu a^2}$$

$$h_o = S_1(K) \frac{\cos \theta}{\cos \gamma} \frac{\Delta \beta K}{4\pi i \mu a}$$

where: μ is the rigidity

Δ is the volume of the cavity

K is the wave number

$P_1(K)$ and $S_1(K)$ are the fourier components of the normal and tangential stresses.

The application of the wave displacements to the boundary conditions between the layers showed the wave displacements for the incident and reflected P wave as (Brekhovskikh, 1960):

$$u_1 = - \int_{\Gamma_1} \sigma f_o V_{11} H_1^{(1)}(\sigma r) \exp[-\alpha'(Z + Z_o)] \sin\theta d\theta$$

$$w_1 = - \int_{\Gamma_1} \alpha f_o V_{11} H_o^{(1)}(\sigma r) \exp[-\alpha'(Z + Z_o)] \sin\theta d\theta$$

The displacements for the incident and reflected SV wave were:

$$u_4 = - \int_{\Gamma_1} \sigma \beta g_o V_{22} H_1^{(1)}(\sigma r) \exp[-\beta'(Z + Z_o)] \sin\gamma d\gamma$$

$$w_4 = - \int_{\Gamma_1} \sigma^2 g_o V_{22} H_o^{(1)}(\sigma r) \exp[-\beta'(Z + Z_o)] \sin\gamma d\gamma$$

and the wave displacement for the incident, reflected SH wave was:

$$v_1 = - \int_{\Gamma_1} \sigma h_o V_{33} H_1^{(1)}(\sigma r) \exp[-\beta'(Z + Z_o)] \sin\gamma d\gamma$$

where: V_{11} , V_{22} , V_{33} are the reflection coefficients for incident P, SV, and SH waves respectively,

$$\sigma = K \sin\theta = K' \sin\theta' = k \sin\gamma = k' \sin\gamma'$$

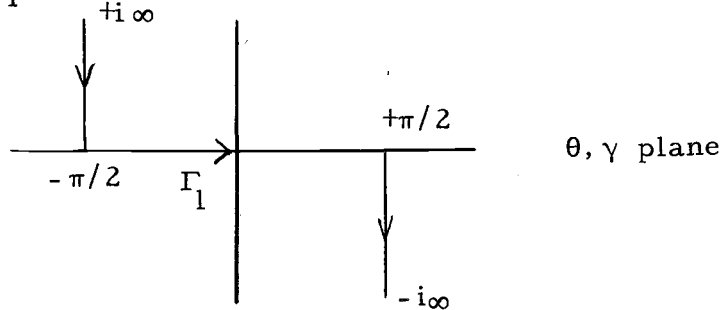
$$\alpha' = -i K \cos\theta$$

$$\beta' = -i k \cos\gamma$$

Z is the distance the receiver is above interface,

Z_0 is the distance the source is above interface,

$H_0^{(1)}(\sigma r)$, $H_1^{(1)}(\sigma r)$ are Hankel functions.



The path of the intervals Γ_1 is from $-\pi/2 + i\infty$ to $\pi/2 - i\infty$ for the variable θ or γ . The transformation from this path Γ_1 to the path which determines the displacement of a head wave or reflected wave can be made after considering the singularities.

The poles are determined from (Brekhovskikh, 1960, p. 310-311).

$$\alpha''P = -Q$$

where P and Q comprise the reflection coefficients and are functions of wave numbers, rigidities and angles of incidence across the boundary.

The displacements u_1 , w_1 , u_4 , w_4 and v_1 have been evaluated in the present study. To illustrate the procedure used in determining these displacements u_1 will be used as an example.

V_{11} , the reflection coefficient in the integrand of u_1 , has three branch points:

$$\theta_{K'} = \arcsin \frac{K'}{K} \quad (1)$$

$$\theta_k = \arcsin \frac{k}{K} \quad (2)$$

$$\theta_{k'} = \arcsin \frac{k'}{K} \quad (3)$$

In the present analysis, only the branch point $\theta_{K'}$ will be considered.

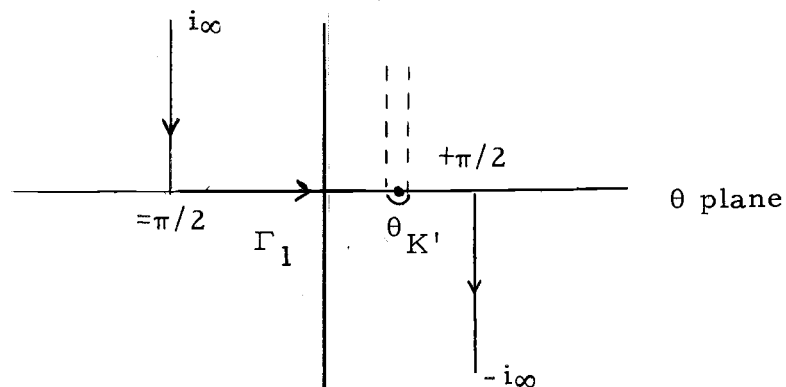
The Hankel function can be replaced by its asymptotic function provided $Kr \gg 1$

$$H_1^{(1)}(\sigma r) = \sqrt{\frac{2}{\pi \sigma r}} \exp \left[i \sigma r - \frac{3}{4} \pi i \right]$$

The displacement can be written:

$$u_1 = - \sqrt{\frac{2}{\pi r}} \int_{\Gamma_1} K^{1/2} \sin^{3/2} \theta f_o V_{11}(\theta) \exp \left[iK(r \sin \theta + \cos \theta (Z + Z_o)) - \frac{3}{4} i \pi \right] d\theta$$

The contribution from the branch point (1) gives the head wave for u_1 . The path of integration is modified from Γ_1 to an integration along the branch cuts and the branch point $\theta_{K'}$.



The displacement u_1 will be

$$u_1 = -\sqrt{\frac{2}{\pi r}} \int_{\theta'_k}^{i\infty} \Phi(\theta) K^{1/2} \sin^{3/2} \theta f_0 \exp [iK(r \sin \theta + \cos \theta (Z + Z_0)) - \frac{3}{4} \pi i] d\theta$$

where: $\Phi(\theta) = V_{11}^+(\theta) - V_{11}(\theta)$

For convenience Φ can be written

$$\Phi(\theta) = 2\alpha'' V_{11}^*(\theta)$$

where: $\alpha'' = iK \left(\frac{K'^2}{K^2} - \sin^2 \theta \right)^{1/2}$

The integral can be modified from the two-layer medium to the multi-layered medium (Berry and West, 1966) by the following substitutions.

Replace $(Z + Z_0) \cos \theta$ by $\sum_{j=1}^{2n} h_j \frac{(1 - p_j^2 V_j^2)^{1/2}}{V_j}$ where,

in the case of n layers, h_j is the thickness of the layer and V_j is the velocity ratio defined as

$$j \leq n \quad n+1 \leq j \leq 2n-1 \quad 2n$$

$$V_j = a_j / a_1 \quad \frac{a_{2n+1-j}}{a_1} \quad 1$$

Replace $\theta_{K'} = p_c = \frac{a_1}{a_{n+1}}$ and $\alpha'' = iKV_{n+1}^{-1} (1 - V_{n+1}^2 p^2)^{1/2}$

Also, $\Phi(\theta)$ includes the transmission coefficients for the P waves incident at each of the n layers.

The integral is rewritten in the new form using $p = \sin \theta$ as:

$$u_1 = -\sqrt{\frac{2}{\pi r}} \int_{p_c}^{i\infty} \Phi(p) \frac{K^{1/2} p^{3/2}}{(1-p^2)^{1/2}} f_0 \exp \left[iK(pr + \sum_j h_j \frac{(1-p^2 V_j^2)^{1/2}}{V_j} \right) - (3/4)\pi i \right] dp$$

The integral is now determined by the method of steepest descents. The path of integration is modified along the branch cut so that the exponential function decreases most rapidly.

This is accomplished by replacing the arguments of the exponential function by its Taylor series expansion which is:

$$K(p_c r + \sum_{j=1}^{2n} h_j \frac{(1-p_c^2 V_j^2)^{1/2}}{V_j}) + iq K(r - p_c \sum_{j=1}^{2n} V_j h_j (1-p_c^2 V_j^2)^{-1/2})$$

where $p = p_c + iq$ and $dp = idq$ so the limits are from 0 to ∞ for q .

The term $2a''$ becomes

$$2a'' = 2iKV_{n+1}^{-1} (1 - V_{n+1}^2 p_c^2 - 2iq p_c V_{n+1}^2 + q^2 V_{n+1}^2)^{1/2}$$

Since the path of most rapid decrease has been chosen, only small values of q are important. Therefore, the equation becomes

$$2\alpha'' = -2\sqrt{2} p_c^{1/2} i^{1/2} q^{1/2}$$

Making these modifications the integral equation is

$$u_1 = \frac{+4}{\sqrt{\pi r}} \int_0^\infty \frac{p_c^2}{(1-p_c^2)^{1/2}} f_o V_{11}^* \exp[iK(p_c r + \sum_{j=1}^{2n} h_j \frac{(1-p_c^2 V_j^2)^{1/2}}{V_j})] \\ \exp[-qK(r-p_c \sum_{j=1}^{2n} h_j V_j (1-p_c V_j^2)^{-1/2})] i\sqrt{i} \exp[-3/4\pi i] q^{1/2} dq$$

This integral equation can be expressed in the form

$$\int_0^\infty A(p_c) \exp[-aq] q^{1/2} dq$$

which can be integrated, letting $q = x^2$, $dq = 2x \cdot dx$ as

$$\int_0^\infty \exp[-ax^2] 2x^2 dx = \frac{2}{4} \frac{1}{a} \sqrt{\frac{\pi}{a}} = \frac{1}{2} \frac{\sqrt{\pi}}{K^{3/2} L^{3/2}}$$

The final form of the integral is written

$$u_1 = \frac{2}{r^{1/2} L^{3/2}} \frac{p_c^2}{(1-p_c^2)^{1/2}} f_o V_{11}^* (p_c) \exp[iK(p_c r + \sum_{j=1}^{2n} h_j \frac{[1-p_c^2 V_j^2]^{1/2}}{V_j})]$$

where

$$L = r - \sum_{j=1}^{2n} p_c h_j (1 - p_c^2 v_j^2)^{-1/2}$$

The displacements for P, SV and SH waves are:

$$u_1 = \frac{2}{r^{1/2} L^{3/2}} \frac{p_c^2}{(1 - p_c^2)^{1/2}} Q_{PP}$$

$$w_1 = \frac{2}{r^{1/2} L^{3/2}} p_c Q_{PP}$$

$$v_1 = \frac{2}{r^{1/2} L^{3/2}} \frac{p_c^2}{(1 - p_c^2)^{1/2}} Q_{SHSH}$$

$$u_4 = \frac{-2}{r^{1/2} L^{3/2}} p_c^2 Q_{SVSV}$$

$$w_4 = \frac{2}{r^{1/2} L^{3/2}} \frac{p_c^3}{(1 - p_c^2)^{1/2}} Q_{SVSV}$$

$$\text{where: } Q_{PP} = f_o V_{11}^*(p_c) \exp\left[ik(p_c r + \sum_{j=1}^{2n} h_j \frac{[1 - p_c^2 v_j^2]^{1/2}}{v_j}) \right]$$

$$Q_{SV,SV} = ik g_o V_{22}^*(p_c) \exp\left[ik(p_c r + \sum_{j=1}^{2n} h_j \frac{(1 - p_c^2 v_j^2)^{1/2}}{v_j}) \right]$$

$$Q_{SH,SH} = h_o V_{33}^*(p_c) \exp\left[ik(p_c r + \sum_{j=1}^{2n} h_j \frac{[1 - p_c^2 v_j^2]^{1/2}}{v_j}) \right]$$

Form of amplitude conversion factor for P wave (when ratio is used) is:

$$\frac{Q_{pp}/V^*}{(u_1^2 + w_1^2)^{1/2}} = \frac{r^{1/2} L^{3/2}}{V_{11}^*} \left[\frac{(1 - p_c^2) + p_c^2}{p_c^4} \right]^{1/2}$$

APPENDIX II

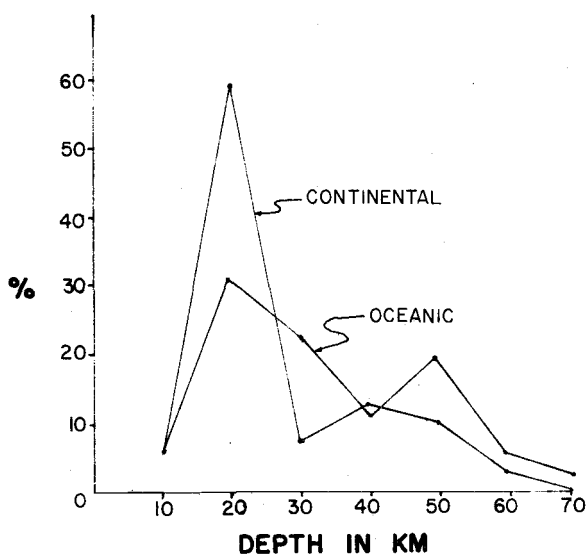
DEPTH OF FOCUS DETERMINATION

A statistical analysis of focal depths of earthquakes occurring from 1962 to 1966 was made, using U. S. Coast and Geodetic Survey Preliminary Earthquake Determination Cards. (See Engdahl and Gunst, 1966.)

All focal depths of 25 km in 1962 earthquakes and focal depths of 33 km in 1963-1966 earthquakes were eliminated.

The statistical average for each geographic region is given below. Numbers in parentheses are the number of earthquakes studied. Oceanic and continental curves represent the frequency of earthquakes with focal depth.

CENTRAL IDAHO	26.9 km (7)
MONTANA	18.8 km (8)
OFF COAST OF OREGON AND NORTHERN CALIFORNIA	27.6 km (11)
VANCOUVER ISLAND	24.8 km (13)
NORTHWEST OREGON	37.3 km (3)
WASHINGTON	40.0 km (2)



When p and P arrival times were available, focal depths were calculated in the present study based on a modified Hodgson-Gutenberg method (Macelwane, 1932). The method used the epicenter determined by the U.S. Coast and Geodetic Survey, average or representative velocities at the Moho in the earthquake region, and horizontal layers.

The theoretical equations for the travel times of the p and Ph waves were:

$$T = \sqrt{\frac{\Delta^2 - h^2}{V_1}}$$

$$T = \frac{\Delta}{V_2} + (2D - h) \sqrt{\frac{V_2^2 - V_1^2}{V_1 V_2}}$$

where:

V_1 is the average velocity of the crust

V_2 is the velocity below the Moho

T is the travel time of the Pn or p wave

D is the crustal thickness

h is the focal depth

A focal depth was determined by adjustment of the origin time and crustal thickness until the difference between the observed and calculated travel times was a minimum.

APPENDIX III

COMPUTER PROGRAMS

Programs written in Fortran IV for a CDC 3300 computer are as follows:

S Wave: Angle of Incidence and Polarization

This program computes the ratios of the ground components \bar{U}_R , \bar{U}_H and \bar{U}_Z in terms of the angle of incidence of the S wave at the surface of the earth (Nuttli 1961 equation). The angular phase between the radial and vertical components of the SV wave also is computed.

Data Input

READ 11: P and S wave velocity at the surface of the earth, maximum calculated angle of incidence

Data Output

PRINT: Angle of incidence, horizontal ground displacement, radial ground displacement, vertical ground displacement, ratio of horizontal to radial displacement, ratio of horizontal to vertical displacement, ratio of radial to vertical displacement, angular phase of radial component, angular phase of vertical component, difference in phase of radial and vertical components.

Computer program (SWAVE) listing follows:

```

PROGRAM SWAVE
READ 11,A,B,XN,P
11 FORMAT(4(2X,F8.4))
X1=1.0
XJ=0.0
X1)=(3.1415926*X1)/180.0
2 XJ=X1+X1
C=A/R
AM=ASINF(C)
CS=C*C
C1=COS(XJ)
C12=COS(2.0*XJ)
S1=SIN(XJ)
S12=SIN(2.0*XJ)
IF(XJ-AM)6,7,7
6 X1=ASINF(S1/C)
C2=COS(2.0*X1)
C2=COS(X1)
S2=SIN(X1)
S22=SIN(2.0*X1)
Q1=(C12*C12+CS*S12*S22)
F1=((C12*C12)-CS*S12*S22)/Q1
F2=((2.0*C*S12*C12)/Q1)
PH=2.0
PR=(C1+F1*C1+F2*S2)
P7=(S1-F1*S1+F2*C2)
DHR=PH/PR
DH7=PH/PZ
DRZ=PR/PZ
XJR=XJ*57.295
PRINT 120,XJR,PH,PR,PZ,DHR,DH7,DRZ
120 FORMAT(7(2X,F8.4))
GO TO 1A
7 R1=SQRT(S1*S1-CS)
R21=(C15*C12*C1)
R22=(R1*S12**2.0)
Z21=2.0*R1*S1*S12
Z22=C12*C12
Q2=(C12*C12*C12*C12+4.0*(R1*R1)*S12*S1*S1)
PH2=2.0
APR2=2.0*C12*R21/Q2
BPR2=2.0*C12*R22/Q2
PR2=SQRT(APR2*APR2+BPR2*BPR2)
APZ2=2.0*S12*R1*Z21/Q2
BPZ2=2.0*S12*R1*Z22/Q2
PZ2=SQRT(APZ2*APZ2+BPZ2*BPZ2)
DHR2=PH2/PR2
DHZ2=PH2/PZ2
DRZ2=PR2/PZ2
XJR=XJ*57.295
PRINT 130,XJR,PH2,PR2,PZ2,DHR2,DHZ2,DRZ2,APR2,BPR2,APZ2,BPZ2
130 FORMAT(11(2X,F8.4))
AG1=ATAN((-BPR2)/APR2)
AG2=ATAN((-BPZ2)/APZ2)
AG1=AG1*57.2958
AG2=AG2*57.2958
DAG=AG1-AG2
WT1=AG1*0.0027777
WT2=AG2*0.0027777
DWT=DAG*0.0027777
PRINT 131,AG1,AG2,DAG,WT1,WT2,DWT
131 FORMAT(6(2X,F8.4))
1A IF(XJ-XN) 2,220,220
220 STOP
END

```

Epicentral Distance Determination

This computer program determines the epicentral distance in degrees, back-azimuth and azimuth between two points on a spherical earth (method, Bullen, 1963). The accuracy of the method ranges from 0.05° standard error at an epicentral distance of 1° to a 0.007° error at a 20° epicentral distance, using four placed tables.

Data Input

READ 101: No. of earthquakes, No. of stations

READ 102: Name of earthquake, latitude, longitude (E)

READ 102: Name of station, latitude, longitude (E)

Data Output

PRINT: Name of earthquake, name of station, azimuth, back-azimuth, epicentral distances in degrees and kilometers.

The listing for this program is (EPDAZM):

i_h As a Function of Epicentral Distance

This program determines the epicentral distance that straight rays travel through a spherical layered earth, using the angle of incidence i_h at the focus. An experimental crustal section is used as the basis for the spherical layers.

```

PROGRAM EPDAZM
DIMENSION NAME(40),NAMA(400),THE(300),PHI(300),THP(300),PHP(300)
READ 101,N,M
101 FORMAT(2X,I3,2X,I3)
READ 102,(NAME(I),THE(I),PHI(I),I=1,N)
102 FORMAT(A5,1X,2F9.4)
DO 20 I=1,N
THE(I)=(90.0-THE(I))*0.0174533
20 PHI(I)=PHI(I)*0.0174533
READ 103,(NAMA(J),THP(J),PHP(J),J=1,M)
DO 30 J=1,M
THP(J)=(90.0-THP(J))*0.0174533
30 PHP(J)=PHP(J)*0.0174533
DO 40 I=1,N
PRINT 104,
104 FORMAT(/////)
DO 40 J=1,M
C=CCS(THE(I))
D=SIN(PHI(I))
E=-COS(PHI(I))
HK=-SIN(THE(I))
A=HK*E
B=-HK*D
G=C*E
H=C*D
CP=CCS(THP(J))
DP=SIN(PHP(J))
EP=-COS(PHP(J))
HKP=-SIN(THP(J))
AP=HKP*EP
BP=-HKP*DP
GP=-CP*EP
HP=CP*DP
X1=(A-AP)*(A-AP)
Y1=(B-RP)*(B-RP)
Z1=(C-CP)*(C-CP)
CDEL=((X1+Y1+Z1)-2.0)/2.0
SDEL=SQRT(1.0-(CDEL*CDEL))
DELA=ATAN(ABS(SDEL)/ABS(CDEL))
X2=(A-D)*(A-D)
Y2=(B-E)*(B-E)
Z2=(C*CP)
SAZ1=((Y2+Z2+Z2)-2.0)
X12=(A-G)*(A-G)
Y12=(B-H)*(B-H)
Z12=(C-HK)*(C-HK)
CAZ1=((X12+Y12+Z12)-2.0)
A71=ARCTAN(SAZ1,CAZ1)
X3=(A-OP)*(A-OP)
Y3=(B-EP)*(B-EP)
Z3=(C*C)
SAZ2=((X3+Y3+Z3)-2.0)
X13=(A-GP)*(A-GP)
Y13=(B-HP)*(B-HP)
Z13=(C-HKP)*(C-HKP)
CAZ2=((X13+Y13+Z13)-2.0)
AZ2=ARCTAN(SAZ2,CAZ2)
AZ1=AZ1+57.295
AZ2=AZ2+57.295
DELD=DEL*57.295
DELK=DELD*111.0
40 PRINT 106, NAME(I),NAMA(J),AZ1,AZ2,DELD,DELK
106 FORMAT(2X,A4,1X,A4.5X,4(5X,F9.4))
END

```

```

FUNCTION ARCTAN(ANUM,ADEN)
IF(ADEN)2,3,4
2 IF(ANUM)5,6,6
5 A12=ATAN(ANUM/ADEN)+3.1415926
GO TO 12
6 A12=3.1415926+ATAN(ANUM/ADEN)
GO TO 12
3 IF(ANUM)7,8,9
7 A12=4.7123889
GO TO 12
9 A12=1.5707963
GO TO 12
8 STOP
4 IF(ANUM)10,11,11
10 A12=6.2831852+ATAN(ANUM/ADEN)
GO TO 12
11 A12=ATAN(ANUM/ADEN)
12 ARCTAN=A12
RETURN
END

```

Data Input

- READ (1, 1): depth of focus, radius of spherical earth, limit angle for rays leaving the source, angular increment of each ray, number of velocities used, - according to Bullen (1963, p. 123), starting angle of incidence at source,
- READ (1, 2): depth, radius to top and velocity of each layer.
- READ (1, 7): number of different Moho layers,
- READ (1, 190): different radii and velocities for Moho layer.

Data Output

- WRITE (2, 901): Angle of incidence at a boundary.
- WRITE (2, 3): } Angular distance ray traveled, angle of incidence
 WRITE (2, 6): } of ray at source, total travel time, total distance ray traveled.
- WRITE (2, 4): Angular distance ray traveled, angle of incidence of ray at source, total travel time, angle of incidence at surface of earth, total distance ray traveled, and its reciprocal.
- WRITE (2, 202): Travel time for curved ray, angular distance curved ray traveled, number of layer.
- WRITE (2, 201): Section used, angle of incidence of ray, angular distance ray traveled, travel time of ray.
- Abbreviations: PN RA means the ray has been critically refracted.
 REFLECTED means the ray has been reflected.

The listing for CRUCRSSR is:

Fault Plane Determination

This program calculates the theoretical amplitude and direction of first motions from a given wave radiation pattern and

```

PROGRAM CRUCSSR
DIMENSION D(20),R(1,20),V(1,20),DFL(30),TIM(30),A(1)
COMMON VX(10),RS(10)
908 READ(1,1) DD,RE,XLIM,ANG,M,J,AML,SAL
1  FORMAT(2F7.2,F10.8,F10.2,I2,F1,F9.3,F9.3)
READ(1,2) (D(K),R(1,K),V(1,K),K=1,M)
2  FORMAT(5(F5.1,F7.2,F4.2))
READ(1,7) NX
7  FORMAT(I3)
READ(1,910) (RS(I),VX(I),I=1,NX)
910 FORMAT(RF10,4)
IF(J)150,909,150
909 ALR=SAL
Q=ALR
I=1
XR=0.0
5  L=1
DF=DD
P=0.0
RF=RE-DD
TTL=0.0
TDEL=0.0
TTIM=0.0
DO 10 K=1,M
IF(DD=0(K)) 11,150,10
10 CONTINUE
11 IF((3.14159265/2.0)-ALR)43,15,15
15 IF (ALR)150,16,26
16 IF(L-1)150,18,17
17 DE=0(K)
18 SRU=DE-D(K-1)
TTL=TTL+SRU
DEL(L)=0.0
TIM(L)=SRU/V(1,K)
TTIM=TTIM+TIM(L)
TDEL=TDEL+DEL(L)
IF(K-2)150,38,20
20 RF=R(1,K-1)
K=K-1
L=L+1
GO TO 11
26 XL=(RF/R(1,K-1))*SIN(ALR)
THE=ASINF(XL)
THE1=THE*57.2958
WRITE(2,901) THE1
901 FORMAT(2X,F8.4)
IF(THE)150,27,29
27 ALR=0.0
GO TO 11
29 DEL(L)=ALR-THE
IF(DEL(L))150,27,30
30 DIST=(R(1,K-1)/SIN(ALR))*SIN(DEL(L))
TTL=TTL+DIST
TIM(L)=DIST/V(1,K)
XL2=(V(1,K-1)/V(1,K))*SIN(THE)
XL2=ASINF(XL2)
TTIM=TTIM+TIM(L)
TDEL=TDEL+DEL(L)
IF(XL2-(3.14159265/2.0))32,32,151
32 CONTINUE
33 ALR=XL2
L=L+1
RF=R(1,K-1)
IF(K-2)150,38,36
36 K=K-1
37 GO TO 11
38 TDEL=TDEL/0.0174533
ALR=ALR/0.0174533
Q=Q/0.0174533
THE=THE/0.0174533
SR=1.0/TTL
WRITE(2,4) TDEL,ALR,Q,TTIM,P,THE,TTL,SR
4  FORMAT(3F9.4,F9.3,F2.1,F9.3,2(E9.3))
LX=L
WRITE(2,906) (TIM(L),L=1,LX)
906 FORMAT(7(2X,F8.4))
39 ALR=(Q+ANG)*0.0174533
40 Q=ALR
IF(XLIM-ALR)160,160,5
43 IF(3.14159265-ALR)150,150,44
44 IF(M-K)150,45,49
45 IF(RF-R(1,K-1))160,46,150
46 ALR1=ALR/0.0174533
TDEL1=TDEL/0.0174533
Q1=Q/0.0174533
THE1=THE/0.0174533
SR=1.0/TTL
WRITE(2,4) Q1,ALR1,TDEL1,TTIM,P,THE1,TTL,SR
THE=(3.1415926-ALR)
THE1=THE*57.2958
WRITE(2,901) THE1
CALL MCHO(THE,K,R(1,K-1),M,NX)

```

```

AMQ=SQRTF(AML*AML-1.0)
XAM=AMQ/COS(THF)
TX=((R(I,K-1)/(AMQ*V(I,K)))*LOGF((AML*XAM)/(AML-XAM)))
DY=2.0*ATAN(1.0/((SIN(THF)/COS(THF))*AML))
DY=DY/0.0174533
WRITE(2,202)TX,DY,AML,K
202 FORMAT(2X,3F9.4,I2)
DEL(L)=(3.14159265*2.0*THF)
DIST=(R(I,K-1)/SIN(3.14159265-ALR))*SIN(DEL(L))
TTL=TTL+DIST
TIM(L)=DIST/V(I,K)
TTIM=TTIM+TIM(L)
XL3=(V(I,K-1)/V(I,K))*SIN(THF)
XL3=ASTNF(XL3)
TDEL=TDFL+DEL(L)
TDEL1=TDEL/0.0174533
Q1=Q/0.0174533
THE1=THF/0.0174533
SR=1.0/TTL
WRITE(2,4) Q1,ALR1,TDEL1,TTIM,P,THE1,TTL,SR
47 XL2=XL3
GO TO 33
49 IF(SIN(3.1415965-ALR)-SIN(R(I,K)/RF))300,300,60
300 XL4=(RF/R(I,K))*SIN(3.14159265-ALR)
THE=ASTNF(XL4)
THE1=THF*57.2958
WRITE(2,901) THE1
DEL(L)=THE*ALR-3.14159265
TDEL=TDFL+DEL(L)
DIST=((R(I,K)/SIN(3.14159265-ALR))*SIN(OEL(L)))
TTL=TTL+DIST
TIM(L)=DIST/V(I,K)
TTIM=TTIM+TIM(L)
IF(SIN(THF)-SIN(V(I,K)/V(I,K+1)))74,149,151
149 TDEL=TDEL/0.0174533
ALR=90.0
Q=Q/0.0174533
WRITE(2,3)TDEL,ALR,Q,TTIM,TTL
3 FORMAT(I2H PN RA ,3F9.4,2F9.3)
GO TO 39
74 XL5=(V(I,K+1)/V(I,K))*SIN(THF)
XL5=ASTNF(XL5)
70 THAL=XL5
ALR=(3.14159265-THAL)
RF=R(I,K)
L=L+1
K=K+1
GO TO 11
60 ALR=3.14159265-ALR
XL6=(RF/R(I,K-1))*SIN(ALR)
THE=ASTNF(XL6)
CALL MCHO(THF,K,R(I,K-1),M,NX)
THE1=THF*57.2958
WRITE(2,901) THE1
DEL(L)=(3.14159265-(ALR+THE))
61 GO TO 30
151 TDEL=TDEL/0.0174533
ALR=ALR/0.0174533
Q=Q/0.0174533
WRITE(2,6)TDEL,ALR,Q,TTIM,TTL
6 FORMAT(I2H REFLECTED ,F9.4,F9.4,F9.4,F9.3,F9.3)
152 GO TO 39
160 GO TO 908
150 END

SUBROUTINE MCHO(THF,K,R,M,NX)
COMMON VX(10),RS(10)
IF(M=K)21,20,21
20 DO 200 J=1,NX
ZM=((RS(J)*SIN(THF))/R)
TEH=ATAN(ZM/SQRTF(1.0-ZM*ZM))
DEH=(3.1415926-(TEH+THF))
SIM=((SIN(DEH)*R)/(SIN(TEH)*VX(J)))
DEH=DEH*57.2958
TEH=TEH/0.0174533
200 WRITE(2,201)J,TEH,DEH,SIM
201 FORMAT(IH SECTION,I2,E9.3,2F9.3)
21 RETURN
END

```

compares these values with experimentally determined values. The difference between the values is calculated for numerous fault-plane orientations.

Data Input

READ 50: IF statement condition, number of seismic stations used.

READ 70: Angular increment shifts.

READ 1: Angle of incidence of ray at source and station azimuth.

READ 130: Direction of motion for each station.

READ 122: Experimental amplitude ratios for all seismic stations.

Data Output

PRINT 1: Angle of incidence of ray at source and station azimuth.

PRINT 200: Angular increments.

PRINT 120: Fractional deviations, plot of fractional deviations.

PWAVE is listed as follows:

```

PROGRAM PWAVE
DIMENSION F1(3),FP(3),P(3)
DIMENSION PQ(3),CX(3),D(3),PQT(3)
51 READ 50,NV,NS
50 FORMAT(2I3)
   READ 70,W1,W2,W3
70 FORMAT(3(2X,F8.4))
   READ 1,(FT(I),FP(I),I=1,NS)
1  FORMAT(2(2X,F8.4))
   PRINT1,(FT(I),FP(I),I=1,NS)
   READ 130,(CX(I),I=1,NS)
130 FORMAT(3(2X,F8.4))
   READ 122,(PQT(I),I=1,NS)
122 FORMAT(3(2X,F8.4))
   PRINT 119
119 FORMAT(2X,3HLPR,2X,3HLTR,2X,3HLSR)
   XN=1,0
   DO 60 I=1,NS
   FP(I)=(360.0-FP(I))*0.0174533
60 FT(I)=FT(I)*0.0174533
   DO 3 N=1,19
   DO 2 M=1,19
   DO 2 L=1,19
   RN=N-1
   RM=M-1
   RL=L-1
   PP=0.0174533*W1*RN*10.0*0.0174533
   PT=0.0174533*W2*RM*10.0*0.0174533
   PS=0.0174533*W3*RL*10.0*0.0174533
   A1=CCS(PS)
   A2=SIN(PS)
   R1=CCS(PP)
   R2=SIN(PP)
   C1=CCS(PT)
   C2=SIN(PT)
   DO 8 I=1,NS
   X=CCS(FP(I))*SIN(FT(I))
   Y=SIN(FP(I))*SIN(FT(I))
   Z=CCS(FT(I))
   XP=(A1*R1-C1*R2*A2)*X+(A1*B2+C1*B1*A2)*Y+(A2*C2)*Z
   YP=(-A2*R1-C1*R2*A1)*X+(-A2*B2+C1*B1*A1)*Y+(A1*C2)*Z
   ZP=(C2*R2)*X+(-C2*R1)*Y+C1*Z
   VFP=ARCTAN(ZP,XP)
   XPP=SQRT(ZP*ZP+XP*XP)
   VFT=ARCTAN(XPP,YP)
   P(I)=0.5*SIN(2.0*VFT)*CCS(VFP)
   XEQ=P(I)*CX(I)
   IF(XEQ)2,7,7
7  IF(I-2)8,11,8
11 PQ(1)=P(1)/P(2)
   D(1)=ARS((PQ(1)-PQT(1))/PQT(1))
   IF(D(1)-1.0)8,8,2
8  CONTINUE
   PQ(1)=P(1)/P(2)
   PQ(2)=P(2)/P(3)
   PQ(3)=P(3)/P(1)
   D(1)=ARS((PQ(1)-PQT(1))/PQT(1))
   D(2)=ARS((PQ(2)-PQT(2))/PQT(2))
   D(3)=ARS((PQ(3)-PQT(3))/PQT(3))
   DO 4 I=1,3
   IF(D(I)-1.00)4*4,2
4  CONTINUE
   PTR=PT*57.295
   PPR=PP*57.295
   PSR=PS*57.295
   IF(XN-1.0)40,41,40
41 XN=2,0
   GO TO 42
40 XN=3,0
42 PRINT 200, PPR,PTR,PSR
200 FORMAT(3(2X,F8.4))
   CALL LPLST(D(1),D(2),D(3),XN)
2  CONTINUE
3  CONTINUE
   IF(INV-1)10,51,10
10 CONTINUE
END

```

```

FUNCTION ARCTAN(Y,X)
  IF (X)1,2,3
  3 IF (Y)4,5,5
  2 IF (Y)7,11,8
  4 ARCTAN=6.28319*ATAN(Y/X)
  RETURN
  5 ARCTAN=ATAN(Y/X)
  RETURN
  1 ARCTAN=3.14159*ATAN(Y/X)
  RETURN
  7 ARCTAN=4.71239
  RETURN
  8 ARCTAN=1.57080
  RETURN
11 STOP
END

SUBROUTINE LPLCT(P,Q,R,YN)
  DIMENSION X(3),LINE(51)
  X(1)=P
  X(2)=Q
  X(3)=R
  DO 3 I=1,3
  IF (X(I)-1.00)3,4,4
  4 X(I)=1.00
  3 CONTINUE
  IP=(X(1)+0.01)*50.0
  IQ=(X(2)+0.01)*50.0
  IR=(X(3)+0.01)*50.0
  X(1)=IP
  X(2)=IQ
  X(3)=IR
  X(1)=X(1)/5.0
  X(2)=X(2)/5.0
  X(3)=X(3)/5.0
  IF (YN=2.0)8,6,8
  6 DO 5 J=1,51
  5 LINE(J)=1H*
  LINE(1)=LINE(11)=LINE(21)=LINE(31)=LINE(41)=1H*
  PRINT 1R, (LINE(I),I=1,51)
  18 FORMAT(29X,51A1)
  8 DO 30 I=1,51
  30 LINE(I)=1H
  IF (X(1)-X(2))9,10,9
  10 IF (X(1)-X(3))11,12,11
  12 J=5.*X(1)+1.0
  LINE(J)=1HS
  GO TO 17
  11 J=5.*X(1)+1.0
  LINE(J)=1HC
  J=5.*X(3)+1.0
  LINE(J)=1HZ
  GO TO 17
  9 IF (X(1)-X(3))13,14,13
  14 J=5.*X(1)+1.0
  LINE(J)=1MC
  J=5.*X(2)+1.0
  LINE(J)=1MY
  GO TO 17
  13 IF (X(3)-X(2))15,16,15
  16 J=5.*X(2)+1.0
  LINE(J)=1MC
  J=5.*X(1)+1.0
  LINE(J)=1HX
  GO TO 17
  15 J=5.*X(1)+1.0
  LINE(J)=1HX
  J=5.*X(2)+1.0
  LINE(J)=1HY
  J=5.*X(3)+1.0
  LINE(J)=1HZ
  17 PRINT 120,P,Q,R,(LINE(I),I=1,51)
  120 FORMAT(3(2X,F7.4),2X,51A1)
  END

```

APPENDIX IV

PRELIMINARY STUDY OF TRAVEL TIMES IN BRITISH COLUMBIA

Eight earthquakes located along the continental slope of British Columbia, the northern Cascadia Basin and on the continental shelf of British Columbia were used to obtain P, S and R wave arrivals.

The seismic stations used in the study are listed in Table II and seismic arrival times in Table VII. Earthquake locations used are those determined by the United States Coast and Geodetic Survey. Six earthquake foci were at normal depths (33 km); two had focal depths of 7 and 37 km.

All arrivals were selected where a change in wave frequency or energy occurred; in particular, waves arriving after Pn were used to ascertain changes in velocity with depth. Arrival times were accurate to within 0.5 seconds.

Velocities of Pn waves increased from 8.12 to 8.28 km/sec with increasing epicentral distance out to 18°. The corresponding Sn velocity was 4.52 km/sec.

P phases

$$T = \frac{\Delta}{8.12} + 5.0$$

$$T = \frac{\Delta}{8.28} + 10.6$$

S phase

$$T = \frac{\Delta}{4.52} + 16.0$$

Other P and R velocities are not as well defined.

Travel-time curves are enclosed in envelope.

Table VII. Travel Times of Seismic Waves from British Columbia Earthquakes.

Earthquake	Station	Epicentral Distance	Vertical Component or First Arrival	North or Radial Component	East or Transverse Component	Reference
Sept. 2, 1965 18:01:19.4	COR	5.1	79.6			A
	BMO	8.4	121.6			A
	ORV	10.0	143.6			A
	EUR	12.5	180.4			A
	DUG	13.8	193.8			A
	GSC	15.5	219.6			A
	UBO	15.6	225.2			A
	TFO	18.9	260.7			A
	COL	19.6	268.6			A
Sept. 2, 1965 19:41:25.2	BMO	8.4	121.8			A
	ORV	10.1	144.8			A
	EUR	12.6	180.9			A
	DUG	13.8	204.9			A
	UBO	15.7	226.4			A
	PAS	16.1	226.8			A
	TFO	19.0	261.1			A
Oct. 11, 1965 15:47:55.4	GSC	17.8	247.6			A
		"	254.6			A
	CED	18.5	255.5			A
	RCD	18.9	260.6			A
	LON	6.3	93.0			A
	COR	7.3	107.5			A
	SPO	8.4	122.5			A
	BMO	10.0	142.9			A
	HHM	10.3	147.9			A
	EDM	10.3	149.6			A
	ORV	12.4	174.7			A
	BOZ	12.9	183.1			A
		"	364.6			A
	MHC	14.4	206.3			A
	EUR	14.6	206.8			A
		"	210.1			A
		"	229.4			A
DUG	15.6	219.2			A	
PRI	15.8	221.2			A	
COL	17.3	239.6			A	
UBO	17.3	240.4			A	
	"	441.6			A	
March 30, 1966 12:40:01.0	NEW	8.4	120			A
	BMO	9.8	140.4			A

Continued

Table VII Continued.

Earthquake	Station	Epicentral Distance	Vertical Component or First Arrival	North or Radial Component	East or Transverse Component	Reference	
Mar. 30, 1966	EDM	10.7	153.0			A	
	ORV	11.8	167.7			A	
	"	"	184.0			A	
	"	"	316.7			A	
	SID	14.1	198.5			A	
	"	"	371.			A	
	"	"	490.			A	
	EUR	14.2	201.8			A	
	UBO	17.1	238.7			A	
	BCN	17.6	245.6			A	
	"	"	479.5			A	
	COL	17.9	246.0			A	
	"	"	246.5			A	
	"	"	252.5			A	
	"	"	463.0			A	
	"	"	464.			A	
	PAS	17.8	246.0			A	
	"	"	437.0			A	
	"	"	443.			A	
	CMC	19.5	265.0			A	
	"	"	479.0			A	
	FSJ	5.7	81.8			81.8	B
	"	"	139.3			113.3	B
	"	"	174.3				B
	"	"	235.5				B
	BKS	13.1	187.6		187.6		B
	"	"			188.4		B
	"	"	342.6				B
	"	"	348.0				B
	COL	17.8	244.8				B
"	"	245.9				B	
"	"	247.6		247.6	247.6	B	
"	"				455	B	
"	"			456.0		B	
"	"	458.0				B	
"	"	508.5				B	
VIC	4.3	63.7		63.7	62.8	B	
"	"			114.7		B	
"	"	116.7			118.7	B	
PNT	6.6	95.5		96.	95.	B	
"	"	177.		136.	105.	B	
"	"	318.		331.		B	

Continued

Table VII Continued.

Earthquake	Station	Epicentral Distance	Vertical Component or First Arrival	North or Radial Component	East or Transverse Component	Reference
Mar. 30, 1966	LON	6.1	89.1	89.6		B
		"	90.3			B
		"	159.0	158.6	162.6	B
		"	248.1	227.8	253.3	B
		"			270.6	B
	BOZ	12.8	182.2	182.4	182.3	B
		"	183.2	183.2	183.2	B
		"	335.	335.	332.8	B
		"	349.8	365.9		B
		"	397.9			B
		"	416.2	407.	414.1	B
		"	419.			B
		"	440.			B
		"	480.7	427.6		B
May 20, 1966 23:58:51.7	COR	7.1	99.6			A
	BMO	9.9	142.4			A
	HHM	10.4	148.8			A
		"	155.0			A
		"	278.5			A
		EDM	10.6	157.3		
	ORV	12.1	172.5			A
	BKS	13.4	190.3			A
	JAS	13.9	198.0			A
		"	205.8			A
		MHC	14.1	199.9		
	"	"	207.8			A
	SLD	14.5	203.8			A
	EUR	14.5	204.5			A
	PRI	15.5	217.0			A
	LAO	15.9	223.2			A
	UBO	17.2	241.0			A
		"	440.3			A
	COL	17.5	243.3			A
	PAS	18.1	250.3			A
		"	461.3			
	LON	6.3	92.8	92.9	93.3	B
	COL	17.5	242.8			B
	FSJ	5.4	79.2	79.4	79.7	B
		"	114.2	115.2	115.2	B
		"	143.3	143.7	144.2	B
		PNT	6.6	96.5		
"	"		99.3	101.3	B	

Continued

Table VII Continued.

Earthquake	Station	Epicentral Distance	Vertical Component or First Arrival	North or Radial Component	East or Transverse Component	Reference
May 20, 1966	PNT	6.6	223.3			B
	VIC	4.4	68.6	69.1	68.6	B
Nov. 4, 1966 20:30:13.3	LON	5.2	76.7			A
	NEW	7.6	110.7			A
	BMO	8.9	127.9			A
	EDM	10.3	149.7			A
	ORV	11.0	153.4			A
	BOZ	12.1	172.0			A
	JAS	12.8	185.2			A
	MHC	13.0	187.7			A
	SLD	13.4	188.0			A
	EJR	13.4	191.5			A
	PRI	14.4	201.4			A
	LAO	15.2	214.7			A
	GSC	16.5	230.7			A
	UBO	16.2	232.8			A
	COL	18.6	255.7			A
	TFO	19.8	272.4			A
	LON	5.3	78.2	77.7	78.2	B
	BOZ	12.0	172.0		172.9	B
	"	"	182.8		185.4	B
	VIC	3.5	53.0	54.7	53.5	B
"	"	96.5	96.5	97.5	B	
PNT	5.8	86.7	88.2	87.2	B	
"	"	102.5	100.7	100.7	B	
"	"	"	157.7	167.7	B	
FSJ	5.7	86.2	86.5	86.5	B	
"	"	92.8			B	
"	"	156.0	167.0	155.0	B	
"	"	178.7		169.0	B	
April 19, 1967 18:12:24.6	LON	8.6	125.2			A
	HHM	11.9	169.7			A
	"	"	371.7			A
	SCM	12.5	173.1			A
	BMO	12.1	173.4			A
	"	"	180.5			A
	BOZ	14.7	205.4			A
	"	"	213.9			A
"	"	461.9			A	

Continued

Table VII Continued.

Earthquake	Station	Epicentral Distance	Vertical Component or First Arrival	North or Radial Component	East or Transverse Component	Reference
April 19, 1967	COL	14.8	210.4			A
	PJD	14.8	211.4			A
	TNN	16.3	227.7			A
	EUR	16.9	237.4			A
	JAS	16.6	238.6			A
	LAO	17.3	241.8			A
	UBO	19.4	267.0			A
	"	"	276.7			A
	PNT	8.1	127.4		132.4	B
	"	"	149.9	149.2	157.4	B
	"	"	255.9	263.6		B
	"	"	271.7	270.4		B
	FSJ	4.6	69.9		70.3	B
	"	"	90.4	70.4	87.9	B
	"	"	109.4	91.4	111.6	B
	"	"		113.6		B
	COL	14.8	208.2	211.1	213.1	B
	"	"	210.9	238.3		B
	"	"		262.9		B
	LON	8.6	124.3	128.6	123.9	B
"	"	128.6	136.7	128.6	B	
"	"		143.3	142.0	B	
"	"			149.3	B	
April 29, 1967 00:04:41.8	COL	16.4	234.6	239.2	240.2	B
	"	"	238.8	261.7	263.4	B
	"	"			307.8	B
	"	"	427.7	422.7	427.2	B
	"	"		435.7		B
	"	"		462.2		B
	"	"		483.4		B
	"	"	542.8	525.7	525.7	B
	SIT	6.6	99.2			A
	COR	8.1	121.7			A
	NEW	9.1	133.2			A
	EDM	10.7	156.2			A
	BMO	10.8	157.2			A
	HHM	10.9	159.9			A
	"	"	164.4			A
	"	"	277.4			A
	UKI	13.0	188.2			A
BOZ	13.6	195.4			A	

Continued

Table VII Continued.

Earthquake	Station	Epicentral Distance	Vertical Component or First Arrival	North or Radial Component	East or Transverse Component	Reference	
April 29, 1967	BOZ	13.6	364.2			A	
	SCM	14.2	201.2			A	
	BKS	14.5	207.5			A	
	PMR	14.7	209.7			A	
	JAS	15.0	213.2			A	
	MHC	15.1	216.0			A	
	EUR	15.4	220.4			A	
	EUR	15.4	501.7			A	
	SLD	15.5	221.0			A	
	"	"	"	523.7		A	
	LF4	15.7	226.0			A	
	BIG	16.3	232.2			A	
	DUG	16.4	233.1			A	
	"	"	"	437.4		A	
	COL	16.5	234.2		434.2	A	
	PRI	16.5	235.7			A	
	PJD	16.5	237.2			A	
	TNN	18.0	251.2			A	
	UBO	18.1	253.8			A	
	"	"	"	259.9		A	
	PAS	19.2	267.2			A	
	"	"	"	272.2		A	
	"	"	"	486.2		A	
	VIC	5.2	79.2		79.9	78.6	B
	"	"	"			173.4	B
	PNT	7.1	106.2		106.4	107.2	B
	"	"	235.7				B
	"	"	345.2				B
	"	"	"		482.2		B
	FSJ	4.9	77.4		77.0	77.3	B
	"	"	"			159.2	B
	"	"	"		318.3	359.8	B
	LON	7.2	106.9		107.1	107.9	B
"	"	228.0		179.8	224.0	B	
"	"	"		221.5		B	
"	"	"		242.1		B	
"	"	"	344.5	360.4	379.9	B	
BKS	14.5	207.7		209.4	209.8	B	
"	"	209.8			228.7	B	
"	"	"			259.0	B	

APPENDIX V

THE TACOMA AND OTHER EARTHQUAKE FAULT-PLANE
SOLUTIONS OBTAINED WITH THE BYERLY METHODLocal Determination of the Tacoma Earthquake

In the preliminary analysis of faulting in the Pacific Northwest, a fault-plane solution was obtained for the Tacoma earthquake of April 29, 1965, using the first motion of the P wave. The eighteen stations used in this analysis were at epicentral distances of less than 15° and in all azimuths. This solution was unique in that four seismic stations were less than 1° from the earthquake, which placed first motions at these stations on the upper hemisphere of the focal sphere. This earthquake had a focal depth of about 60 km and magnitude of 6.5. This fault-plane solution differs from other solutions, using world-wide station coverage, but is comparable to a solution which used the three station technique.

The solution from first motions of P waves recorded at seismic stations, located at epicentral distances less than $14\frac{01}{2}$ is:

Plane A N 24.0° W, Dip 50° W

Plane B N 02.0° E, Dip 42° E

The solution from first motions of P waves recorded at a world distribution of stations (Algermissen and Harding, 1965) is:

N 18.0° W, Dip 69° E

N 53.0° W, Dip 35° W

The solution from first motions and amplitudes of the P waves at three seismic stations is:

N 26.0° W, Dip 32° W

N 05.0° W, Dip 59° E

^{1/}Data from Algermissen and Harding, 1965, p. 24.

Byerly Method Applied

Fault-plane solutions attempted for some earthquakes were not obtained in the present study. These earthquakes and others, for which no amplitudes of P waves were available, were solved using the Byerly method.

Using the angle i_h and azimuth for each seismic station, the direction of first motion of the P wave was plotted on a projection (Wulff's Net) of the focal sphere. If a nodal plane drawn on the projection was constrained by the first motions of the P wave at seismic stations, the pole of the plane fixed a point through which the other nodal plane must pass.

The difficulty of determining fault-plane solutions using a limited number of first motions is indicated in the following earthquake studies (see related illustrations).

The earthquake of February 1, 1963 had only one solution--

Plane A Strike N 42° W, Dip 58° SW

Plane B Strike N 42° W, Dip 32° NE

The earthquake of December 27, 1963 had Plane A well defined while Plane B can have any values between the strike given by the dash lines--

Plane A Strike N 74° E, Dip 2° SE

Plane B Strike N 14° E, Dip 88° W

to Strike N 37° E, Dip 90° NW

The earthquake of August 2, 1963 had Plane B fixed with Plane A variable between two strikes--

Plane A Strike N 17° E, Dip 90.0°

to Strike N 38° W, Dip 90.0°

Plane B Strike N 0° E, Dip 0.0°

The earthquake of August 19, 1963 had Plane B fixed with

Plane A variable between two strikes--

Plane A Strike N 72° E, Dip 90°

to Strike N 82° E, Dip 90°

Plane B Strike N 0° E, Dip 0°

The earthquake of January 27, 1963 had Plane A fixed and

Plane B fixed in solid black lines--

Plane A Strike N 08° W, Dip 34° W

Plane B Strike N 18° E, Dip 60° E

The earthquake of August 27, 1963 had Plane B fixed and Plane

A variable between two strikes--

Plane A Strike N 84° E, Dip 90°

to N 108° E, Dip 90°

Plane B Strike N 06° E, Dip 03° E

The earthquake of December 31, 1962 had several possible solutions--

in the black lines

Plane A Strike N 92° E, Dip 51° N

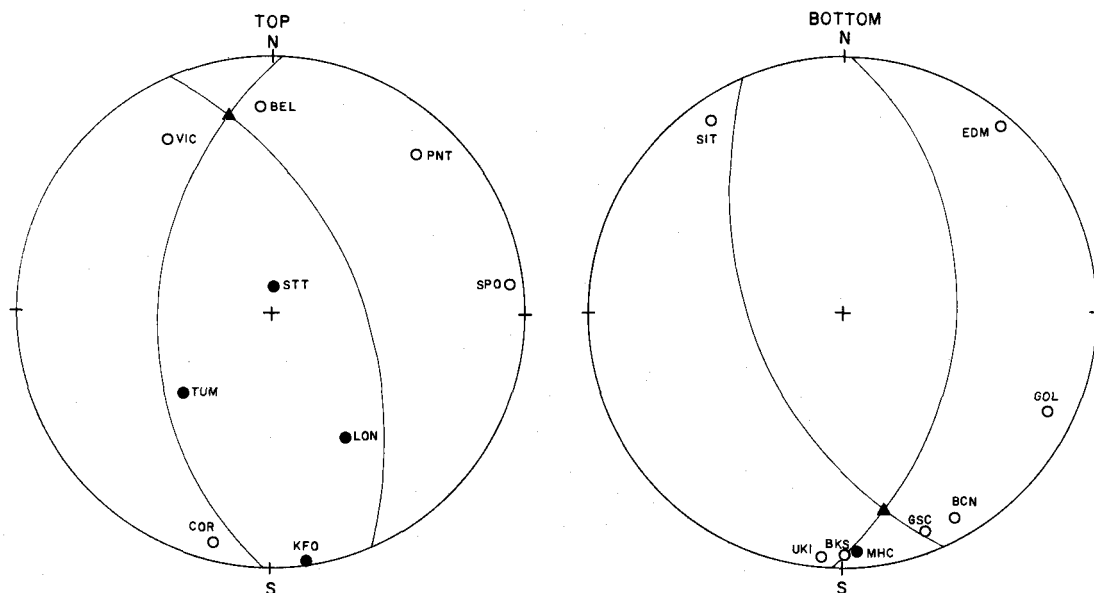
to N 28° W, Dip 76° NE

Plane B Strike N 85° E, Dip 38° S

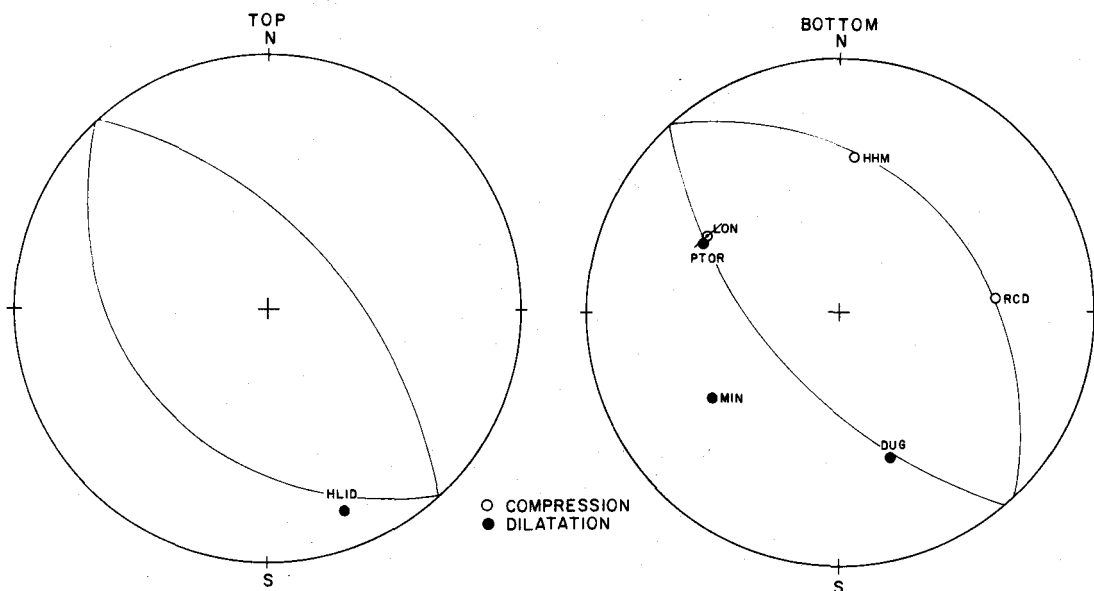
and in black dash lines

Plane A Strike N 87° E, Dip 63° S

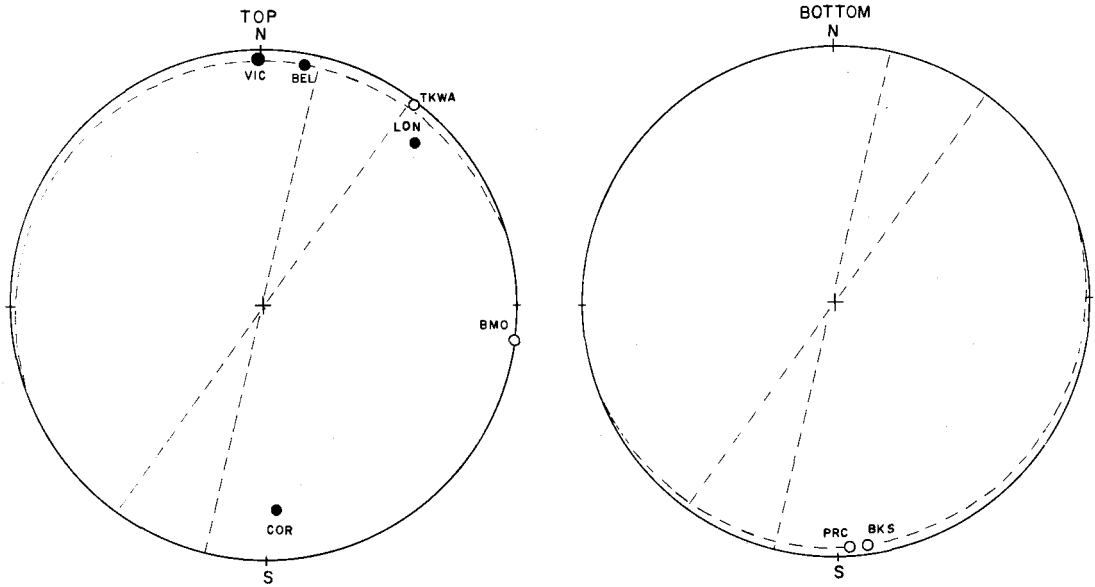
Plane B Strike N 122° E, Dip 30° NE



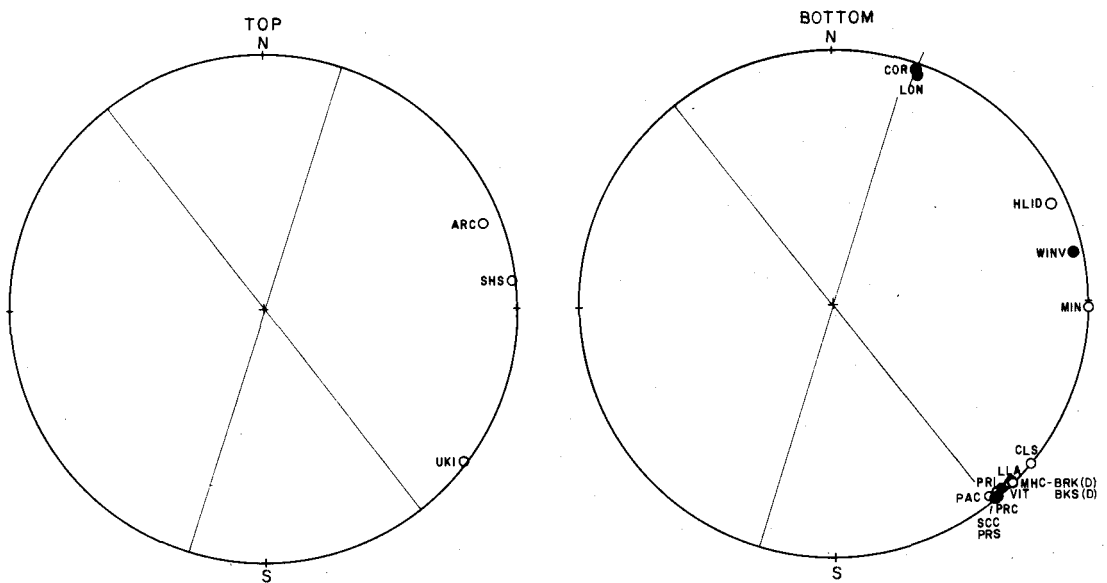
Fault-plane solution for earthquakes of April 29, 1965 projected on top and bottom half of focal sphere.



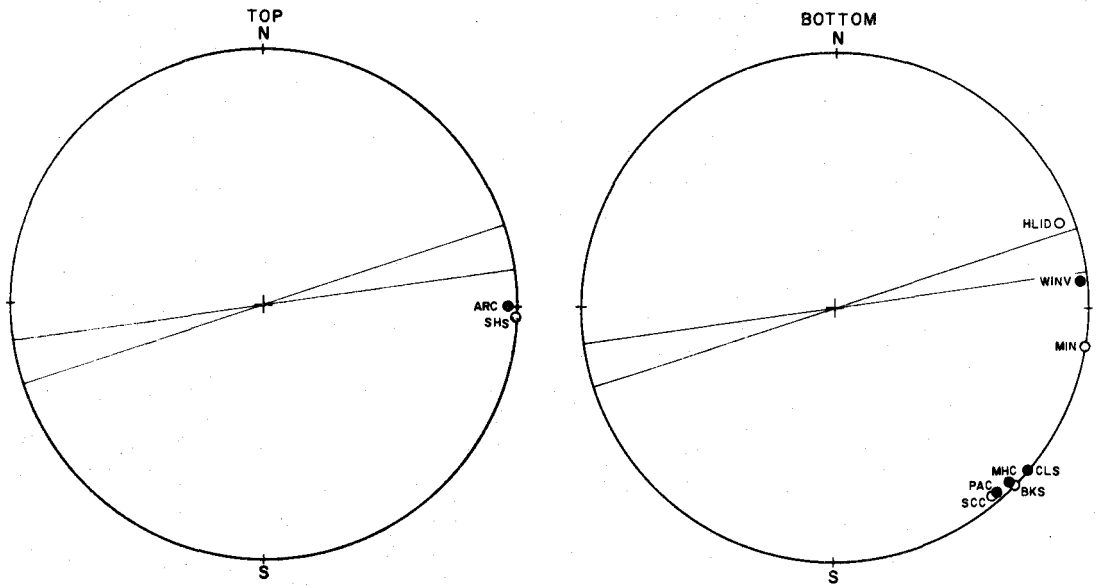
Fault-plane solution for earthquake of February 1, 1963 projected on top and bottom half of focal sphere.



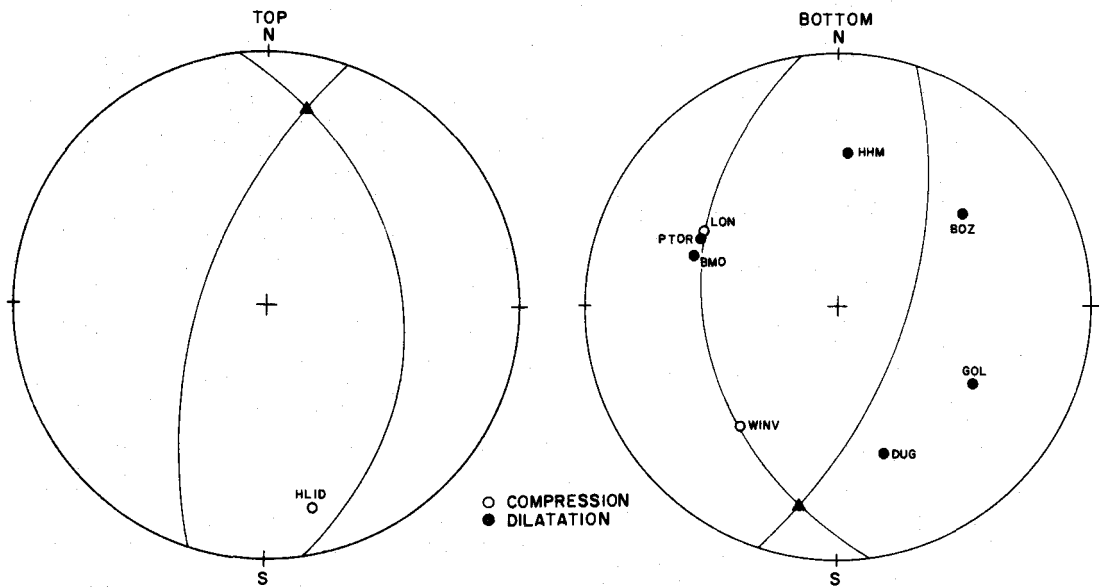
Fault-plane solutions for earthquake of December 27, 1963 projected on top and bottom half of focal sphere.



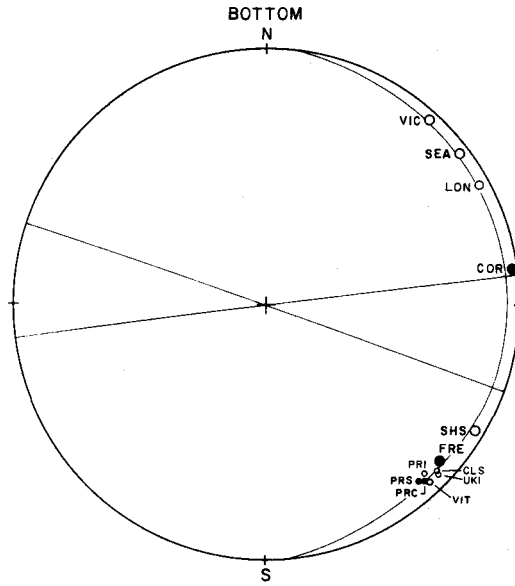
Fault-plane solutions for earthquake of August 2, 1963 projected on top and bottom half of focal sphere.



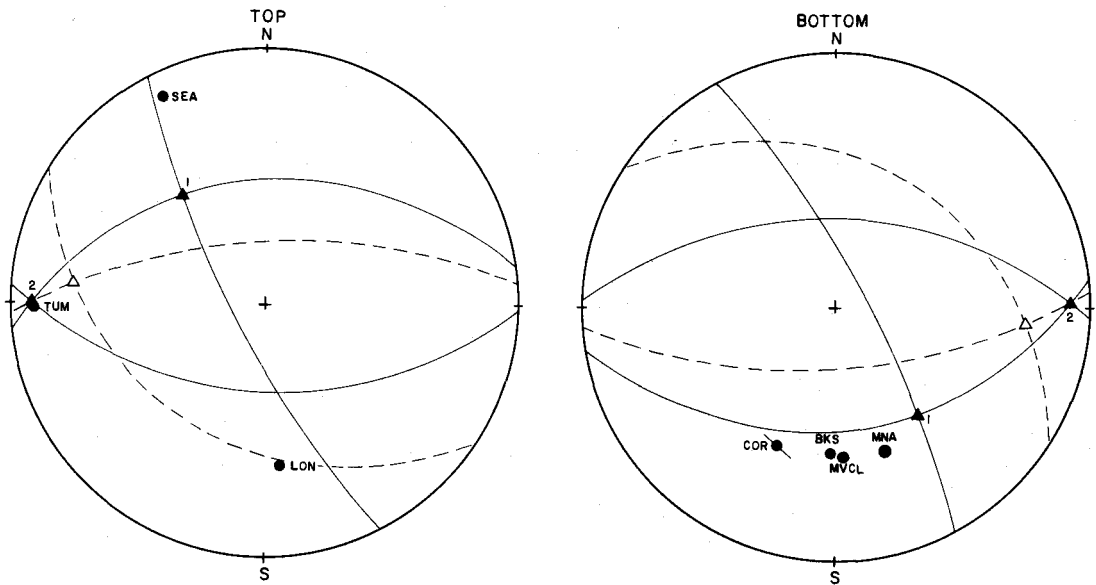
Fault-plane solutions for earthquake of August 19, 1963 projected on top and bottom half of focal sphere.



Fault-plane solutions for earthquake of January 27, 1963 projected on top and bottom half of focal sphere.



Fault-plane solutions for earthquake of August 27, 1963 projected on bottom of focal sphere.



Fault-plane solutions for earthquake of December 31, 1963 projected on top and bottom of focal sphere.

APPENDIX VI

EXPERIMENTAL EARTHQUAKE DATA

Notations used in the following tables;

- C compression
- D dilatation
- * in the Angle of Incidence column means that the angle of incidence is based on averages.
- * in the Arrival Time column indicates no time correction was available.

In the column designated Reference the following symbols are used:

- A data from the U.S. Coast and Geodetic Survey, Earthquake Data Reports
- B data from the University of California, Preliminary Seismological Bulletins
- C data from Verril Rinehart (1964)
- D data from the University of Washington, Preliminary Earthquake Data Reports

P_1 , P_2 , P_3 refers to the first and second arrival of the short-period P wave, and first arrival of the long-period P wave.

S_1 , S_3 refers to the short-period and long-period arrivals of an S wave.

Only the three stations used in the Computer program are shown for crustal shocks of March 7, 1963 and October 14, 1963.

All P and S phases not designated P_1 , P_2 , P_3 , S_1 or S_3 are either P_1 or S_1 .

Earthquake of April 29, 1965 (15:28:43.6) at Tacoma, Washington.

Station	Time	Onset	Source Amplitude of P Wave 10^{10} mm	Crustal Conversion 10^{15}	Angle of Incidence of P wave in degrees	Epicentral Distance in degrees	i_h in degrees	Azimuth in degrees	Reference
BBC P ₃	35:14	C	665.5	21.4	29.8	13.8	95.6	158.9	
BKS	31:00.7	C	66.4	16.2	20.5	9.4	92.6	180.2	
CMC P ₁	33:22.5	C	110.0	27.6	11.5	20.9	99.8	7.5	
P ₃		C	7620.9	27.6	33.8	20.9	99.8	7.5	
COL	33:37.5	D				22.3	100.5	331.2	
DUG	31:14.7	C	511.4	16.8	55.5	9.8	93.0	133.0	
EDM P ₁	30:42.1	C	72.5	14.5	7.3	8.2	91.9	40.4	
P ₃		C	2341.7	14.5	33.7*	8.2	91.9	40.4	
FSJ P ₁	30:28.4	D	35.4	12.9	29.5	7.3	91.0	350.5	
P ₃		D	921.8	12.9	43.3	7.3	91.0	350.5	
HL2ID	30:22.3	C	281.2	11.8	37.8	6.6	90.2	121.6	
MNA	31:00	C	12.8	15.8	44.5	9.3	92.5	160.1	
PHC P ₃	29:55.1	C	1121.4	7.5	33.7*	4.8	88.9	316.7	
PNT	29:27.6	C				2.7	84.0	39.5	
SGAZ P ₁	31:56.3	C	187.6	21.0	58.0	13.4	95.5	147.0	
P ₂			430.9	21.0	53.5	13.4	95.5	147.0	
SNAZ P ₁	32:24.8	C	34.5	23.2	33.7*	15.6	96.5	145.7	
P ₃		C	75.2	23.2	45.5	15.6	96.5	145.7	
VIC P ₁	29:06.4	D				1.5	77.0	326.7	
P ₃		C				1.5	77.0	326.7	
YKA	32:20	D	20.5	23.4	39.8	15.8	96.8	13.0	

Earthquake of May 8, 1968 (12:17:13.4) off coast of Oregon.

Station	Time	Onset	Source Amplitude of P Wave 10^{10} mm	Crustal Conversion 10^{15}	Angle of Incidence of P wave in degrees	Epicentral Distance in degrees	i_h in degrees	Azimuth in degrees	Reference
ARC	18:11.5	D				3.9	91.1	132.6	
BEL	18:45.5	D				6.4	93.0	34.2	
BKS	18:57.3	D	254.1	15.3	34.9	7.2	93.0	141.2	
BMO	19:04.1	C	8.9	15.7	37.2	7.7	93.2	77.0	
COR	18:05.5	C	3572.0	8.7	27.1*	3.4	91.0	71.8	
DUG	20:02.0	C	197.5	19.5	33.5	11.7	95.0	101.7	
FRE	19:28.6	D				9.2	94.0	135.1	
GOL	21:23.0	C				17.2	98.1	95.3	
JAS	19:09.6	D				8.0	93.1	132.5	
MHC	19:07.6	D				7.9	93.0	140.7	
OMSI	18:17	C				4.2	91.0	60.9	
PRI	19:27.1	D				9.3	94.0	140.9	
SAO	19:14.4	D				8.4	93.5	142.1	
SPO	19:14.3	C	60.6	17.0	31.2*	8.4	93.3	57.1	
TFO	21:00.1	C	36.4	21.7	31.2*	15.9	98.0	120.3	
UBO	20:33.3	C	1717.6	21.1	2.3	14.0	95.6	97.3	

Earthquake of August 22, 1963 (09:27:07.3) off the Coast of Oregon.

Station	Time	Onset	Source Amplitude of P Wave 10 ¹⁰ mm	Crustal Conversion 10 ¹⁵	Angle of Incidence of P waves in degrees	Epicentral Distance in degrees	i _h in degrees	Azimuth in degrees	Reference
ARC	27:40.2	D				2.0	88.5	126.8	C
BKS	28:26.3	C	53.8	12.5	26.3	5.2	91.8	143.0	
BRK	28:23.9	C				5.2	91.8	143.2	C
CLS	28:13.6	C				4.4	91.0	140.3	C
COR P ₁	27:59.3	D	77.4	8.0	24.5	3.3	90.0	39.3	
P ₃	28:01.6	D	345.4	8.0	61.3	3.3	90.0	39.3	
FRE	28:59.7	D				7.3	93.0	135.1	C
HLID	29:17.5	C	5.3	17.3	47.3	8.9	93.8	75.9	
LLA	28:48.5	D				6.8	92.6	141.8	C
MHC	28:34.5	C				5.9	92.0	142.1	C
MIN	28:07.1	C				3.9	90.9	115.4	C
PAC	28:31.7	C				5.6	92.0	145.3	C
PRC	28:18.5	D				4.8	91.2	146.5	C
PRI	28:56.8	C				7.3	92.9	142.4	C
PRS	28:47.8	D				6.9	92.5	145.5	C
SCC	28:36.0	C				6.0	92.0	146.2	C
SEA	28:44.8	C	17.9	14.0	31.6	6.2	92.0	25.0	
SFC	28:27.2	D				5.2	91.8	145.2	C
SHS	27:57.5	C				3.2	90.2	114.9	C
UKI	28:06.0	D				3.7	90.5	141.6	C
VIT	28:43.0	D				6.5	92.2	143.7	C
WINV	28:46.3	C	6.0	14.5	25.8	6.6	92.5	93.6	

Earthquake of October 14, 1962 (10:14:27.7) off the Coast of Northern California.

Station	Time	Onset	Source Amplitude of P wave 10^{10} mm	Crustal Conversion 10^{15}	Angle of Incidence of P wave in degrees	Epicentral Distance in degrees	i_h in degrees	Azimuth in degrees	Reference
BKS P ₁	14:56.0	C	77.8	3.4	39.5	1.6	88.0	120.2	
P ₃	15:00.0	C	311.7	3.4	18.5	1.6	88.0	120.2	
BMO	16:27.2	D	2.6	16.5	32.0	7.9	93.1	36.9	
BRK	14:56.0	C				1.6	88.0	120.6	
CLS	14:48.5	C				1.1	86.2	92.8	C
CNC	14:57.3	C				1.7	88.1	115.2	C
HLID	16:41.5	C	4.2	17.3	48.0	8.8	93.8	52.9	
LLA	15:18.2	C				3.2	90.1	129.8	C
MHC	15:06.2	C				2.3	89.0	125.4	C
MIN	15:08.1	C				2.5	89.2	47.6	C
PAC	15:02.3	C				1.9	88.5	131.3	C
PRC	14:49.4	C				1.1	86.0	124.6	C
PRI	15:26.4	D				3.7	90.5	133.0	C
PTOR	16:29.6	C	17.3	16.4	38.8	7.9	93.0	27.1	
REN	15:23.5	D				3.4	90.2	74.2	C
SCC	15:06.6	D				2.3	89.0	136.3	C
SHS	15:07.0	D				2.4	89.0	31.4	C
VIT	15:14.2	D				2.8	90.0	132.5	C
WINV	15:53.3	C	3.5	13.2	35.5	5.7	92.0	60.0	
Crustal									
BKS	14:56.0	C	34.5	1.5	39.5	1.6	119.3	120.2	
PTOR	16:29.6	C	37.0	35.0	38.8	7.9	119.3	27.1	
WINV	15:53.3	C	5.3	20.2	35.5	5.7	119.3	60.0	

Earthquake of March 7, 1963 (23:53:22.3) near Valsetz, Oregon.

Station	Time	Onset	Source Amplitude of P wave 10^{10} mm	Crustal Conversion 10^{15}	Angle of Incidence of P wave in degrees	Epicentral Distance in degrees	i_h in degrees	Azimuth in degrees	Reference
BKS	55:06.5	D	40.3	11.3	32.0*	7.0	91.6	170.1	
BMO	54:32.4	C				4.6	89.9	86.9	
CLS	54:56.7	C				6.2	90.0	171.6	
COR	53:35	C				0.4	51.0	121.8	
HLID	55:04.2	C	3.3	11.2	37.3	6.9	91.5	96.1	
LLA	55:29	C				8.4	92.6	164.5	
LOV	54:55.7	C	20.9	9.8	6.0	6.1	90.8	141.5	
MHC	55:15.1	C	15.7	12.2	32.0*	7.6	92.0	167.2	
MIN P ₁	54:36*	D	17.6	7.6	27.3*	4.7	90.0	159.7	
P ₂		D	51.4	7.6	27.3*	4.7	90.0	159.7	
MNA P ₁	55:17.4	C	1.8	12.2	37.8	7.6	92.0	144.7	
P ₂		D	11.3	11.7	29.5	7.6	92.0	144.7	
MVCL	54:52.2	C	7.5	9.5	43.8	5.9	90.6	161.0	
PNT	54:43	C	93.1	8.6	8.5	5.3	90.1	30.4	
PRI	55:36.1	C				9.0	92.9	163.8	
PRS	55:31.4	C				8.6	92.8	167.1	
PTOR	54:18	C				3.5	88.2	74.7	
SCC	55:20.4	C				7.9	91.5	169.7	
STW	55:03.2	C	11.2	10.6	20.0	6.6	91.2	142.6	
VIT	55:26	C				8.2	92.0	166.7	
WINV	54:50.4	C	5.4	9.3	16.5	5.7	90.5	124.6	
YAWA	54:12.6	D	67.5	4.7	47.5	3.2	87.8	56.0	
Crustal Shock									
PNT	54:43	C	189.2	17.5	8.5	5.3	119.3	30.4	
HLID	55:04.2	C	8.8	30.0	37.3	6.9	119.3	96.1	
MNA	55:17.4	C	5.4	36.5	37.8	7.6	119.3	144.7	

Continued

March 7, 1963

Components of SWAVE 10^{-4} mm

Station	Time	Vertical	Radial	Transverse	Angle of Incidence	Polarization
LOV	56:07.4	-1.90	3.79	-5.40	25.0	32.0
					32.0	34.0
					36.0	45.0
MNA	56:30.5	.04	.02	-.01	40.0	21.0
					59.5	16.0

Earthquake of April 19, 1967 (18:12:25) off the Coast of British Columbia.

Station	Time	Onset	Source Amplitude of P wave 10^{10} mm	Crustal Conversion 10^{15}	Angle of Incidence of P wave in degrees	Epicentral Distance in degrees	i_h in degrees	Azimuth in degrees	Reference
COL	15:55.2	C	8.5	22.4	33.7*	14.8	95.5	332.0	
FSJ	13:34.9	C	9.6	6.9	30.5	4.6	87.8	64.9	
JAS	16:18.1	D				16.6	96.2	148.3	B
LON P ₁	14:29.6	C	6.5	16.1	33.0	8.6	91.9	130.1	
P ₂			5.5	16.2	42.0	8.6	91.9	130.1	
MBC	17:38.2	C				24.0	101.0	7.0	A
MIN	15:52.8	C				14.0	95.5	147.7	B
PNT	14:32.3	C	14.1	15.6	34.4*	8.1	91.0	109.9	

Earthquake of April 29, 1967 (00:04:41.8) near Vancouver Island.

Station	Time	Onset	Source Amplitude of P wave 10^{12} mm	Crustal Conversion 10^{17}	Angle of Incidence of P wave in degrees	Epicentral Distance in degrees	i_h in degrees	Azimuth in degrees	Reference
BKS P ₁	08:09.2	D	4.8	1.4	38.8*	14.5	126.9	153.4	
P ₂	08:11.6	D	16.1	1.4	55.0	14.5	126.9	153.4	
COL P ₁	08:36	C	1.7	1.9	33.7*	16.4	126.9	333.3	
P ₂	08:40.4	C	9.8	1.9	41.0	16.4	126.9	333.3	
FSJ P ₁	05:59.3	D	0.4	0.2	50.5	4.9	126.9	46.6	
P ₂	06:09.7	C			35.0	4.9	126.9	46.6	
HHM	07:21.7	C				10.9	126.9	98.7	A
JAS	08:15.0	C				15.0	126.9	148.2	B
LON P ₁	06:28.6	C	0.5	0.5	31.5	7.2	126.9	125.0	
P ₂	06:29.5	D				7.2	126.9	125.0	
MBC	10:13.3	D				25.4	126.9	6.1	A
MHC	08:17.8	D				15.2	126.9	152.5	B
MIN	07:43.5	D				12.4	126.9	147.3	B
PNT P ₁	06:28.2	C	.6	0.5	34.4*	7.1	126.9	101.1	
P ₂		D			55.5	7.1	126.9	101.1	
PRI	08:37.5	C				16.6	126.9	151.4	B
VIC	06:01.2	C	1.1	0.2	42.5	5.2	126.9	118.1	

Earthquake of March 30, 1966 (12:40:01.0) off British Columbia.

Station	Time	Onset	Source Amplitude of P wave 10^{10} mm	Crustal Conversion 10^{15}	Angle of Incidence of P wave in degrees	Epicentral Distance in degrees	i_h in degrees	Azimuth in degrees	Reference
BKS P ₁	43:08.6	C	203.9	25.3	32.8	13.1	96.0	153.0	
P ₃		C	1329.7	25.3	61.3	13.1	96.0	153.0	
BOZ P ₁	43:03.0	C	16.8	25.1	44.5	12.8	96.0	102.2	
P ₂		D	33.6	25.1	38.0	12.8	96.0	102.2	
P ₃		C	40.7	25.1	44.8	12.8	96.0	102.2	
CMC	44:26.0	C				19.4	99.0	16.6	A
COL P ₁	44:07.7	C	25.7	28.3	27.5	17.8	98.6	334.5	
P ₂		C	131.1	28.3	50.0	17.8	98.6	334.5	
P ₃		C	2201.6	28.3	57.3	17.8	98.6	334.5	
COR P ₁	41:42.7	C	183.3	19.2	54.8	6.8	93.0	137.8	
P ₃	41:41	C	768.6	19.2	38.8*	6.8	93.0	137.8	
FSJ	41:21.3	C	59.2	17.6	34.3*	5.7	92.5	33.7	
JAS	43:12.5	C				13.6	96.4	147.3	B
LON P ₁	41:31.1	C	31.1	18.2	43.3	6.1	92.8	117.2	
P ₃		C	1358.0	18.2	46.3	6.1	92.8	117.2	
MHC	43:13.1	C				13.7	96.5	152.0	B
MIN	42:39.7	C				11.0	95.0	145.9	B
PNT P ₁	41:36.2	D	76.1	18.9	38.3	6.6	93.0	90.4	
P ₂		C	155.1	18.9	56.3	6.6	93.0	90.4	
PRI	43:34.7	D				15.2	97.4	151.0	B
VIC	41:03.8	C	35.1	15.4	38.8*	4.3	91.5	104.9	

Continued

March 30, 1966

Components of S wave 10^{-4} mm.

Station	Time	Vertical	Radial	Transverse	Angle of Incidence	Polarization
BKS S ₃	45:40.5	22.5	-7.47	28.88	40.5	4.0
					54.0	3.0
BOZ S ₃	45:34.2	-2.64	-3.65	6.97	36.5	28.0
COL S ₁	47:47.7	-0.14	-1.62	3.83	4.0	23.0
COL S ₃	47:47.4	11.20	-4.46	-27.98	40.0	3.0
					57.5	2.0
COR	43:12	-8.26	8.85	-0.04	45.0	0.0
PNT	42:57	-1.07	11.95	-7.20	4.5	59.0

Earthquake of May 20, 1966 (23:58:51.7) off Coast of Vancouver Island.

Station	Time	Onset	Source Amplitude of P wave 10^{10} mm	Crustal Conversion 10^{15}	Angle of Incidence of P wave in degrees	Epicentral Distance in degrees	i_h in degrees	Azimuth in degrees	Reference
BKS	02:02	D				13.4	96.2	153.8	B
COR	00:36.1	D	51.8	19.6	38.8*	7.1	93.1	140.0	
COL	02:55	C	90.5	28.1	26.5	17.5	98.2	334.0	
FSJ	00:10.8	D	77.3	17.2	28.3	5.4	92.2	36.1	
JAS	02:09.7	D				13.9	96.8	148.2	B
LON	00:24.6	D	16.6	18.5	38.8*	6.3	92.8	120.4	
MHC	02:11.6	D				14.1	96.9	152.8	B
MIN	01:35.6	D				11.4	95.0	147.0	B
PNT	00:28.2	D	29.9	18.9	34.4*	6.6	93.0	93.8	
PRI	02:28.7	D				15.5	97.6	151.7	B
VIC	00:00.3	C	32.1	15.5	38.8	4.4	91.6	109.9	

May 20, 1966 Components of S wave 10^{-4} mm.

Station	Time	Vertical	Radial	Transverse	Angle of Incidence	Polarization
COR	02:05.1	.07	-.36	-.13	10.0	68.8
FSJ	01:15.7	-.41	-1.45	-.76	12.5	82.0
					34.3	84.0
					35.0	85.0
PNT	01:49.5	-.28	-1.25	-.32	38.0	7.0

Earthquake of November 4, 1966 (20:30:13.0) off Coast of British Columbia.

Station	Time	Onset	Source Amplitude of P wave 10^{10} mm	Crustal Conversion 10^{15}	Angle of Incidence Of P wave in degrees	Epicentral Distance in degrees	i_h in degrees	Azimuth in degrees	Reference
BOZ	33:05.2	D	3.8	24.5	31.3*	12.1	95.2	101.9	
FSJ	31:39.8	C	32.0	17.6	24.5	5.7	92.5	26.4	
JAS	33:18.5	D				12.9	96.0	149.8	B
LON	31:31.6	C	9.1	17.1	38.8*	5.3	91.8	117.7	
MHC	33:21.0	D				13.1	96.0	154.8	B
MIN	32:41.4	D				10.3	94.5	148.8	B
PNT	31:40.3	D	140.7	17.8	31.5	5.8	92.5	87.4	
PRI	33:34.7	C				14.5	97.0	153.5	B
VIC	31:06.3	D	13.2	13.7	38.8*	3.5	91.1	102.5	

November 4, 1966

Components of S wave 10^{-4} mm.

Station	Time	Vertical	Radial	Transverse	Angle of Incidence	Polarization
FSJ	32:49.3	.38	.11	-.38	41.0	3.0
					52.1	6.0
LON	32:32	.19	-.16	.33	38.0	18.0
PNT	32:51.0	.24	-.65	.67	18.3	42.0
					33.5	48.0
					35.6	57.0
VIC	31:50.8	.20	-.14	.49	38.5	11.0

Earthquake of June 25, 1963 (08:26:21.7) off the Coast of Oregon.

Station	Time	Onset	Source Amplitude of P wave 10^{10} mm	Crustal Conversion 10^{15}	Angle of Incidence Of P wave in degrees	Epicentral Distance in degrees	i_h in degrees	Azimuth in degrees	Reference
CLS	28:05.8	C				7.4	93.0	137.0	C
COR	27:24.8	C	37.5	10.0	20.5	4.1	91.0	82.6	
HLID	28:58.2	C	7.8	18.4	56.5	10.6	94.8	87.8	
LON	27:46.8	C	16.6	11.4	19.0	5.6	92.0	60.6	
MIN	28:00.6	C				6.7	92.5	122.6	
PTOR	28:09.5	D	14.2	15.6	24.5	7.3	93.0	75.3	
SHS	27:51.7	C				6.0	92.0	123.4	C
WINV	28:35.2	C	4.0	17.3	30.0	8.9	93.5	104.6	

Earthquake of July 4, 1963 (05:50:47.5) off the Coast of Oregon.

Station	Time	Onset	Source Amplitude of P wave 10^{10} mm	Crustal Conversion 10^{15}	Angle of Incidence of P wave in degrees	Epicentral Distance in degrees	i_h in degrees	Azimuth in degrees	Reference
COR	51:28.2	C	51.6	5.8	18.0	2.4	89.0	64.4	
PTOR	52:14.2	C	22.1	13.2	34.5	5.6	92.0	66.6	
WINV	52:29.5	C	4.3	15.0	42.2	6.9	92.5	106.0	

Earthquake of June 25, 1963 (09:39:27.7) off the Coast of Oregon.

Station	Time	Onset	Source Amplitude of P wave 10^{10} mm	Crustal Conversion 10^{15}	Angle of Incidence of P wave in degrees	Epicentral Distance in degrees	i_h in degrees	Azimuth in degrees	Reference
COR	40:31.2	D	23.5	10.2	28.5	4.1	91.0	84.0	
HLID	42:05.8	C	3.6	18.7	59.5	10.7	94.9	88.3	
LON	40:52.9	C	6.5	13.2	31.8	5.7	92.0	61.8	
MIN	41:07.4	C				6.8	92.5	122.9	C
SHS	40:59.4	C				6.1	92.0	123.8	
WINV	41:42.4	C	4.9	17.4	39.8	9.0	93.8	105.0	

Earthquake of February 21, 1963 (12:01:16.4) off the Coast of Northern California.

Station	Time	Onset	Source Amplitude of P wave 10^{10} mm	Crustal Conversion 10^{15}	Angle of Incidence of P wave in degrees	Epicentral Distance in degrees	i_h in degrees	Azimuth in degrees	Reference
ARC	01:11	C	8.2	0.7	30.3*	.9	66.0	54.8	
BKS	02:08.3	C				3.3	86.0	137.4	C
BMO	03:04.7	C	6.1	12.9	47.0	7.3	91.0	49.2	
BRK	02:04.9	D				3.3	85.8	137.7	C
CLS	01:58.5	C				2.6	84.0	131.0	
CNC	02:09.3	C				3.3	86.0	134.7	C
COR	02:25.1	C	8.9	6.5	30.3*	4.4	88.2	16.5	
HLID	03:25.5	D	5.2	15.2	29.3*	8.7	92.0	64.1	
MHC	01:28	D	5.3	5.8	30.3*	4.0	87.2	137.3	
MIN	01:55	D	6.9	3.3	31.8*	2.6	84.0	89.0	
PAC	02:12.9	D				3.7	86.4	141.6	C
PRC	02:01.8	C				2.8	84.6	142.4	
PRS	02:31.0	D				5.0	88.9	143.0	C
PTOR	03:00.0	D	8.8	12.4	19.0	6.9	90.8	38.6	
REN	02:24.3	D				4.1	87.5	99.7	C
SCC	02:28.1	C				4.1	87.5	143.4	
SHS	01:13.8	C	5.6	2.3	30.3*	2.1	81.0	79.5	
UKI	01:50.2	D				1.9	80.0	129.7	C
VIT	02:25.9	D				4.6	88.2	140.2	C
WINV	02:43.8	C	2.7	10.2	36.0	5.8	89.9	77.7	

Earthquake of November 6, 1962 (03:36:43.0) near Portland, Oregon.

Station	Time	Onset	Source Amplitude of P wave 10^{10} mm	Crustal Conversion 10^{15}	Angle of Incidence of P wave in degrees	Epicentral Distance in degrees	i_h in degrees	Azimuth in degrees	Reference
ARC	37:58.5	C	100.2	7.8	32.0*	4.8	90.0	192.9	
BKS P ₁	38:41.4	D	76.2	12.3	21.3	7.7	91.2	177.6	
P ₃		C	146.0	12.3	67.0	7.7	91.2	177.6	
BMO	37:42.5	C	7.9	5.5	40.3	3.8	88.9	99.4	
COL	41:58*	D				23.7	101.0	333.4	
COR	37:03.5	D	33.9	0.70	32.0*	1.1	78.0	204.7	
DUG P ₁	38:57.8	C	35.3	13.7	31.5	9.0	92.9	123.4	
P ₃		C	2200.8	13.7	49.5	9.0	92.9	123.4	
FRE	39:08.6	C	229.3	13.8	40.8	9.1	92.8	165.4	
HLID	38:17.2	C	9.1	10.2	60.0	6.3	91.0	105.1	
LON	37:07.3	D	5.8	0.8	32.0*	1.3	80.6	26.5	
MBC	42:59.5	D				30.7		1.5	
MHC	38:50.2	D	67.9	12.9	32.0*	8.3	92.2	174.4	
MIN	38:06.5	D	24.5	8.6	27.3*	5.3	90.1	171.4	
MNA	38:43.4	C	41.2	13.8	34.3	7.9	91.5	153.4	
MVCL	38:23.2	C	3.5	10.5	26.8	6.5	91.0	170.6	
PAC	38:46.5	C	45.1	12.8	32.0*	8.2	92.2	177.4	
PNT	37:48.5	C	9.8	6.7	24.5	4.2	89.2	27.8	
PTOR	37:29.2	C	11.9	3.1	24.0	2.6	86.9	88.4	
REN P ₁	38:24?	C	154.3	10.4	51.5	6.4	91.0	160.0	
P ₂		C	431.9	10.4	24.5	6.4	91.0	160.0	
SEA P ₁	37:18	D	573.0	2.0	21.5	2.1	85.0	6.4	
P ₃	37:18	D	375.8	2.0	32.0*	2.1	85.0	6.4	
SFC	38:42.3	D	89.3	12.5	32.0*	7.8	92.0	178.8	
SIT	40:05.2*	C	56.7	18.4	33.7*	13.9	95.5	330.2	
VIC	37:30	D	12.4	4.1	32.0*	3.0	87.2	350.1	
WINV	38:10.5	D	2.8	9.2	18.0	5.7	90.5	136.6	

Earthquake of January 24, 1963 (21:43:11.8) east of Seattle.

Station	Time	Onset	Source Amplitude of P wave 10^{10} mm	Crustal Conversion 10^{15}	Angle of Incidence on P wave in degrees	Epicentral Distance in degrees	i_h in degrees	Azimuth in degrees	Reference
COR	44:01	C	25.9	7.8	24.0	3.0	126.9	197.6	
HLID P ₁	44:49.5	C	5.6	25.5	56.0	6.6	126.9	122.4	
P ₂		D	11.0	25.5	37.5	6.6	126.9	122.4	
LON P ₃	43:24.6	D	35.0	1.6	32.0*	0.7	86.0	169.1	
MNA P ₁	45:34.3	C	22.2	75.0	16.8	9.5	126.9	161.3	
P ₂		C	98.6	75.0	34.0	9.5	126.9	161.3	
MVCL	45:15.3	C	16.2	57.0	43.5	8.3	126.9	176.1	
PNT	43:51.1	D	5.1	3.4	57.0	2.4	126.9	40.1	
PTOR	43:56.8	C	8.6	7.0	29.0	2.9	126.9	129.8	
SEA	43:18.0	D				0.3	76.0	311.2	
WINV	44:45	D	11.6	27.5	27.3	6.9	126.9	150.4	

Earthquake of September 26, 1962 (05:07:11.2) in Southwestern Montana.

Station	Time	Onset	Source Amplitude of P wave 10^{10} mm	Crustal Conversion 10^{15}	Angle of Incidence of P wave in degrees	Epicentral Distance in degrees	i_h in degrees	Azimuth in degrees	Reference
BMO	08:04.8	D	3.1	6.6	36.8	3.4	117.3	275.3	
BUT	07:35.9	C	5.3	1.0	34.8*	1.4	117.3	359.1	
DUG	08:23.8*	D	2.2	11.4	22.0	4.4	117.3	182.8	
HHM	08:21.2	C	1.7	8.5	34.8*	3.9	117.3	345.1	
HLID	07:40.3	C	18.6	1.3	33.8	1.6	117.3	231.9	
PTOR	08:22.3	C	11.3	11.8	34.8*	4.6	117.3	284.5	Continued

September 26, 1962

Components of S wave 10^{-4} mm.

Station	Time	Vertical	Radial	Transverse	Angle of Incidence	Polarization
HLD	08:01.3	3.76	-2.59	-1.15	38.3	53.0
PTOR	09:16.1	26.12	-52.29	-24.60	25.0	62.0
					32.0	64.0
					36.0	69.0

Earthquake of February 16, 1963 (03:01:37.8) in Southwestern Montana.

Station	Time	Onset	Source Amplitude of P wave 10^{10} mm	Crustal Conversion 10^{15}	Angle of Incidence of P wave in degrees	Epicentral Distance in degrees	i_h in degrees	Azimuth in degrees	Reference
BMO	02:48.1	D	3.7	12.3	37.5	4.7	117.3	256.7	
DUG	03:11.9	D	1.6	21.5	34.8*	6.1	117.3	193.8	
GOL	03:34.6	D	3.4	33.0	37.8	7.6	117.3	145.7	
HHM	02:29.4	D	5.2	5.4	34.8*	3.1	117.3	317.9	
HLID	02:31.8	C	6.2	6.6	38.4	3.4	117.3	225.1	
LON	03:28.8	D	13.6	32.0	33.0*	7.5	117.3	278.9	
PTOR	03:02.2	D	13.6	17.9	20.0*	5.6	117.3	267.8	
WINV	03:17.8	C	3.3	26.0	32.8*	6.7	117.3	227.2	

Earthquake of October 18, 1962 (18:03:14.0) in Central Idaho.

Station	Time	Onset	Source Amplitude of P wave 10^{10} mm	Crustal Conversion 10^{15}	Angle of Incidence of P wave in degrees	Epicentral Distance in degrees	i_h in degrees	Azimuth in degrees	Reference
BMO	03:45.7	D	2.4	2.0	43.3	1.8	117.3	291.0	
DUG	04:24.2	D	0.8	10.5	34.8	4.3	117.3	158.4	
HLID	03:27.9	D	4.5	2.4	45.0	0.7	84.8	141.1	
PTOR	04:04.6	C	4.3	5.6	31.0	3.2	117.3	297.6	
WINV	04:10.0	C	1.0	6.6	15.0*	3.4	117.3	214.3	

October 18, 1962 (18) Component of S wave 10^{-4} mm.

Station	Time	Vertical	Radial	Transverse	Angle of Incidence	Polarization
PTOR	04:42.5	-.26	.59	-.20	21.0	70.0
					33.0	73.0
					35.9	75.0

Earthquake of October 18, 1962 (20:31:02.6) in Central Idaho.

Station	Time	Onset	Source Amplitude of P wave 10^{10} mm	Crustal Conversion 10^{15}	Angle of Incidence of P wave in degrees	Epicentral Distance in degrees	i_h in degrees	Azimuth in degrees	Reference
BMO	31:24.5	D	13.0	2.0	27.3	1.8	117.3	291.0	
DUG	32:13.5	C	4.4	10.5	51.8	4.3	117.3	158.4	
HLID	31:16.5	D	3.2	2.4	50.0	0.7	84.8	141.1	
LON	32:25.6	C	1.1	17.2	50.0	5.5	117.3	300.0	
PTOR	31:53.5	C	4.6	5.6	40.0	3.2	117.3	297.6	
WINV	31:59.2	C	0.7	6.6	15.0*	3.4	117.3	214.3	

October 18, 1962 (20) Component of S wave 10^{-4} mm.

Station	Time	Vertical	Radial	Transverse	Angle of Incidence	Polarization
PTOR	32:34.8	-.37	-.19	-.98	39.5 65.0	4.0 2.0

Earthquake of January 6, 1963 (18:07:42.9) in Southwestern Montana.

Station	Time	Onset	Source Amplitude of P wave 10^{10} mm	Crustal Conversion 10^{15}	Angle of Incidence of P wave in degrees	Epicentral Distance in degrees	i_h in degrees	Azimuth in degrees	Reference
DUG	08:54.6	C	4.4	12.5	15.0	4.7	117.3	186.8	
GOL	09:31.0	C	8.5	29.0	35.3	7.2	117.3	133.7	
HLID	08:16.5	D	2.8	2.2	34.0	2.0	117.3	233.0	
LON	09:28.8	C	47.7	28.5	15.0	7.0	117.3	289.1	
PTOR	08:58.2	C	10.0	13.4	48.8	4.9	117.3	281.4	
WINV	09:03.6	C	3.2	15.5	15.0*	5.3	117.3	230.1	

Earthquake of February 24, 1963 (15:24:51.8) in Southwestern Montana.

Station	Time	Onset	Source Amplitude of P wave 10^{10} mm	Crustal Conversion 10^{15}	Angle of Incidence of P wave in degrees	Epicentral Distance in degrees	i_h in degrees	Azimuth in degrees	Reference
HHM	25:55.5	C	2.2	8.4	34.8*	3.9	117.3	338.1	
HLID	25:27.4	C	1.4	2.4	25.2	2.1	117.3	236.8	
PTOR	26:08.5	C	14.5	14.0	35.0	5.0	117.3	281.8	
WINV	26:21.4	C	1.0	18.9	12.5	5.3	92.5	231.8	

Earthquake of September 2, 1965 (18:01:19.4) off the Coast of British Columbia.

Station	Time	Onset	Source Amplitude of P wave 10^{10} mm	Crustal Conversion 10^{15}	Angle of Incidence of P wave in degrees	Epicentral Distance in degrees	i_h in degrees	Azimuth in degrees	Reference
COL	05:31.9	D	31.0	29.8	33.7	19.6	99.2	335.1	
LON	02:30.5	D	17.6	16.2	38.8*	4.7	91.9	106.8	
JAS	04:09.3	D				11.9	95.1	147.9	B
MIN	03:34.6	C				9.3	94.0	146.1	B

Earthquake of October 11, 1965 (15:47:55.4) off the Coast of British Columbia.

Station	Time	Onset	Source Amplitude of P wave 10^{10} mm	Crustal Conversion 10^{15}	Angle of Incidence of P wave in degrees	Epicentral Distance in degrees	i_h in degrees	Azimuth in degrees	Reference
BOZ	50:54.0	C	10.8	25.1	18.0	12.8	96.0	106.0	
COR	49:43.0	C	70.5	19.9	38.8*	7.3	93.1	143.4	
JAS	51:21.7	C				14.2	96.9	149.9	B
LON	49:28.5	D	43.6	18.5	33.5	6.3	92.9	124.6	
MHC	51:21.7	C				14.4	97.0	154.4	B
MIN	50:41.8	D				11.6	95.0	149.1	B
PRI	51:36.6	C				15.8	97.8	153.2	B
SPO	49:57.9	D				8.4	93.9	105.4	A

Earthquake of July 8, 1963 (04:19:08.4) off the coast of Oregon.

Station	Time	Onset	Source Amplitude of P wave 10^{10} mm	Crustal Conversion 10^{15}	Angle of Incidence of P wave in degrees	Epicentral Distance in degrees	i_h in degrees	Azimuth in degrees	Reference
BKS P_1	20:08.4	C	19.1	9.8	39.3	4.0	90.9	135.5	
P_3		C			27.3	4.0	90.9	135.5	
COR	20:09	C	45.6	10.3	35.0	4.2	91.0	25.0	
UKI	20:49.5*	C	13.4	6.6	30.3*	2.6	89.5	129.1	

Earthquake of August 19, 1963 (09:38:56.2) off the Coast of Oregon.

Station	Time	Onset	Source Amplitude of P wave 10^{10} mm	Crustal Conversion 10^{15}	Angle of Incidence of P wave in degrees	Epicentral Distance in degrees	i_h in degrees	Azimuth in degrees	Reference
ARC	39:17	D				1.5	87.5	90.3	
BKS	40:05.3	C				4.2	91.0	134.9	C
CLS	39:50.9	D				3.5	90.4	129.7	C
HLID	40:11.5	C				9.1	94.0	68.6	
MHC	40:11.9	D				4.9	91.5	135.1	C
MIN	39:49.4	C				3.4	90.2	98.0	C
PAC	40:06.0	D				4.6	91.1	138.4	C
SCC	40:11.4	C				5.0	91.5	140.1	C
SHS	39:40.1	C				2.7	89.8	93.1	C
WINV	40:33.3	D				6.5	92.2	83.2	

Earthquake of February 1, 1963 (16:38:55.8) near Idaho.

Station	Time	Onset	Source Amplitude of P wave 10^{10} mm	Crustal Conversion 10^{15}	Angle of Incidence of P wave in degrees	Epicentral Distance in degrees	i_h in degrees	Azimuth in degrees	Reference
DUG	40:00.5	D	3.8	9.8	34.8*	4.2	117.3	161.8	
HHM	40:01.5	C	5.8	10.0	34.8*	4.2	117.3	4.4	
HLID	39:06.6	D	8.9	0.4	34.8*	0.6	81.0	159.7	
LON	40:21.9	C	17.7	18.5	28.5	5.7	117.3	299.4	
MIN	40:31 *	D	45.6	24.2	15.0*	6.5	117.3	236.4	
PTOR	39:50.2	D	13.0	6.6	37.0	3.4	117.3	296.5	
RCD	41:00.3	C				8.1	117.3	86.7	

February 1, 1963

Components of S wave 10^{-4} mm.

Station	Time	Vertical	Radial	Transverse	Angle of Incidence	Polarization
LON	41:25.7	-.21	-.25	.75	36.5	21.0

Earthquake of January 27, 1963 (15:24:41.9) in Central Idaho.

Station	Time	Onset	Source Amplitude of P wave 10^{10} mm	Crustal Conversion 10^{15}	Angle of Incidence of P wave in degrees	Epicentral Distance in degrees	i_h in degrees	Azimuth in degrees	Reference
BMO	25:18.9	D	8.7	2.6	34.8*	2.2	117.3	289.3	
BOZ	25:32	D	1.8	4.7	34.8*	2.4	117.3	53.0	
DUG	25:48.4	D	2.1	9.7	34.8*	4.1	117.3	162.8	
GOL	25:46.1	D	20.6	37.0	21.3	8.1	117.3	120.5	
HHM	25:48.7	D	26.7	10.0	34.8*	4.2	117.3	3.5	
HLID	24:54.0	C				0.5	79.0	167.0	
LON	26:09.7	C	19.6	19.1	38.5	5.8	117.3	299.1	
PTOR	25:37.2	D	4.3	7.0	33.0	3.5	117.3	296.1	
WINV	25:39.9	C	18.2	7.4	17.5	3.6	117.3	219.5	

Earthquake of December 27, 1963 (02:36:18.5) in Northwestern Oregon.

Station	Time	Onset	Source Amplitude of P wave 10^{10} mm	Crustal Conversion 10^{15}	Angle of Incidence of P wave in degrees	Epicentral Distance in degrees	i_h in degrees	Azimuth in degrees	Reference
BEL	37:08.9	D				3.2	87.8	10.8	
BKS	38:25	C	6.8	12.4	30.3*	7.8	92.0	173.3	
BMO	37:25.9	C				4.4	89.5	98.2	
COR P ₃	36:37.8	D				1.1	78.0	176.9	
LON	36:45.9	D	22.6	1.2	20.3	1.6	82.6	43.7	
PRC	38:12	C				7.6	92.0	176.9	
TKWA	37:22.5	C	1.7	6.4	46.0	4.1	89.0	37.8	
VIC	37:02.3	D				2.9	87.1	359.6	

Earthquake of December 31, 1962 (20:49:34.4) east of Seattle.

Station	Time	Onset	Source Amplitude of P wave 10^{10} mm	Crustal Conversion 10^{15}	Angle of Incidence of P wave in degrees	Epicentral Distance in degrees	i_h in degrees	Azimuth in degrees	Reference
BKS	51:50.1	D	148.4	51.0	32.0*	9.2	119.3	181.9	
COR P ₃	50:17.0	D	598.0	4.5	60.5	2.7	119.3	203.0	
LON	49:40	D				0.3	65.0	174.5	
MNA P ₁	51:50	D	10.0	50.0	25.0	9.0	119.3	161.2	
P ₂		C	58.6	50.0	24.5	9.0	119.3	161.2	
MVCL P ₁	51:31.8	D	17.4	34.5	35.5	7.8	119.3	176.8	
P ₂		C	39.5	34.5	42.3	7.8	119.3	176.8	
SEA	49:46.5	D				0.7	85.0	333.6	
TUM	49:45.5	D				0.7	85.2	268.9	

December 31, 1962

Components of S wave 10^{-4} mm.

Station	Time	Vertical	Radial	Transverse	Angle of Incidence	Polarization
COR S ₃	50:50.2	-16.60	-17.34	37.74	37.8	19.0

Earthquake of August 2, 1963 (22:17:18.2) off the Coast of Northern California.

Station	Time	Onset	Source Amplitude of P wave 10^{10} mm	Crustal Conversion 10^{15}	Angle of Incidence of P wave in degrees	Epicentral Distance in degrees	i_h in degrees	Azimuth in degrees	Reference
ARC	17:40.6	C				1.1	85.6	69.0	C
BKS	18:15.3	D	123.1	8.9	85.0	3.6	90.5	135.9	
BRK	18:12.5	D				3.6	90.5	136.2	C
CIS	18:03.7	C				2.9	90.0	129.7	C
COR	18:30.5	D	27.3	10.7	36.8	4.4	91.0	20.0	
HLID	19:32	C	8.5	17.3	45.0	8.8	93.5	65.5	
LLA	18:36.3	C				5.2	91.7	136.7	C
LON	19:04.2	D	6.8	14.8	42.8	6.8	92.5	21.4	
MHC	18:23.6	C				4.3	91.0	136.0	C
MIN	18:06.0	C				2.9	90.0	91.8	C
PAC	18:20.1	C				4.0	90.8	140.0	C
PRC	18:06.8	D				3.1	90.1	140.2	C
PRI	18:44.3	C				5.7	91.9	138.1	C
PRS	18:36.3	D				5.2	91.7	141.6	C
SCC	18:24.3	D				4.4	91.0	141.7	C
SHS	17:57.8	C				2.3	89.0	84.1	C
UKI	17:56.5*	C	18.7	5.0	30.3*	2.2	89.0	128.3	
VIT	18:32.0	D				4.9	91.4	138.8	C
WINV	18:49.7	D	2.8	13.8	40.5*	6.1	92.1	79.3	

August 2, 1963 Component of S wave 10^{-4} mm.

Station	Time	Vertical	Radial	Transverse	Angle of Incidence	Polarization
COR	19:18	-0.10	1.15	0.08	4.0	86.0

Earthquake of August 27, 1963 (05:51:34. 1) off the Coast of Oregon.

Station	Time	Onset	Source Amplitude of P wave 10^{10} mm	Crustal Conversion 10^{15}	Angle of Incidence of P wave in degrees	Epicentral Distance in degrees	i_h in degrees	Azimuth in degrees	Reference
CLS	53:25.5	C				7.5	93.0	134.1	C
COR	52:42.0	D	72.6	10.8	30.4*	4.5	91.0	81.6	
FRE	53:11.4	D				10.4	94.6	131.6	C
PRI	53:24.0	C				10.4	94.7	136.7	C
PRC	53:24.5	D				7.8	93.5	138.1	C
PRS	53:24.0	D				9.9	94.2	138.6	C
SEA	53:08.8	C	1237.7	13.9	42.0	6.1	92.1	52.1	
SHS	53:12.4	C				6.3	92.1	120.5	C
UKI	53:18.5	C				6.8	92.5	134.4	C
VIC	53:03.5	C				6.1	92.0	41.4	C
VIT	53:33.0	C				9.6	94.0	137.3	C